Improving Fault Location through Interpole Analysis of Circuit Breaker and Automatic Reclose Scheme Operation

Thesis presented for the degree of

Doctor of Philosophy

at the University of Strathclyde

by

LIANG JI

Supervisors: Dr Campbell Booth, Dr Adam Dyśko

Department of Electronic and Electrical Engineering
University of Strathclyde

2012

Acknowledgments

I wish to gratefully acknowledge the financial and technical support from Toshiba International (Europe) Ltd. and the University of Strathclyde that allowed me to carry out this research.

I would like to express my whole-hearted gratitude to Dr Campbell Booth and Dr Adam Dyśko for their professional advice, guidance and kind support throughout this project. I would like to sincerely thank them for the time and effort that they spent on my studies and project. Without them, it would have been impossible for me to complete this degree. Also, I would like to thank Professor Phil Moore for the great help and providing me this great opportunity to do this research.

I am grateful to all of my friends. I would like to thank them for giving me great help in my study and life. With them, I never feel lonely.

Finally, I would like to thank my parents, Mr Pengfei Ji and Ms Meiru Zhang, for their great love and support. Without them, how can I stand on today's stage? No matter what happens, I know they are always there to share my happiness and accompany me for my every achievement.

Declaration of Author's Right

Signed: _____ Date: _____

Abstract

This research concentrates on the development and evaluation of novel single ended impedance based fault location methods, which are easy and economical to implement in practice. The conventional single ended impedance based fault location methods normally suffer from negative effects associated with variability and inaccuracies in fault resistance, distance to fault and from the impact of variable remote end short circuit level. A novel concept of a single ended impedance based fault location method using analysis of 'interpole' states, which arise during the operation of the circuit breaker as the individual poles open sequentially, has been developed. The proposed fault location technique has been shown to have a very high theoretical accuracy by eliminating the aforementioned negative effects associated with conventional single ended impedance based methods. The thesis describes how the developed technique operates through comparing simulated voltage and currents during the interpole states with the actual measured voltage and currents, and searches for a match that may be indicative of fault location. When a match is found within a pre-specified tolerance error from analysis of the initial "during fault" state, the ranges of corresponding possible fault locations, fault resistances and remote end short circuit levels used in the simulation are noted. The ranges of all possible values are subsequently reduced through analysis of the consecutive interpole stages as each pole of the circuit breaker opens sequentially to finally interrupt the flow of current in all three phases. The final, most accurate, fault location is obtained following on from analysis of the final state.

Another single ended impedance based fault location method has been developed that extends the analysis to the operation of single/three phase auto-reclose schemes. Similarly with previous method, the second method also uses the analysis of different system states, which are arisen during the auto-reclose operation, and improves on the accuracy of the method that only analyses the single operation of the circuit breaker. The methods are demonstrated using EMTP/ATP simulation models for a variety of different cases and it is shown how high accuracy has been achieved, with improved performance when compared with conventional single ended impedance based method (Takagi method and network impedance method). Additionally, it is a potentially economic solution, as only local end data is required. The thesis concludes with an overview of ongoing and future work that has the intention of moving the work forward towards implementation within commercially available relay hardware.

Glossary

CB:	Circuit Breaker
GPS:	Global Position System
DFT:	Discrete Fourier Transform
LSM:	Least Squared Method
CT	Current Transformer
VT	Voltage Transformer
SCL1:	Local end short circuit level
SCL2:	Remote end short circuit level
$\mathbf{Z_L}$**:**	Transmission line impedance
n :	Fault location as a proportion of total line length
R_f:	Fault resistance
K:	Fault matrix
E_L	Local source voltage
E_R	Remote source voltage
$\mathbf{Z_{loc,}}$ **:**	Local end source impedances
$\mathbf{Z_{rem}}$	Remote end source impedance
$\mathbf{E_f}$**:**	Voltage at the fault location in the pre-fault network
SPAR:	Single Phase Auto Reclose Scheme
TPAR:	Three Phase Auto Reclose Scheme
γ:	Propagation constant of transmission line
d:	Transmission line length
Z_c:	Surge impedance of transmission line

Note that matrices are denoted by bold text.

List of Tables

List of Figures

CONTENTS

Chapter 1. Introduction

1.1 Basic concepts of fault location

It is critical for transmission and distribution system operators to supply power with high continuity, dependability and reliability; this is becoming ever more important as the level of interconnectivity grows, and the reliance on electrical power increases. Furthermore, the increasing levels of renewable generation, particularly in the UK where a large amount of wind energy is being installed in offshore locations, places even greater emphasis on the need for transmission circuits with the highest possible levels of availability, particularly for those that transmit power from remote generation locations/offshore generation infeeds to major load centres. As a result, it is critical that accurate and fast-acting power system protection and fault location functions are available.

Fault location plays an important role in the overall function of system protection and post-fault remedial actions. There are many causes of faults on transmission and distribution lines. These include breakdown of insulation, problems initiated by storms and other weather phenomena, overgrown vegetation, animals and human error; any of which may result in the connection of a power line to earth or a fault

between phases. Permanent faults involving physical damage to equipment must be located and repaired before the supply can be restored. In today's modern power system, customers are more sensitive to outages and sustained outages can lead to significant damages and financial losses for the operating companies. Therefore, fast and accurate fault location techniques are desired to reduce restoration times and to increase the continuity and dependability of power supply.

1.2 Motivation for research

According to the nature of the input signal(s) used, fault location techniques can be subdivided into single ended methods, two ended methods and multi ended methods. Single ended fault location methods are generally the simplest and most economical to implement. Only local end data is required. It can obtain good accuracy with minimum requirements for processing or communications. Compared with single ended methods, two ended and multi-ended methods, which require voltage and current data from two/multiple locations, require additional facilities such as communication channels and, in some cases, Global Position System (GPS) timing synchronising devices. While more complex and costly, such techniques generally offer higher accuracy of fault location than single ended methods.

Impedance based and travelling wave based fault location methods are the main fault locating techniques that have been implemented in practice. Impedance based methods are relatively simple and easy to implement, and estimate the distance to fault using measured fundamental current and voltage phasors. However, the accuracy of conventional single ended impedance based methods, such as the simple

reactance method and the Takagi method [1-3], may suffer from the effects of variable fault resistance, fault position, remote end short circuit level and pre-fault load level. Some algorithms [4-7] have been developed to reduce the negative impacts on conventional single ended method, for example by requiring a definition of the remote end short circuit level as an input. Very good levels of accuracy have been achieved by such improved single ended fault location techniques. However, the remote end short circuit level is uncertain, and changes if the system configuration beyond the remote end bus changes, so cannot be relied upon as an input to such techniques.

Compared with conventional single ended impedance based methods, two ended methods [8-17] do not suffer from the effects of factors such as fault resistance, fault distance variations and uncertain remote end short circuit level, and a generally higher accuracy is therefore obtained when compared with single ended techniques. As the synchronisation of the measurement data from both ends is critical within such methods, GPS timing technology has been used in some cases [8, 9, 11, 16-18].

Travelling wave methods offer significant improvements in accuracy compared with impedance based methods [5-7, 11, 15, 19-26]. However, this method is relatively expensive to implement compared with impedance based method. High data sampling frequency and dedicated devices is required. Some problems associated with the travelling wave method still need to be improved, including accurately waveform detection and interpretation, discriminating between initial waveforms and subsequent reflections and time tagging of measurements.

In summary, the single ended impedance based fault location method is the most attractive if it can be made sufficiently accurate: it is potentially economic and simple to implement as only local fundamental frequency phasors are required. However, the accuracy of conventional single ended impedance based fault location techniques may suffer from effects of variable pre-fault loading level, uncertain remote end short circuit level, the actual fault position and the fault resistance.

To address these shortcomings, two fault location algorithms, which use only single ended data and which analyse the electrical data during and after circuit breaker and auto-reclose scheme operation, have been developed and are reported in this dissertation. Such methods provide great accuracy of fault location, and not only eliminate, but can also quantify the magnitude of the parameters that normally have a negative impact on single-ended impedance methods (namely remote end short circuit level and fault resistance). The developed techniques are potentially as economic to implement as conventional single ended techniques because only the local phasors are only required.

During circuit breaker operation, several system states, which are termed “interpole states”, arise due to the different stages of interruption of each of the three individual phases, which are not interrupted simultaneously due to the requirement for interruption of current flow in each phase around the point of a current zero crossing. There are three main elements of the algorithm: (a) transmission line modelling, (b) matching, and (c) recording.

(a) The transmission line modelling is to compute voltage and current phasors using assumed fault location, fault resistance and remote end short circuit level. The ranges of possible fault locations, fault resistances and remote end short circuit levels are pre-estimated first using a conventional fault location technique (Takagi method). The computations are iteratively stepped through pre-set ranges of fault locations, fault resistances and remote end short circuit levels. For each combination of these parameters the method calculates voltage and current phasors during the consecutive circuit breaker interpole states (using transmission line fixed impedance model).

(b) At each iteration, the computed data is compared with the simulated data (matching) using pre-defined comparison tolerance levels.

(c) When a match is established between the calculated and simulated data, the candidate group (including fault location, fault resistance and remote end short circuit level) is stored (recording).

This process is repeated for each interpole state and this is then used to obtain the exact fault location (and other parameters) at the final interpole state (where all three phases have been interrupted). A steady state transmission line model underpins the methods and is used to demonstrate the accuracy of this method. The duration of each interpole state is short (3.33ms in theory in a 50Hz system); it is, therefore, difficult to extract the fundamental frequency phasor in such a short time. However, it is believed that this shortcoming can be resolved as DSP techniques develop in the future.

In order to overcome this shortcoming associated with reliably of extracting fundamental frequency phasors during such a short time period, a second fault location algorithm, based on analysis of data during the operation of auto-reclose schemes, has also been researched and developed in this thesis. This is prudent, as auto reclose is used on the vast majority of overhead systems, and any permanent fault will obviously involve "open-reclose-open" states as the system attempts to reclose, which will be unsuccessful due to the permanent nature of the fault. It should be noted that location of transient faults is also important as such faults may occur repeatedly at the same location, and therefore, need to be identified and attended to promptly. However, this thesis, primarily deals with permanent faults.

There are several individual system states that arise during auto-reclose scheme operation. This new method applies the similar principle as the first fault location algorithm that analyses interpole states during circuit breaker operation. Compared with fault location algorithm based on the interpole state analysis, this algorithm avoids the difficulty in accurately extracting fundamental frequency phasors as the duration of individual system states that arise from auto-reclosing operation has sufficient time for accurate phasor extraction, and it is believed that it could be readily implemented in practice.

1.3 Research objectives

The objective in this research work is to study the conventional fault location techniques and to develop novel fault location algorithms which improve fault location accuracy by eliminating the negative factors associated with conventional

techniques, including the negative impact of variable fault resistance, remote end short circuit level and pre-fault load level. This research is sub-divided into three main elements:

- An investigation into the influences and impacting factors on established fault location techniques and comparative analyses of the performance of such techniques under these negative influences.
- Design and demonstration of fault location algorithms based on the analysis of circuit breaker operation and evaluation of the performance of the proposed algorithm against the best existing techniques under a range of fault conditions.
- Design and demonstration of fault location algorithms based on auto-reclose operation and evaluation of the performance of the proposed algorithm against the best existing techniques under a range of fault conditions.

1.4 Research contribution

Based on the above research objectives, the following original contributions can be claimed:

- A new fault location algorithm, which analyses the interpole states of circuit breakers during fault clearing operation. As the basic principle is based on the comparison between simulated data and calculated data, a steady state transmission line modelling approach has been used to compute a range of states relating to different fault locations (and other parameters – fault resistance and remote end short circuit level) during circuit breaker operation has been developed using a lumped parameter line model. Results of the novel fault location algorithm show that the algorithm is capable of accurate fault location

in situations where the remote end short circuit level and fault resistance are unknown. The performance compares favourably against existing fault location methods, and has the potential for achieving very high accuracy with low cost of implementation

- A novel fault location algorithm, which analyses the different states arising during the operation of auto-reclose schemes. This uses similar principles to the previous method, but employs an increased amount of input data (from the auto reclose phases of operation) that enhances accuracy and reliability of the output results. A large number of evaluations, which include the negative effects of fault distance, fault resistance, remote end short circuit level, inaccurate local end short circuit level and measurement error, have been carried out to prove the success of the proposed algorithm.

1.5 Scope of the thesis

Chapter 1: Introduction

In this chapter, fault location theory is defined. The motivation for the research work is presented and the objectives of this thesis are defined.

Chapter 2: Review of fault location techniques

In this chapter, the background information of fault location is included; the main fault location techniques that are used and/or have been the subject of research by others are introduced.

Chapter 3: Comparative performance analysis of impedance based fault location techniques

In this chapter, an evaluation and comparative analyses of the simple reactance method, the Takagi method, the network impedance method and the two-ended method are presented.

Chapter 4: Fault location through analysis of data from inter-pole states during circuit breaker operation

In this chapter, the novel fault location technique based on the analysis of circuit breaker operations is introduced and described in detail. Case studies and evaluation of this technique are included and results illustrate and quantify the accuracy of this method. The challenges and difficulties associated with this method are also described.

Chapter 5: Fault location through analysis of data from auto-reclose operations

In this chapter, the novel fault location technique based on the analysis of auto reclose scheme operations is introduced and described in detail. This novel technique is based on similar principles to the fault location technique introduced in chapter 4. However, this method avoids the difficulties and challenges of the other technique by analysing data from the various stages of the auto-reclose scheme operation. Case studies using EMTP/ATP simulations and evaluation of this technique are included.

Chapter 6: Evaluation of sensitivity of auto-reclose based location to variations in input parameters

In this chapter, the new fault location technique introduced in chapter 5 has been evaluated to ascertain its ability to counteract the traditional negative effects associated with impedance based methods, such as fault resistance, uncertain remote end short circuit level, inaccurate local end short circuit level setting and measurement error brought by measurement instrument. A detailed comparison with the Takagi method is also presented.

Chapter 7: Conclusions and future work

Conclusions are presented and future work is outlined.

1.6 Publications

Based on the results of the research work reported in this thesis, the following papers have been published:

- L.Ji, C.Booth, A.Dysko, F.Kawano, G.Baber, "Improving fault location by analysis of electric parameters during circuit breaker operation," *presented at the PSCC*, Stockholm Sweden, 2011
- L.Ji, C.Booth, A.Dysko, F.Kawano, G.Baber, "Improved Fault Location through Analysis of System Parameters during Auto-Reclose Operations on Transmission Lines," *IEEE transaction on Power Delivery* (submitted for fourth round review)

1.7 References

[1] T. Takagi, *et al.*, "Development of a New Type Fault Locator Using the One-Terminal Voltage and Current Data," *Power Apparatus and Systems, IEEE Transactions on*, vol. PAS-101, pp. 2892-2898, 1982.

[2] K. Zimmerman and D. Costello, "Impedance-Based Fault Location Experience," in *Rural Electric Power Conference, 2006 IEEE*, 2006, pp. 1-16.

[3] E. O. Schweitzer, "A review of impedance-based fault locating experience," presented at the Proc of 14th Annual Iowa¨CNebraska System Protection Seminar, Omaha, 1990.

[4] L. Eriksson, *et al.*, "An Accurate Fault Locator With Compensation For Apparent Reactance In The Fault Resistance Resulting From Remore-End Infeed," *Power Apparatus and Systems, IEEE Transactions on*, vol. PAS-104, pp. 423-436, 1985.

[5] C. E. de Morais Pereira and L. C. Zanetta, Jr., "Fault location in transmission lines using one-terminal postfault voltage data," *Power Delivery, IEEE Transactions on*, vol. 19, pp. 570-575, 2004.

[6] S. Harmeet and T. Raghuveer, "A new design distance to fault locator for power transmission lines," presented at the Proc of Int Conf on Modern Trends in the Protection Schemes of Elelctrical Power Apparatus and System, New Delhi, 1998.

[7] M. B. Djuric, *et al.*, "Distance protection and fault location utilizing only phase current phasors," *Power Delivery, IEEE Transactions on*, vol. 13, pp. 1020-1026, 1998.

[8] C. Ching-Shan, *et al.*, "A new adaptive PMU based protection scheme for transposed/untransposed parallel transmission lines," *Power Delivery, IEEE Transactions on,* vol. 17, pp. 395-404, 2002.

[9] M. Kezunović, *et al.*, "An accurate fault location algorithm using synchronized sampling," *Electric Power Systems Research,* vol. 29, pp. 161-169, 1994.

[10] M. Kezunovic and B. Perunicic, "Automated transmission line fault analysis using synchronized sampling at two ends," *Power Systems, IEEE Transactions on,* vol. 11, pp. 441-447, 1996.

[11] D. A. Tziouvaras, *et al.*, "New multi-ended fault location design for two- or three-terminal lines," in *Developments in Power System Protection, 2001, Seventh International Conference on (IEE),* 2001, pp. 395-398.

[12] R. K. Aggarwal, *et al.*, "A practical approach to accurate fault location on extra high voltage teed feeders," *Power Delivery, IEEE Transactions on,* vol. 8, pp. 874-883, 1993.

[13] E. G. Silveira and C. Pereira, "Transmission Line Fault Location Using Two-Terminal Data Without Time Synchronization," *Power Systems, IEEE Transactions on,* vol. 22, pp. 498-499, 2007.

[14] Y. Liao, "Unsynchronized Fault Location Based on Distributed Parameter Line Model," *Electric Power Components and Systems,* vol. 35, pp. 1061-1077, 2007/06/27 2007.

[15] A. L. Dalcastagne, *et al.*, "An Iterative Two-Terminal Fault-Location Method Based on Unsynchronized Phasors," *Power Delivery, IEEE Transactions on,* vol. 23, pp. 2318-2329, 2008.

[16] Z. Q. Bo, *et al.*, "Application of GPS based fault location scheme for distribution system," in *Power System Technology, 1998. Proceedings. POWERCON '98. 1998 International Conference on*, 1998, pp. 53-57 vol.1.

[17] P. F. Gale, "The use of GPS for precise time tagging of power system disturbances and in overhead line fault location," in *Developments in the Use of Global Positioning Systems*, 1994, pp. 5/1-5/2.

[18] K. E. Martin, "Precise timing in electric power systems," in *Frequency Control Symposium, 1993. 47th., Proceedings of the 1993 IEEE International*, 1993, pp. 15-22.

[19] P. F. Gale, *et al.*, "Fault location based on travelling waves," in *Developments in Power System Protection, 1993., Fifth International Conference on*, 1993, pp. 54-59.

[20] L. J. Lewis, "Traveling Wave Relations Applicable to Power-System Fault Locators," *American Institute of Electrical Engineers, Transactions of the,* vol. 70, pp. 1671-1680, 1951.

[21] L. Yi-Feng and C. Ping, "The Principle of the Modern Travelling Wave Based on Fault Location and the Applications to Actual Fault Analysis," in *Power and Energy Engineering Conference, 2009. APPEEC 2009. Asia-Pacific*, 2009, pp. 1-4.

[22] P. A. Crossley and P. G. McLaren, "Distance Protection Based on Travelling Waves," *Power Apparatus and Systems, IEEE Transactions on,* vol. PAS-102, pp. 2971-2983, 1983.

[23] P. F. Gale, *et al.*, "Practical experience with travelling wave fault locators on Scottish Power's 275 & 400 kV transmission system," in *Developments*

in Power System Protection, Sixth International Conference on (Conf. Publ. No. 434), 1997, pp. 192-196.

[24] L. M. Wedepohl, "Application of matrix methods to the solution of travelling-wave phenomena in polyphase systems," *Electrical Engineers, Proceedings of the Institution of,* vol. 110, pp. 2200-2212, 1963.

[25] H. W. Dommel, "Digital Computer Solution of Electromagnetic Transients in Single-and Multiphase Networks," *Power Apparatus and Systems, IEEE Transactions on,* vol. PAS-88, pp. 388-399, 1969.

[26] M. S. Sachdev and R. Agarwal, "A technique for estimating transmission line fault locations from digital impedance relay measurements," *Power Delivery, IEEE Transactions on,* vol. 3, pp. 121-129, 1988.

Chapter 2. Review of fault location techniques

2.1 Introduction

Fast and accurate fault location methods assist power system operators in locating and repairing elements of the system that have been damaged due to electrical faults. It is critical that the system is restored as quickly as possible following an outage so that the overall availability and integrity of the system is maximised. This is particularly important in modern and future systems, where the location and nature of generation means that even greater reliance will be placed on transmission and distribution systems. There are a large number of fault location techniques that have been proposed, and in some cases, implemented within power systems. This chapter reviews several of these techniques and places the work reported in the remainder of this dissertation in the context of existing work.

2.2 Faults within power systems

2.2.1 Power line faults

As mentioned in Chapter 1, there are many causes of faults on transmission and distribution lines. These include breakdown of insulation, problems initiated by

storms and other weather phenomena, overgrown vegetation, animals and human error; any of which may result in the connection of a power line to earth or a fault between phases.

According to different voltage level and weather conditions, there are statistics relating to faults on systems. The majority of statistics state that approximately 75% of all faults in transmission networks are due to the inherent exposed characteristics of the line and atmospheric conditions [1].

2.2.2 Fault types and statistics

Faults occurring on a transmission line can be categorised as open circuit, transient (or arcing) and permanent short circuit fault. Open circuit faults usually arise from a breakage in a conductor, as shown in Figure 2.2. In some cases, the broken conductor may subsequently result in a single phase to earth fault, which is shown in Figure 2.2b. Transient faults only exist on the power system for a short time (as they are cleared by the fast operating protection) and are normally resolved quickly by using an auto-reclosing scheme. Transient faults represent the majority of faults encountered on overhead power systems. However, faults which are permanent or repetitive cannot be resolved quickly by auto-reclosing action and normally require to be repaired by the maintenance team.

In short circuit faults, a phase conductor (or conductors) may be in in contact with earth or another phase. These are the most common fault types in distribution and transmission systems. Generally, short circuit faults can be catalogued as:

- Single phase to earth fault, as shown in Figure 2.1a
- Phase to phase fault, as shown in Figure 2.1b
- Phase to phase to earth fault, as shown in Figure 2.1c
- Symmetrical fault (three phase/three phase to earth fault, Figure 2.1d, Figure 2.1e)

Data relating to transmission system fault statistics, in terms of fault types and causes, are available from the literature and also from the internet. In order to briefly acquaint the statistics, Table 2.1 shows the statistical occurrence of different categories of short circuit faults [2]. From the table, it is clear that single phase to earth fault represents the vast majority of faults that are encountered on overhead systems.

Fault type	Probability of occurrence (%)
Single phase to earth	85%
Phase to phase	8%
Phase to phase to earth	5%
Symmetrical fault	2%

Table 2.1. Fault category statistics[2]

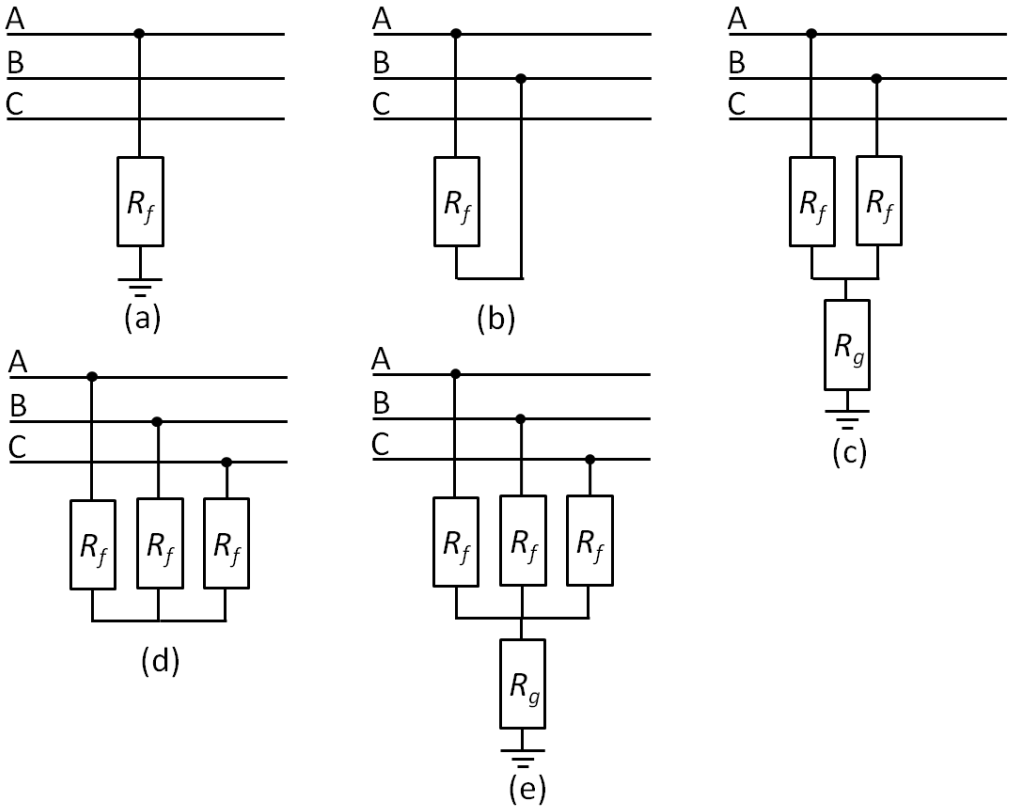

Figure 2.1. Short circuit fault types and their modelled representation

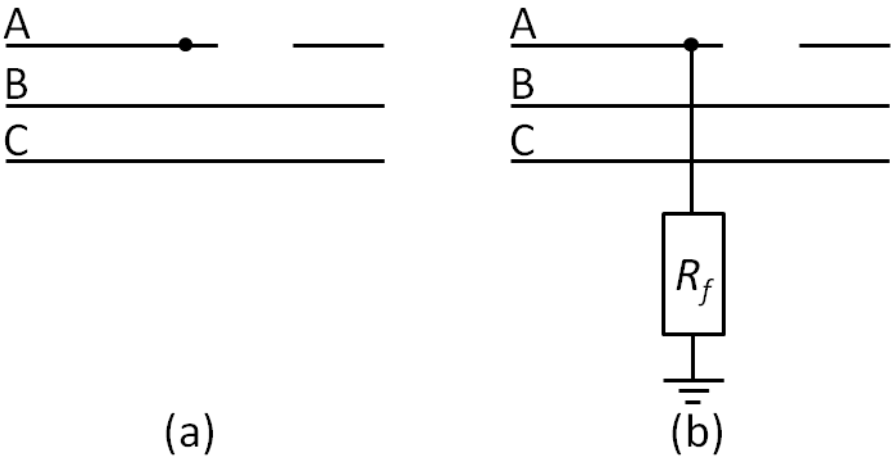

Figure 2.2. Open circuit faults

2.3 Impedance based fault location methods

The impedance method of fault location is the most widely used method in practice as it is relatively economical and easy to install and implement in the system. In this section, several typical single and two ended methods of fault location are reviewed.

2.3.1 Single ended impedance based algorithms

As mentioned previously, single ended impedance based methods are relatively economical and simple to implement when compared with two ended impedance and travelling wave based methods. The algorithms employed within single ended schemes estimate fault location using only current and voltage measured from the local end (i.e. the end at which measurements are taken). In the remainder of this section, the concept of the fault loop model is introduced initially, followed by a review of several typical conventional fault location algorithms including: the simple reactance method which requires only during-fault data; the Takagi method, which requires both pre-fault and during-fault data; and the network impedance, method which requires an input quantifying the local and remote end short circuit levels.

2.3.1.1 Fault loop model

The majority of single ended impedance-based algorithms are based on the use of a fault loop model. Through the entire dissertation, a two ended system model (i.e. a line supplied form both ends – i.e. there are sources of fault current at both ends of the faulted line, typical of interconnected transmission systems) is used to quantify and verify the performance of conventional fault location algorithms (introduced in this chapter) and the novel fault location methods that are reported in Chapters 4 and 5.

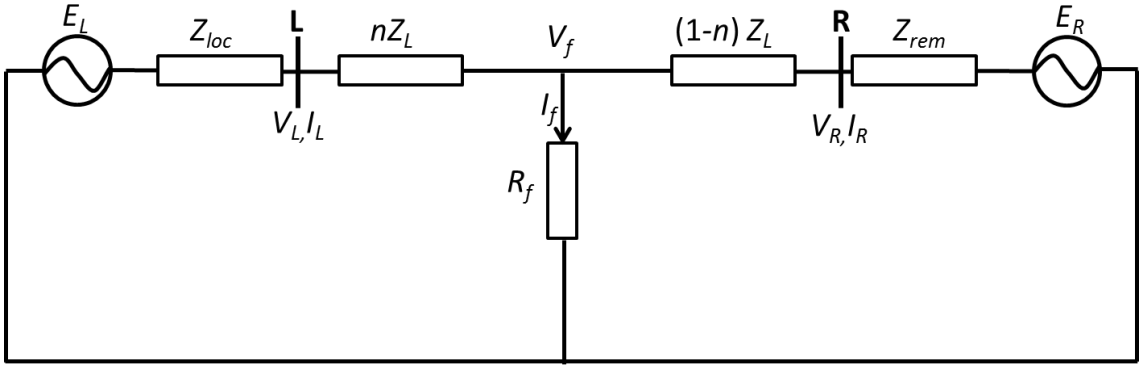

a) Faulted network

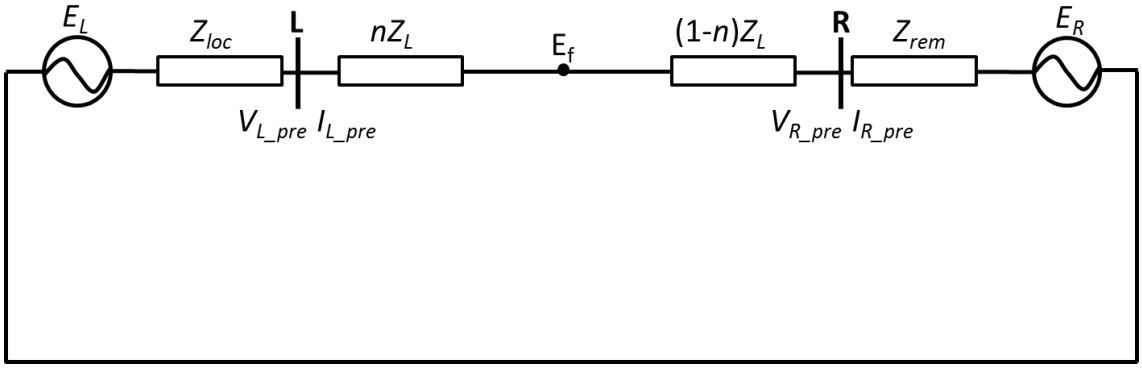

b) Pre-fault network

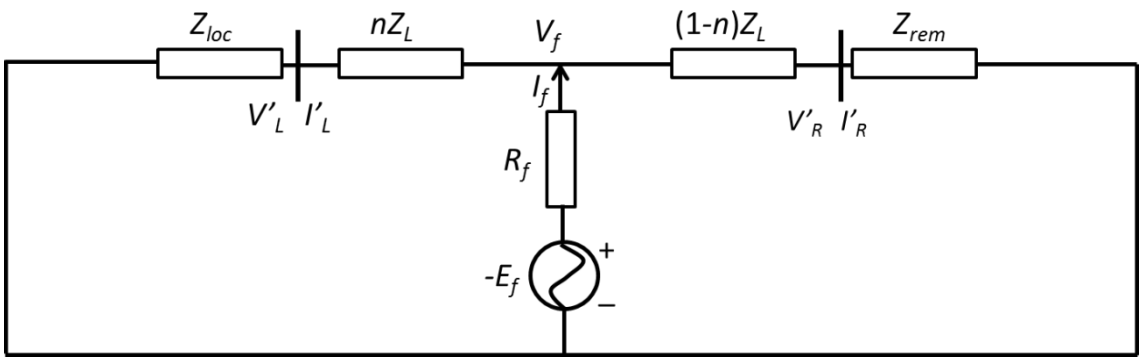

c) Superimposed network

Figure 2.3. Two-ended transmission line network: superposition process

Figure 2.3 represents a faulted network with a phase to earth fault. According to superposition theory, the faulted network, as shown in Figure 2.3a, can be represented as the summation of the pre-fault network (shown in Figure 2.3b) with the superimposed network, as shown in Figure 2.3c. Consequently, the fault voltage and current at local end (V_L and I_L) can be represented as:

$$V_L = V_{L\_pre} + V_L' \tag{2.1}$$

$$I_L = I_{L\_pre} + I_L' \tag{2.2}$$

Note that V_{L_pre} and I_{L_pre} denote the pre-fault voltage and current; V_L' and I_L' denote the superimposed voltage and current. In the figure, **L** and **R** denote the local and remote end of the faulted transmission line.

In the faulted network, as shown in Figure 2.3a, the fault loop from terminal **L** to the fault is represented as:

$$V_L - nZ_L I_L - I_f R_f = 0 \tag{2.3}$$

This fault loop equation is widely applied in majority single end impedance based methods. Typical fault location techniques based on this equation will be reviewed in the following section.

2.3.1.2 Simple Reactance Method

Equation (2.3) represents the fault loop, and the relationship between the various parameters of interest, within the single phase model. By rearranging (2.3), the measured impedance (Z_L) at the local end can be obtained:

$$Z_L = \frac{V_L}{I_L} = nZ_L + \frac{I_f R_f}{I_L} \tag{2.4}$$

In the equation above, the fault location n is the solution objective. The simple Reactance Method [3-5] has been designed to minimise the effect of $\frac{I_f R_f}{I_L}$ by only using the imaginary part of the above equation. Therefore, the fault distance n is calculated using:

$$n = \mathrm{Im}(\frac{V_L}{Z_L I_L}) \tag{2.5}$$

This method has reduced the potential negative impact of R_f by assuming the imaginary part of $\frac{I_f R_f}{I_L}$ is to be equal to 0. The error associated with this method is only equal to 0 if $R_f = 0$ or $\angle I_f = \angle I_L$. In the case of a single end sourced system, this method has excellent accuracy, because $\angle I_f$ is always equal to $\angle I_L$. However, the majority of transmission systems are interconnected and fault current will be supplied form both line ends, and this method will therefore suffer significantly from the impact of non-zero fault resistance and angle mismatches between I_f and I_L, which may change as n, uncertain $SCL2$,R_f and pre-fault load angle.

2.3.1.3 The Takagi method

According to superposition theory, the faulted network can be treated as the sum of the pre-fault and superimposed networks, as shown in Figure 2.3. In the superimposed network, as shown in Figure 2.3c, the fault current I_f passing through the fault resistance is calculated using the following:

$$I_f = \frac{\Delta I_L}{C_m} \tag{2.6}$$

$$I'_L = I_L - I_{L\_pre} \tag{2.7}$$

C_m is defined as the current distribution factor [6], which is equal to:

$$C_m = \frac{Z_{rem} + (1-n)Z_L}{Z_L + Z_{loc} + Z_{rem}} = |C_m|e^{j\gamma} \tag{2.8}$$

The fault loop equation (2.3) can be rewritten as:

$$V_L - nZ_L I_L - R_f \frac{I'_L}{|C_m|e^{j\gamma}} = 0 \tag{2.9}$$

From the above equation, it is clear that γ is represents the angle of the current distribution factor, which depends on the source impedances "behind" both line ends and the distance to fault. As to reduce the effect of R_f, Takagi [7] has developed an algorithm which applies the correction factor I'^{*}_L (* denotes the complex conjugate of I'_L) at both sides of equation (2.9). Thus, the fault distance is obtained as:

$$n = \frac{\mathrm{Im}(V_L I_L'^{*} e^{j\gamma})}{\mathrm{Im}(Z_L I_L I_L'^{*} e^{j\gamma})} \tag{2.10}$$

The key success of the Takagi method is that the influencing element $\mathrm{Im}\left(\frac{R_f I_L' I_L'^{*}}{|C_m| e^{j\gamma}}\right)$ is equal to 0 by assuming$\gamma = 0$. In the majority of situations, there is no significant factor that impacts on the accuracy of this method. However the angle γ is not exactly equal to 0 in the majority of situations. The fault location error arises through a combination of this angle not being non-zero and the additional fact that there is typically a non-zero fault resistance. The fault location error increases as the fault resistance increases, and may become significant when high resistance faults occur. As the angle of fault distribution factor γ depends on *n* and Z_{loc}, Z_{rem}, as shown in (2.8), the change of *n* or Z_{loc}, Z_{rem} will cause a different value of γ. The fault location error may be influenced as a result.

2.3.1.4 Network Impedance Method

The algorithm introduced by Eriksson [6] attempts to address the errors associated with the Takagi method (as explained in the previous section) by requiring both ends source impedance or fault level as an input, normally represented as short circuit level.

Through combining equations (2.8) and (2.9), the following can be obtained:

$$V_L - nZ_L I_L - R_f \frac{I_L'(Z_L + Z_{loc} + Z_{rem})}{Z_{rem} + (1-n)Z_L} = 0 \tag{2.11}$$

Rearranging the above (2.11) gives:

$$M_2 n^2 + M_1 n + M_0 = 0 \tag{2.12}$$

Where,

$M_2 = {Z_L}^2 I_L$

$M_1 = -V_L Z_L - Z_L I_L Z_{rem} - {Z_L}^2 I_L$

$M_0 = R_f I_L'(Z_L + Z_{loc} + Z_{rem})$

In the equation, there are two unknown variables, *n* and R_f. By using both the real and imaginary parts of the equation, the unknown parameters *n* and R_f can be solved. Note that this equation may produce two solutions, only one of which is representative of the actual fault distance. The other (incorrect) solution lies outside of the line range so usually be easily identified and discarded.

A number of other impedance based fault location techniques utilise the fact that *SCL2* is known. The extraction of the current phasor from the fault current data may be distorted by CT saturation. [8] reported a fault location algorithm with limited requirement to use the current phasor data. Instead, a function relating during-fault voltage to fault distance and fault resistance is utilised. The fault location can be determined by knowledge of the level of *SCL2*. Paper [9] describes a single ended fault location method that operates by solving the zero sequence impedance network. The local end current phasors and *SCL2* are required as an input in this method. As previously mentioned, the Takagi method reduces the effect of fault resistance significantly. However, the angle of fault current distribution factor (γ) is not equal

to 0 in reality. A modified Takagi method introduced in [3] improves fault location accuracy, as it allows for correction of the fault current distribution factor angle (γ) using the levels of both *SCL1* and *SCL2*.

Attempts to reduce the negative effects of variations in R_f. have been made by many researchers as any positive developments in this respect can improve location accuracy. Some algorithms, such as those reported in [6], can actually quantify the value of R_f. However, the value of *SCL2* is required as input, which cannot normally be known with any great degree of certainty, as the system configuration beyond the remote end bus may change. Furthermore, the increase in intermittent renewable energy sources will also act increase the uncertainty of source impedances.

2.3.2 Two ended impedance based algorithms

Two ended impedance methods generally display better fault location accuracy performance when compared with single ended methods. Two ended methods display higher levels of immunity to the detrimental influences of fault resistance, pre-fault load angle and uncertain remote end short circuit level. However, communications channels and data from both ends are required as a pre-requisite for the application of such methods.

The use of either synchronised or unsynchronised data from both ends has been considered by researchers working in this field. The methods using synchronised data [10-15] have improved fault location accuracy with the help of GPS time coding techniques [16, 17]. In the case of loss of the GPS facility or signal, then such

schemes can normally operate with unsynchronised data; other schemes using non-synchronised data from both ends have also been developed. The key challenge for such fault location techniques [15, 18-30] is in solving for the angle difference between the data measured from both ends.

2.3.2.1 Two ended methods employing synchronised data

In the faulted network, as shown in Figure 2.4, the voltage at the fault point can be calculated from both sides of the line, as shown below.

From the perspective of the **L** line end:

$$V_f = V_L - I_L n Z_L \tag{2.13}$$

From the perspective of the **R** line end:

$$V_f = V_R - I_R (1 - n) Z_L \tag{2.14}$$

Through combining and rearranging the above equations, the fault distance *n* is can be calculated as shown below:

$$n = \frac{V_L - V_R + I_R Z_L}{Z_L (I_L + I_R)} \tag{2.15}$$

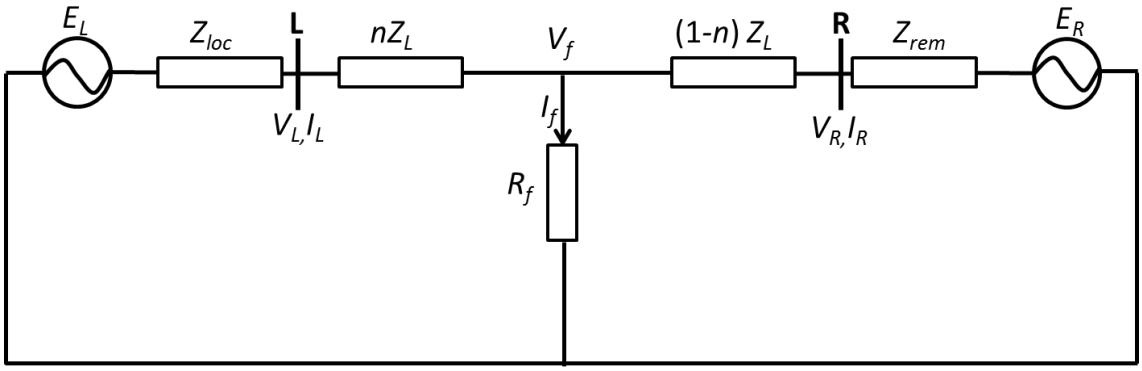

Figure 2.4. Fault network used for two ended method

The above figure represents a single phase network. In a three phase network, the symmetrical sequence components or modal quantities are applied in the calculation steps [31].

2.3.2.2 Use of unsynchronised data methods

In cases where no accurate common time reference (e.g. from GPS) is available, a synchronisation operator $e^{j\theta}$ is applied to ensure proper time alignment of the phasors at opposite sides of the circuit.. The calculation of the angle θ used by the synchronisation operator is described later in this section. In cases where synchronised data is available (e.g. via GPS) and a time reference provided for both ends, then no synchronisation operator is required. In unsynchronised data methods, there is no common time reference available, and normally the remote end data is set as reference (terminal **R** in Figure 2.4), the local end data can be "synchronised" (i.e. angle aligned) by multiplying the local end measurement data by the synchronisation operator. Consequently, the voltage and current at the local end (terminal **L** in Figure 2.4) is represented as $V_L e^{j\theta}$ and $I_L e^{j\theta}$. Accordingly, the fault distance is calculated as shown below:

$$n = \frac{V_L e^{j\theta} - V_R + I_R Z_L}{Z_L (I_L e^{j\theta} + I_R)} \tag{2.16}$$

The objective, when using unsynchronised data from each of the ends, is to calculate or eliminate the synchronisation operator $e^{j\theta}$.

a) Calculation of Synchronisation operator

There are several methods to calculate the synchronisation operator. [18, 21, 25, 27] introduced an algorithm with the use of a pre-fault quantities, as shown in Figure 2.3b. In the pre-fault network, the data from each are represented as shown below:

At **L** end: $I_{L\_pre}e^{j\theta}$, $V_{L\_pre}e^{j\theta}$

At **R** end: V_R , I_R

The calculated voltage V'_{R_pre} at R end is represented in (2.17) using data from the **L** end.

$$V'_{R\_pre} = V_{L\_pre}e^{j\theta} - I_{L\_pre}e^{j\theta}Z_L \tag{2.17}$$

The calculated voltage V'_{R_pre} is equal to the measured voltage at end R.

$$V_{R\_pre} = V'_{R\_pre} \tag{2.18}$$

Thus, the synchronisation operator is,

$$e^{j\theta} = \frac{V_{R\_pre}}{V_{L\_pre} - I_{L\_pre}Z_L} \tag{2.19}$$

As the synchronisation operator has been determined, the fault location is consequently obtained by (2.16).

In addition to methods relying on pre-fault parameters to calculate synchronisation operator parameters, certain algorithms [21, 25] have introduced a method of calculating the synchronisation operator using during-fault quantities. The unsynchronised symmetrical network quantities of both ends are used. A function linking the fault current I_f, as shown in Figure 2.4, with the synchronisation operator $e^{j\theta}$ and the fault location n has been established. The most attractive advantage of this method is that both the parameters of the synchronisation operator and fault location are estimated simultaneously.

b) Elimination of the synchronisation operator

Equations (2.17)-(2.19) show the calculation of the synchronisation operator. Algorithms reported in [19, 26, 28, 30] have calculated the fault distance by solving the synchronisation operator equation, in which the $e^{j\theta}$ term does not require to be calculated.

After rearrangement of (2.16), the synchronisation operator equation can be expressed as shown below:

$$e^{j\theta} = \frac{nI_R - I_R Z_L + V_R}{V_L - nI_L Z_L} \tag{2.20}$$

$\left|e^{j\theta}\right| = 1$, therefore:

$$\left|\frac{nI_R - I_R Z_L + V_R}{V_L - nI_L Z_L}\right|^2 = 1 \tag{2.21}$$

The above equation can be stated in the form shown below:

$$M_2 n^2 + M_1 n + M_0 = 0 \tag{2.22}$$

Where

$M_2 = |Z_L I_L|^2 - |Z_L I_R|^2$

$M_1 = -2\mathrm{Re}[V_L (Z_L I_L)^* + (V_R - Z_L I_R)(Z_L I_R)^*]$

$M_0 = |V_L|^2 - |V_R - Z_L I_R|^2$

The fault distance, *n*, can be calculated by solving (2.22). There are two solutions for this. As is the case for equation (2.12) (used in the network impedance method), the solution that lies within the range of the line length is selected and the other solution discarded.

2.3.3 Fault location in special situations

There are special cases where the use of fault location is more complicated. For example double circuit lines, multi-terminal lines, series-compensated lines, etc. For such types of transmission line, several specific fault location techniques have been designed and propose.

Double circuit lines are extremely common in networks, particularly in power-dense situations and applications where high power transfers are required. As the individual circuits are located in close proximity to each other, they are inductively coupled. The apparent impedance of each line is influenced by the adjacent line. Due to this phenomenon, modifications to the basic impedance based fault location method are

required. Based on the local end data, the fault current distribution factor [32, 33] has been modified to reflect the changes of the line impedance. Further publications [34, 35] propose a method for accurately calculating the fault current distribution factor. In the case of limited measurements at the local end (e.g. the healthy parallel line is switched off and earthed at both ends), [36] has reported a method which only requires three-phase voltage and faulty phase current. Some algorithms locate fault position by using data from both circuit ends [37-41]. As with the single ended methods for double lines, the main task of these algorithms is also focusing on catering for the effect of mutual inductance between adjacent circuits.

Series compensation schemes, normally affected by switching in variable amounts of capacitance to circuits (using thyristor switching), is becoming increasingly popular for power factor correction and optimisation of transmission efficiency and capacity levels [42]. There have been several algorithms proposed that are concerned with locating faults on lines employing series compensation. Among them, the typical method is to apply the equivalent representation of series compensation elements [43-46]. In order to reduce the effect of compensation device, [43, 46] locate the fault position by applying this representation. Such techniques use two “sub-algorithms” which cover both scenarios respectively when that fault is in front of or behind the compensation device. A selection of the correct fault location solution is carried out based on the computation outputs of each “sub-algorithm”.

2.4 Travelling wave based fault location methods

Travelling wave based fault location methods are based on interpretation of relative arrival times and patterns of travelling waves initiated by faults, as measured at the line end(s), and subsequent reflections from line ends (due to the step change in impedance encountered by the original travelling wave) that travel back and forth over the line between the fault location and line ends. The fault locator detects the fault point by recognising the high frequency travelling wave signals and analysing its propagation time. In theory, travelling wave based fault location method can produce extremely accurate results. When compared with impedance based fault location methods, travelling wave methods are immune to fundamental frequency phenomena such as power swings and current transformer saturation [47]. Furthermore, it is insensitive to fault types, fault resistance, pre-fault load flow, and uncertain source parameters (e.g. local and remote end short circuit levels). As with impedance based methods, travelling wave based methods can be subdivided into single ended and two/multi ended methods.

2.4.1 Travelling wave theory

When a fault occurs on a line, voltage and current waves will be initiated and will emanate from the fault location towards the line ends, with subsequent waves being reflected back from the line ends (due to the encountered impedance change) towards the fault location. Further reflections continue until the waves fully attenuate (or a circuit breaker is opened). This phenomenon is depicted in Figure 2.5 [48]. In the figure, L and R denote the local end and remote end. F and M are the fault point and middle point of the line respectively. The initial waves arrive at the L and R

terminals at times T_1 and T_2. As a change of impedance is encountered at the line terminals, waves are reflected from both ends back towards the fault point. The relative timing of the second detected wave at the local end depends on the fault position. Figure 2.5 shows the situation of fault point F is between the M point and remote end. The second wave arriving at the local end is a reflection from the remote end and is represented using a dashed line in the figure. In another case when the fault point F is between the local end and M point, the second detected wave at the local end will be a reflection from the fault point, which is represented using a solid line on the diagram.

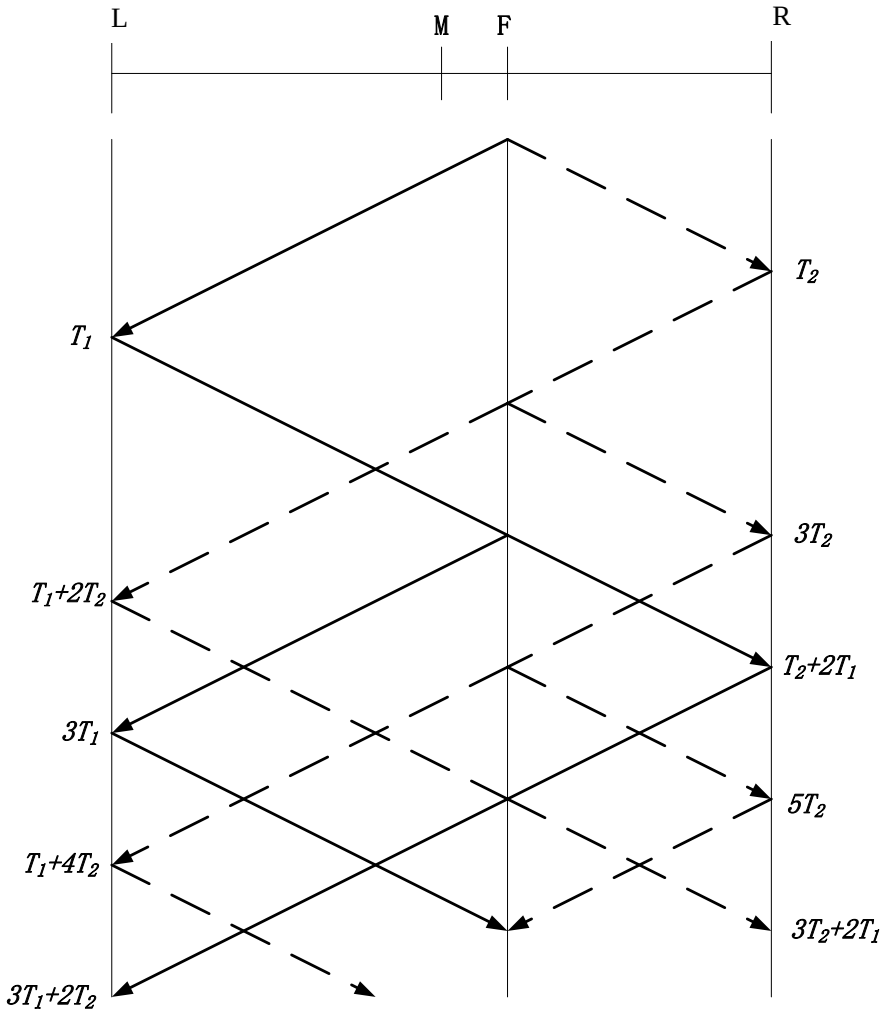

Figure 2.5. Travelling wave propagation in a transmission line in response to a fault

Along the transmission line, the voltage and current at any point *x*, as shown in Figure 2.6, can be expressed as shown in equations (2.23) and (2.24).

$$\frac{\partial v}{\partial x} = -\left(R + L\frac{\partial}{\partial t}\right) i \tag{2.23}$$

$$\frac{\partial i}{\partial x} = -\left(G + C\frac{\partial}{\partial t}\right) v \tag{2.24}$$

Where *L* and *C* are the inductance and capacitance of the line per unit length, and *R* and *G* are resistance and admittance per unit length.

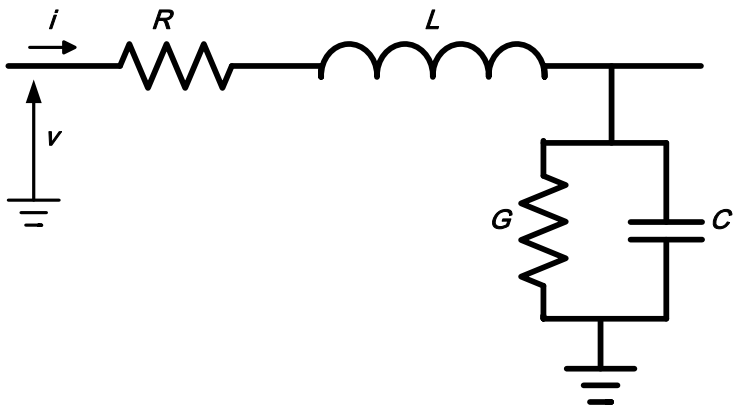

Figure 2.6. Voltage and current at point *x*

If a lossless transmission line is considered, then *R* and *G* can be assumed to be equal to 0, which is suitable for description of the travelling wave theory. According to D'Alembert principle, the voltage and current at time t and at point x can be solved as shown below:

$$v(x,t) = v_f(x - ct) + v_r(x + ct) \tag{2.25}$$

$$i(x,t) = \frac{v_f(x - ct)}{Z_0} - \frac{v_r(x + ct)}{Z_0} \tag{2.26}$$

In the above equations, Z_0 is the characteristic impedance of the transmission line, which is $Z_0 = \sqrt{\frac{L}{C}}$; and v is the propagation velocity of wave along the line, which is $v = \sqrt{\frac{1}{LC}}$.

In a three phase transmission line, the propagation waves of each of the three phases can be converted into three modes using a modal transformation [49-52]. In practical implementations, the target mode chosen for detection needs to satisfy the requirements of small attenuation and good stability.

2.4.2 Classification of travelling wave techniques

The first implementations of travelling wave fault location were realised during the 1950s. Basically, the travelling wave based fault location techniques [53-57] can be classified into five types, which have been denoted as Type A, Type B, Type C, Type D and Type E by other researchers [1, 2].

When a fault occurs on the line, the local end **L** may receive the wave initiated from the fault point and a subsequent wave reflected from the remote end and back along the line. From Figure 2.5, the first arriving wave at the local end is the initial wave from the fault point at time T_1. Generally, Type A technique is single end mode, which is based on measuring the time difference between the first arrived wave which is initiated by the fault, and second arrived wave at local end. It should be noted that the second arrived wave could be reflected either from the fault point or from the remote end. The discrimination of waves that have been reflected from the fault point or from the remote end is obviously critical in this type technique.

Type B fault location techniques utilise the waves received at both ends. The initial wave that propagates from the fault point is the sole requirement for the measurement equipment which is installed at each line end. Such schemes require communications facilities. The fault location is identified by the times of the arrivals of the first travelling waves both ends of the circuit and the signal propagation time through the communication facilities which may be measured in normal system operating conditions.

Type D fault location technique utilises the waves measured at both ends. As with Type B, only the initial waves that propagate from the fault point are required at each end. A Global Position System (GPS) time synchronisation method is used in this type of fault locator. The distance can be easily calculated by the waves arriving time difference between both ends.

Unlike Type A, B and D, Type C and Type E analyse travelling waves which are initiated by the fault sending "to" the line ends. Type C fault location technique relies on the use of pulse generators, which are used to inject a pulse along the line and analyse the reflected pulses from the fault point. The distance can be calculated by measurement of the time gap between sent and subsequently received pulses. Type E fault location techniques use analysis of auto-reclosing events on the system. The principle is similar to that adopted by Type C. This technique utilises the transient generated by reclosing the circuit breaker rather than using an externally-generated pulse as is the case with Type C.

Certain factors, such as fault inception angle, the uncertain and complex bus connections, uncertain transmission line surge impedance, external system interference, and extremities of fault position (e.g. very close to line ends), may introduce difficulties to the process of capturing and analysing the travelling waves/pulses. In recent years, the wavelet transform, which is capable of time and frequency domain analyses has been widely used to underpin travelling wave based fault location techniques [58-62]. Based on the wavelet transform, the magnitude of travelling wave reflected from fault point, remote bus, adjacent bus and unexpected noise reaches maximum in different scales. Accordingly, the target waves (i.e. initial wave from fault and reflected wave from fault, local end and remote end) can be detected and accurately locate the fault.

2.5 Conclusion

This chapter has presented a number of fault location techniques, considering single ended, two ended method. Both impedance-based techniques and travelling wave techniques have been reviewed. The features of reviewed fault location techniques are briefly summarised as in Table 2.2.

Impedance methods based on measurement and analysis of fundamental frequency phasors are relatively simple and economic to implement and are widely used in transmission and distribution systems. As only the fundamental frequency phasor is required, there is no pressing requirement for a very high data sampling rate. However, such methods are susceptible to variable fault resistance, pre-fault loading angle and both ends source impedance. Several proposed methods have attempted to

reduce the impact of such effects, and notable techniques reviewed in this chapter include the Takagi Method [7], the Modified Takagi method [3] and the network impedance method [6].

Methods	Advantages	Disadvantages
Single end impedance based method	Economical and easy to implement	May suffer from fault resistance, fault distance and uncertain remote end short circuit level
Two ended impedance based method	Good accuracy	Relatively expensive to implement; Additional devices may be required
Traveling wave method	Great accuracy	Expensive and difficult to implement; additional devices may be required

Table 2.2. Summary of conventional fault location methods

The Takagi method provides good accuracy by reducing the effects of fault resistance and pre-fault load flow. A fundamental aspect of the Takagi method is that it compensates for potential errors through the use of pre-fault and during fault current. One of the major shortcomings with the method is that inaccuracies may arise due to the fact that there is an assumption that the angle of current distribution factor (γ) is equal to 0, when in reality this may not be the case.

The actual fault position may also impact negatively on the Takagi method. There are certain positions on the transmission line where the angle of current distribution factor reaches a minimum, which can be seen as an "equivalent point". When the fault position moves away from this point, the angle γ increases. As a result, the estimated fault location error increases. Different values of *SCL1* and *SCL2* can be "seen" buy the Takagi method as additions to the line length. The "equivalent point" varies due to different value of *SCL1* and *SCL2*, which influences the estimated fault location accuracy. All of these shortcomings are addressed by the methods researched and developed through the research presented in this dissertation.

Travelling wave methods possess (theoretically) excellent levels of accuracy compared with impedance based methods. However, this method is expensive to implement [1]. High data sampling frequency and, in some cases, external signal generation and synchronising devices are required. Furthermore, there are implementation challenges associated with these methods, such as waveform detection, discrimination between initial and reflected waves, identification of faults very close to line ends and difficulties associated with data synchronisation and time tagging. This remains an active area of research; it is proposed that the techniques proposed later in this dissertation may provide accurate performance without the need for expensive implementations that are typical of travelling wave based methods.

2.6 References

[1] M. M. Saha and E.Rosolowski, *Fault Locaiton On Power Network*. Wrocloaw: Springer, 2011.

[2] G. Yaozhong, *New techniques for protective relaying and fault location*. Xi'an China: Xi'an Jiaotong University Publisher, 2007.

[3] K. Zimmerman and D. Costello, "Impedance-Based Fault Location Experience," in *Rural Electric Power Conference, 2006 IEEE*, 2006, pp. 1-16.

[4] M. M. I. Hashim, *et al.*, "Impedance-based fault location techniques for transmission lines," in *TENCON 2009 - 2009 IEEE Region 10 Conference*, 2009, pp. 1-6.

[5] E. O.Schweitzer, "A Review of Impedance-Based Fault Locating Experience," presented at the Proceedings of the 15th Annual Western Protective Relay Conference, Spokane WA, 1988.

[6] L. Eriksson, *et al.*, "An Accurate Fault Locator With Compensation For Apparent Reactance In The Fault Resistance Resulting From Remore-End Infeed," *Power Apparatus and Systems, IEEE Transactions on*, vol. PAS-104, pp. 423-436, 1985.

[7] T. Takagi, *et al.*, "Development of a New Type Fault Locator Using the One-Terminal Voltage and Current Data," *Power Apparatus and Systems, IEEE Transactions on*, vol. PAS-101, pp. 2892-2898, 1982.

[8] C. E. de Morais Pereira and L. C. Zanetta, Jr., "Fault location in transmission lines using one-terminal postfault voltage data," *Power Delivery, IEEE Transactions on*, vol. 19, pp. 570-575, 2004.

[9] M. B. Djuric, *et al.*, "Distance protection and fault location utilizing only phase current phasors," *Power Delivery, IEEE Transactions on*, vol. 13, pp. 1020-1026, 1998.

[10] B. Fardanesh, *et al.*, "Multifunctional synchronized measurement network [power systems]," *Computer Applications in Power, IEEE*, vol. 11, pp. 26-30, 1998.

[11] M. Kezunović, *et al.*, "An accurate fault location algorithm using synchronized sampling," *Electric Power Systems Research*, vol. 29, pp. 161-169, 1994.

[12] M. Kezunovic and B. Perunicic, "Automated transmission line fault analysis using synchronized sampling at two ends," *Power Systems, IEEE Transactions on*, vol. 11, pp. 441-447, 1996.

[13] K. E. Martin, *et al.*, "IEEE Standard for Synchrophasors for Power Systems," *Power Delivery, IEEE Transactions on*, vol. 13, pp. 73-77, 1998.

[14] A. G. Phadke, *et al.*, "Synchronized sampling and phasor measurements for relaying and control," *Power Delivery, IEEE Transactions on*, vol. 9, pp. 442-452, 1994.

[15] D. A. Tziouvaras, *et al.*, "New multi-ended fault location design for two- or three-terminal lines," in *Developments in Power System Protection, 2001, Seventh International Conference on (IEE)*, 2001, pp. 395-398.

[16] Z. Q. Bo, *et al.*, "Application of GPS based fault location scheme for distribution system," in *Power System Technology, 1998. Proceedings. POWERCON '98. 1998 International Conference on*, 1998, pp. 53-57 vol.1.

[17] K. E. Martin, "Precise timing in electric power systems," in *Frequency*

Control Symposium, 1993. 47th., Proceedings of the 1993 IEEE International, 1993, pp. 15-22.

[18] R. K. Aggarwal, *et al.*, "A practical approach to accurate fault location on extra high voltage teed feeders," *Power Delivery, IEEE Transactions on,* vol. 8, pp. 874-883, 1993.

[19] V. Cook, "Fundamental aspects of fault location algorithms used in distance protection," *Generation, Transmission and Distribution, IEE Proceedings C,* vol. 133, pp. 359-368, 1986.

[20] A. L. Dalcastagne, *et al.*, "An Iterative Two-Terminal Fault-Location Method Based on Unsynchronized Phasors," *Power Delivery, IEEE Transactions on,* vol. 23, pp. 2318-2329, 2008.

[21] A. A. Girgis, *et al.*, "A new fault location technique for two- and three-terminal lines," *Power Delivery, IEEE Transactions on,* vol. 7, pp. 98-107, 1992.

[22] J. Izykowski, *et al.*, "Accurate location of faults on power transmission lines with use of two-end unsynchronized measurements," *Power Delivery, IEEE Transactions on,* vol. 21, pp. 627-633, 2006.

[23] Y. Liao, "Unsynchronized Fault Location Based on Distributed Parameter Line Model," *Electric Power Components and Systems,* vol. 35, pp. 1061-1077, 2007/06/27 2007.

[24] Y. Liao and S. Elangovan, "Unsynchronised two-terminal transmission-line fault-location without using line parameters," *Generation, Transmission and Distribution, IEE Proceedings-,* vol. 153, pp. 639-643, 2006.

[25] D. Novosel, *et al.*, "Unsynchronized two-terminal fault location estimation,"

Power Delivery, IEEE Transactions on, vol. 11, pp. 130-138, 1996.

[26] M. S. Sachdev and R. Agarwal, "A technique for estimating transmission line fault locations from digital impedance relay measurements," *Power Delivery, IEEE Transactions on,* vol. 3, pp. 121-129, 1988.

[27] M. M. Saha, *et al.*, "A two-end method of fault location immune to saturation of current transformers," in *Developments in Power System Protection, 2004. Eighth IEE International Conference on,* 2004, pp. 172-175 Vol.1.

[28] M. M. Saha, *et al.*, "A method of fault location based on measurements from impedance relays at the line ends," in *Developments in Power System Protection, 2004. Eighth IEE International Conference on*, 2004, pp. 176-179 Vol.1.

[29] E. G. Silveira and C. Pereira, "Transmission Line Fault Location Using Two-Terminal Data Without Time Synchronization," *Power Systems, IEEE Transactions on,* vol. 22, pp. 498-499, 2007.

[30] I. Zamora, *et al.*, "Fault location on two-terminal transmission lines based on voltages," *Generation, Transmission and Distribution, IEE Proceedings-,* vol. 143, pp. 1-6, 1996.

[31] A. T. Johns and S. Jamali, "Accurate fault location technique for power transmission lines," *Generation, Transmission and Distribution, IEE Proceedings C,* vol. 137, pp. 395-402, 1990.

[32] Q. Zhang, *et al.*, "Transmission line fault location for phase-to-earth fault using one-terminal data," *Generation, Transmission and Distribution, IEE Proceedings-*, vol. 146, pp. 121-124, 1999.

[33] Q. Zhang, *et al.*, "Fault location of two-parallel transmission line for nonearth

fault using one-terminal data," *Power Delivery, IEEE Transactions on,* vol. 14, pp. 863-867, 1999.

[34] J. Izykowski, *et al.*, "Locating faults in parallel transmission lines under availability of complete measurements at one end," *Generation, Transmission and Distribution, IEE Proceedings-*, vol. 151, pp. 268-273, 2004.

[35] Saha MM, *et al.*, "New fault location algorithm for parallel lines," presented at the Proc of 7th Int Conf on Developments in Power System Protection DPSP, IEE CP476 pp 407, 2001.

[36] Izykowski J, *et al.*, "Accurate location of faults in parallel transmission lines under availability of measurements from one circuit only," presented at the Proc of Power Systems Computation Conference Sevilla,, 2002.

[37] M. Fulczyk, *et al.*, "Two-end unsynchronized fault location algorithm for double-circuit series compensated lines," in *Power and Energy Society General Meeting - Conversion and Delivery of Electrical Energy in the 21st Century, 2008 IEEE*, 2008, pp. 1-9.

[38] J. Izykowski, *et al.*, "Fault Location on Double-Circuit Series-Compensated Lines Using Two-End Unsynchronized Measurements," *Power Delivery, IEEE Transactions on,* vol. 26, pp. 2072-2080, 2011.

[39] C. Ching-Shan, *et al.*, "A new adaptive PMU based protection scheme for transposed/untransposed parallel transmission lines," *Power Delivery, IEEE Transactions on,* vol. 17, pp. 395-404, 2002.

[40] S. Guobing, *et al.*, "Parallel transmission lines fault location algorithm based on differential component net," *Power Delivery, IEEE Transactions on,* vol. 20, pp. 2396-2406, 2005.

[41] A. J. Mazón, *et al.*, "New method of fault location on double-circuit two-terminal transmission lines," *Electric Power Systems Research*, vol. 35, pp. 213-219, 1995.

[42] Z. G, "Application guide on protection of complex transmission network configuration," presented at the CIGRE SC34-WG04, Paris, 1990.

[43] M. M. Saha, *et al.*, "A new accurate fault locating algorithm for series compensated lines," *Power Delivery, IEEE Transactions on*, vol. 14, pp. 789-797, 1999.

[44] R. Dutra, *et al.*, "Fault location on parallel transmission lines with series compensation," in *Transmission and Distribution Conference and Exposition: Latin America, 2004 IEEE/PES*, 2004, pp. 591-597.

[45] J. Sadeh, *et al.*, "Accurate fault location algorithm for series compensated transmission lines," in *Power Engineering Society Winter Meeting, 2000. IEEE*, 2000, pp. 2527-2532 vol.4.

[46] Saha MM, *et al.*, "Accurate location of faults on seriescompensated lines with use of two-end unsynchronised measurements," presented at the Proc of the 9th Int Conf on Developments in Power System Protection-DPSP, IEE CP536, 2008.

[47] S. L. Zimath, *et al.*, "Traveling wave-based fault location experiences," in *Protective Relay Engineers, 2010 63rd Annual Conference for*, 2010, pp. 1-7.

[48] L. Bewley, *Travelling Wave on Transmission System*. New York: John Wiley & Son, Inc, 1963.

[49] L. M. Wedepohl, "Application of matrix methods to the solution of travelling-wave phenomena in polyphase systems," *Electrical Engineers,*

Proceedings of the Institution of, vol. 110, pp. 2200-2212, 1963.

[50] H. W. Dommel, "Digital Computer Solution of Electromagnetic Transients in Single-and Multiphase Networks," *Power Apparatus and Systems, IEEE Transactions on,* vol. PAS-88, pp. 388-399, 1969.

[51] J. A. Brandao Faria and J. Hildemaro Briceno, "On the modal analysis of asymmetrical three-phase transmission lines using standard transformation matrices," *Power Delivery, IEEE Transactions on,* vol. 12, pp. 1760-1765, 1997.

[52] R. W. Long and D. Gelopulos, "Component Transformations - Eigenvalue Analysis Succinctly Defines Their Relationships," *Power Apparatus and Systems, IEEE Transactions on,* vol. PAS-101, pp. 4055-4063, 1982.

[53] P. F. Gale, *et al.*, "Fault location based on travelling waves," in *Developments in Power System Protection, 1993., Fifth International Conference on*, 1993, pp. 54-59.

[54] P. F. Gale, *et al.*, "Practical experience with travelling wave fault locators on Scottish Power's 275 & 400 kV transmission system," in *Developments in Power System Protection, Sixth International Conference on (Conf. Publ. No. 434)*, 1997, pp. 192-196.

[55] L. Yi-Feng and C. Ping, "The Principle of the Modern Travelling Wave Based on Fault Location and the Applications to Actual Fault Analysis," in *Power and Energy Engineering Conference, 2009. APPEEC 2009. Asia-Pacific*, 2009, pp. 1-4.

[56] P. A. Crossley and P. G. McLaren, "Distance Protection Based on Travelling Waves," *Power Apparatus and Systems, IEEE Transactions on,* vol. PAS-102,

pp. 2971-2983, 1983.

[57] L. J. Lewis, "Traveling Wave Relations Applicable to Power-System Fault Locators," *American Institute of Electrical Engineers, Transactions of the,* vol. 70, pp. 1671-1680, 1951.

[58] K. Chul Hwan and A. Raj, "Wavelet transforms in power systems. I. General introduction to the wavelet transforms," *Power Engineering Journal,* vol. 14, pp. 81-87, 2000.

[59] K. Chul Hwan and R. Aggarwal, "Wavelet transforms in power systems. II. Examples of application to actual power system transients," *Power Engineering Journal,* vol. 15, pp. 193-202, 2001.

[60] P. Makming, *et al.*, "Fault diagnosis in transmission lines using wavelet transform analysis," in *Transmission and Distribution Conference and Exhibition 2002: Asia Pacific. IEEE/PES*, 2002, pp. 2246-2250 vol.3.

[61] Z. Q. Bo, *et al.*, "Positional protection of transmission line using fault generated high frequency transient signals," *Power Delivery, IEEE Transactions on,* vol. 15, pp. 888-894, 2000.

[62] Y. Xia, *et al.*, "A new technique using wavelet analysis for fault location," in *Developments in Power System Protection, Sixth International Conference on (Conf. Publ. No. 434)*, 1997, pp. 231-234.

Chapter 3. Comparative performance analysis of impedance based techniques

3.1 Introduction

Performance analysis of the fault location methods included in this chapter focuses primarily on the accuracy aspect of the techniques. The factors which mainly influence the accuracy of impedance based fault location techniques considered here are:

- Distance to fault
- Remote end short circuit level
- Fault resistance
- Pre-fault load angle

An EMTP/ATP simulation model of a 400kV, 100km transmission line (supplied from both ends) is applied to assess the performance of fault location techniques. In the evaluations of those possible negative factors, the transmission line is assumed as homogeneous system and the errors of the simulated data (in terms of measurement error, sensor/sampling error) are not included. In order to improve the reality of the simulation model, the effect of shunt capacitance has been incorporated.

In this chapter, the comparative evaluation and performance analysis of typical impedance fault location techniques introduced in chapter 2 will be carried out. The accuracy of each method is denoted by fault location error in this chapter which is defined as:

$$fault\ location\ Error = \frac{(estimated\ distance - actual\ distance)}{line\ length} \times 100\% \quad (3.1)$$

Some published papers have shown the performance of these existing techniques. Paper [1] shows the implementation of simple reactance method and Takagi method. The example represents a single phase to earth fault at middle point of the line (50% of total line length). The fault resistance is set to 8Ω and the pre-fault loading angle is set to 15^{o}. The fault location estimation errors of simple reactance method and Takagi method as presented in [1] are 1.38% and 0% respectively. Based on the same fault conditions, in the implementations of simple reactance and Takagi methods presented in this chapter, the fault location estimation errors are found to be 1.21% and 0.1% respectively. The accuracies of the implementations in this chapter and paper [1] are, therefore, sufficiently similar. The existing differences may result from the unknown system conditions such as transmission line length, line voltage level and the fundamental frequency phasor extraction accuracy (all of which are not specified in [1] and are likely to be different from those assumed in this thesis).

Paper [2] introduces the network impedance method and shows the result of one example based on 130kV, 76km transmission line. A single phase to earth fault has been detected and located in 67.6km from local end (89% of the line length), while

the actual fault position was set in 67km (88.1% of the line length). The estimated fault location error is 0.9%. In the implementation of the network impedance method in this chapter, the error is 0.7% based on the same fault type and similar transmission line. The estimated errors of both implementations, the one used in this chapter and the one in [2], are therefore, very similar. However, because the system conditions may be different, such as transmission line parameters, local side short circuit level and the fundamental frequency phasor extraction accuracy (all of which are not specified in [2]), a small difference in fault location accuracy between the two implementations exists.

Paper [3] gives an example of two ended method which is based on 345kV, 257km transmission line. A single phase to earth fault was detected and located at 145.92km from local end (56.77% of line length), while the actual fault position was 145.12km (56.46% of line length). The estimated fault location error is 0.31%. In the implementation of the two ended method in this chapter, the error is 0.14% when actual fault position is 56.5% based on the same fault type and similar transmission line. The estimated errors of both implementations (in this chapter and in [3]) are, therefore, similar. Again, due to uncertainty of some system parameters and operation conditions (which are not specified in [3]) the difference in estimated fault location error between the two implementations exists.

Following the above verification of software implementations of the known impedance fault location methods (developed as part of this thesis), it is further assumed that these implementations are sufficiently accurate and can be used in

comparative analysis presented in this chapter.

3.2 Transmission line model

A 400kV, 100km transmission line model (refer to Figure 3.1) is used to evaluate the performances of selected algorithms. Short circuit level *SCL1* is set to 5GVA**.** The zero sequence line impedance Z_{L0}=(0.10+*j*0.76)Ω/km and the positive sequence line impedance Z_{L1}=(0.02+*j*0.25)Ω/km. The zero sequence shunt capacitance Y_{L0}=(0+*j*2.5e^{-6})Ω/km and positive sequence shunt capacitance Y_{L1}=(0+*j*4.7e^{-6})Ω/km. The simulated waveforms are re-sampled with a frequency of 2000 Hz to represent typical sampling rate of existing numerical relays. The range of fault distances considered in the simulation is from 0% to 100%.

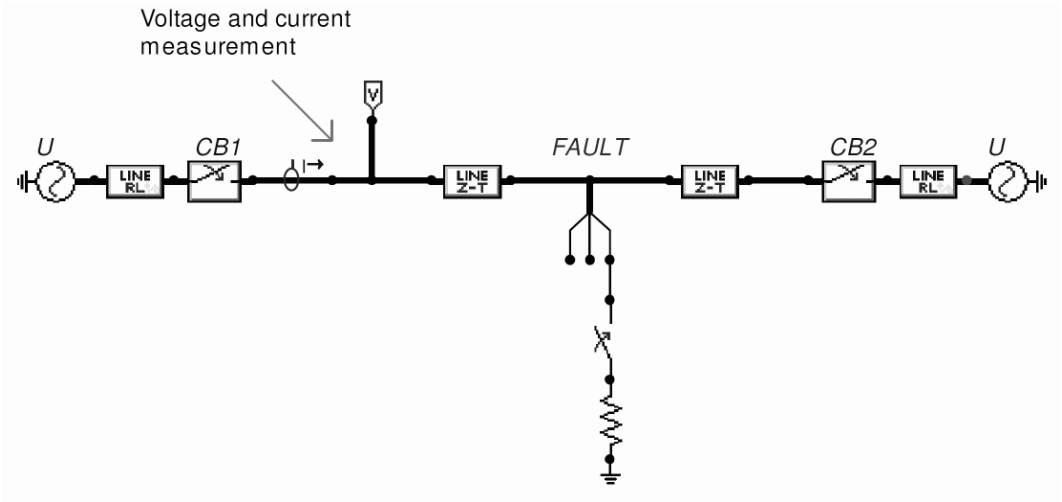

Figure 3.1. EMTP transmission line model

As the impedance based fault location techniques are to be evaluated, the fundamental frequency phasors of phase voltages and currents are required. The

weighted Least Square Method [4] is applied to extract the phasors. The details of this extraction algorithm are introduced in Appendix A2.

3.3 Comparison of selected fault location algorithms

Chapter 2 introduced a number of impedance based fault location techniques that have been developed and demonstrated by other researchers, including:

- Simple reactance method
- Takagi method
- Network impedance method
- Two ended method (using synchronised data)

In the following sections, the performance comparison of these methods will be presented.

3.3.1 Effects of fault resistance

Recalling the fault loop equation from earlier (2.17), the simple reactance method aims to reduce the effect of $R_f I_f$ by only using the imaginary elelment of the equation [3, 5]. According to equations (2.20 – 2.22), the fault current I_f can be represented as:

$$I_f = \frac{\Delta I_s}{|C_m| e^{j\gamma}} \tag{3.2}$$

$$\Delta I_s = I_s - I_{pre} \tag{3.3}$$

The influencing element in the simple reactance method is the imaginary component of $\frac{\Delta I_s R_f}{|C_m|e^{j\gamma}}$. Consequently, fault resistance influences the estimation error associated with the simple reactance method, especially at high values of fault resistance. The Takagi method [6] reduces the effect of fault resistance by applying the complex conjugate value of ΔI_s. In theory, the network impedance method [2] is immune to changing values of $R_{f,}$; however the value of *SCL2* is required as a known input parameter to such techniques, and this is difficult to obtain in practice. The distance to fault is obtained by solving the network impedance equation. The fault resistance can be estimated, along with the fault position, by solving the equation. Two ended methods [5, 7], on the other hand, are not affected by fault resistance. The effect of R_f in this case can be fully eliminated.

In order to evaluate the effect of fault resistance in the above techniques, a model of a transmission line has been simulated in EMTP/ATP with *SCL2* set to 30GVA respectively and the load angle fixed at a value of 10^o. The evaluations of various levels of *SCL2* and pre-fault loading angle, will be carried out in the following sections.

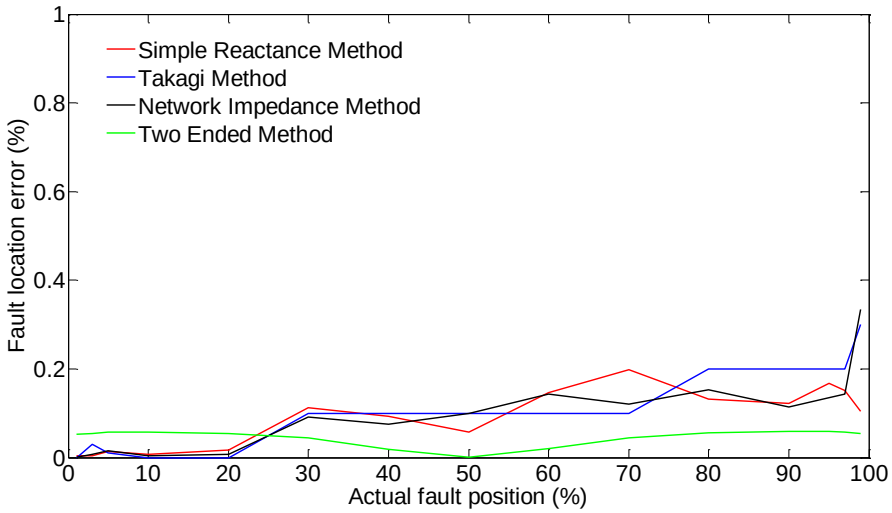

Figure 3.2. Effect of fault resistance R_f = 0.1Ω

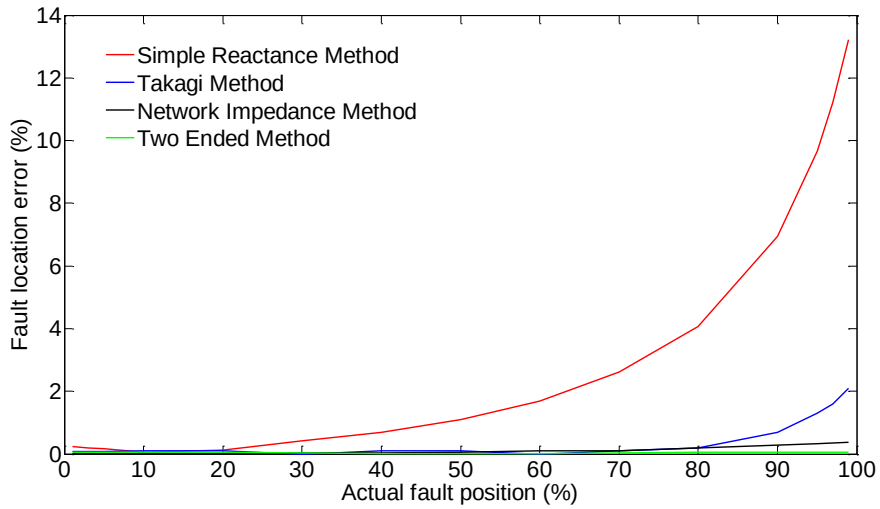

Figure 3.3. Effect of fault resistance R_f = 5Ω

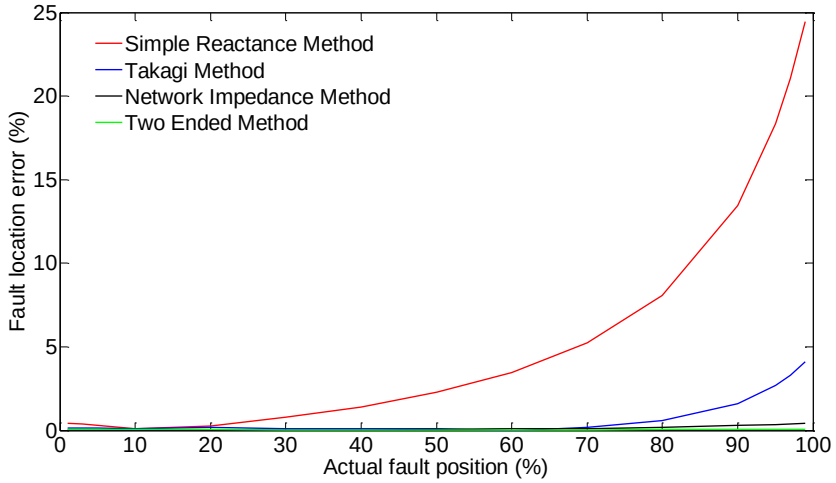

Figure 3.4. Effect of fault resistance R_f = 10Ω

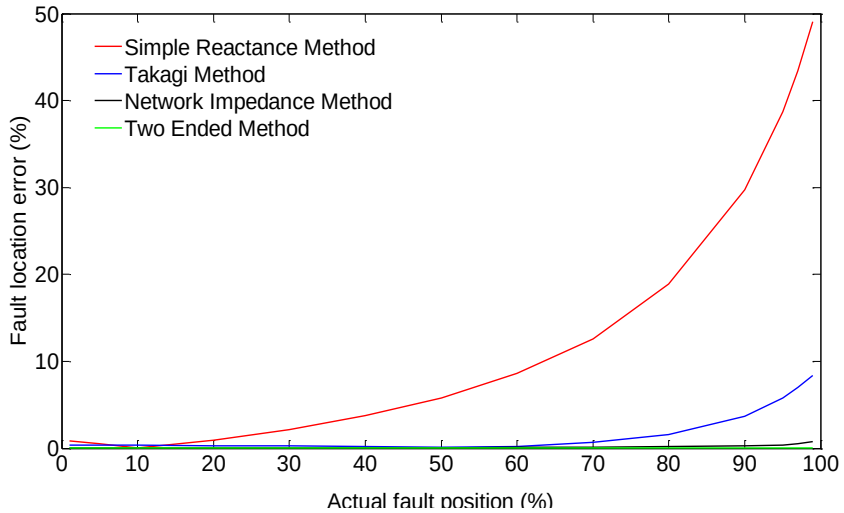

Figure 3.5. Effect of fault resistance R_f = 25Ω

	R_f= 0.1Ω	R_f= 5Ω	R_f= 10Ω	R_f= 25Ω
Simple Reactance method	0.19%	13.2%	24.44%	49.01%
Takagi method	0.30%	2.10%	4.10%	8.40%
Network Impedance method	0.33%	0.38%	0.44%	0.76%
Two ended method	0.06%	0.06%	0.06%	0.07%

Table 3.1 Comparison of maximum estimation error in fault resistance evaluation

Figure 3.2 to Figure 3.5 shows the performances of selected fault location algorithms for various values of fault resistance. In the scenario where R_f= 0.1Ω, all methods are very accurate. The maximum error across all techniques is lower than 0.33%. The error of the simple reactance method increases significantly with increasing fault resistance. In the scenario with R_f= 25Ω, the error reaches 49.01%. As expected, the Takagi method improves the accuracy by reducing the effect of fault resistance but the error remains still significant. In the scenario with R_f= 25Ω, the maximum error reaches 8.4%.

The results confirm that the network impedance method is not influenced by fault resistance. From Table 3.1, the network impedance method has similar accuracy to the Takagi method for R_f=0.1Ω. However, for higher resistances, the network impedance method has a clear advantage over the Takagi method as very good accuracy is maintained for all resistance values included in the test.

Likewise, the two ended method obtains excellent accuracy under all scenarios regardless of fault resistance. The maximum error is lower than 0.07% in all scenarios and is relatively better than all single ended methods.

3.3.2 Effect of remote end short circuit level

Theoretically, both the simple reactance method and the Takagi method are influenced by changes in both end short circuit level. The local end short circuit level can be calculated/measured by using local end data [8, 9]. In this section, the local end short circuit level is set as known; the effect of remote end short circuit level will be evaluated. Recalling equation (2.22), the value remote source impedance (represented by *SCL2*) directly affects the current distribution factor C_m. As both the simple reactance method and the Takagi method utilise C_m, both methods will be influenced by changes in *SCL2*.

The network impedance method calculates the distance to fault by utilising the value of *SCL2*. Therefore, it does not suffer from the effects mentioned above. The two ended method solves the fault position by calculating voltage and current at the fault position using measurements from both ends. In this case, *SCL2* does not influence the calculation. In order to comparatively evaluate the performance of selected fault location algorithms, the fault resistance and load angle are maintained at constant values, set to 5Ω and 10^o respectively in the transmission line simulations carried out.

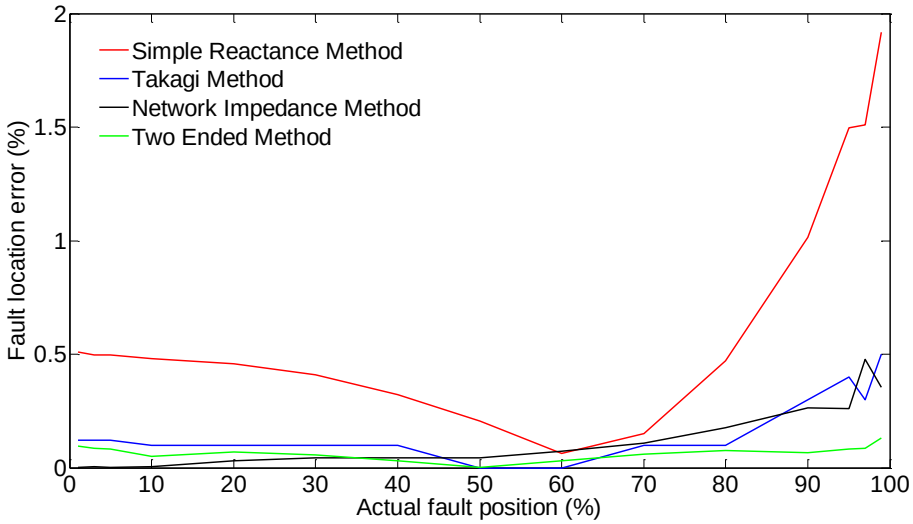

Figure 3.6. Effect of remote end short circuit level when *SCL2*=5GVA

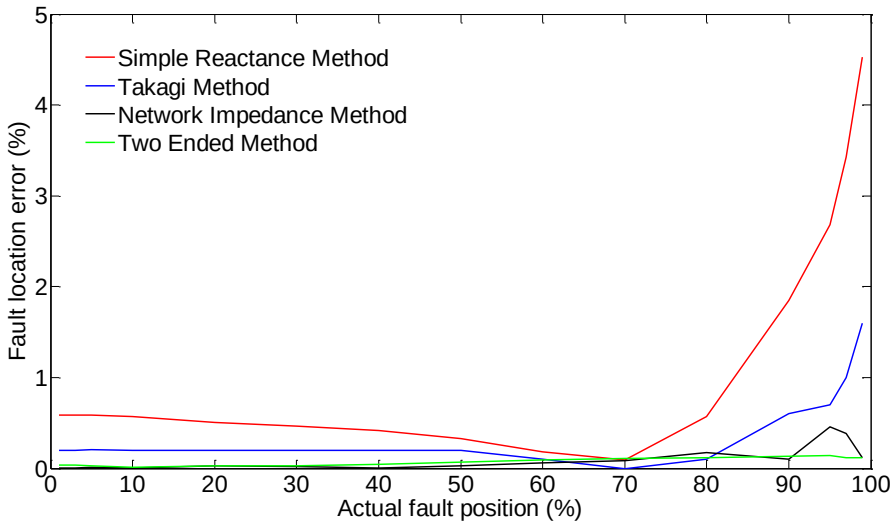

Figure 3.7. Effect of remote end short circuit level when *SCL2*=10GVA

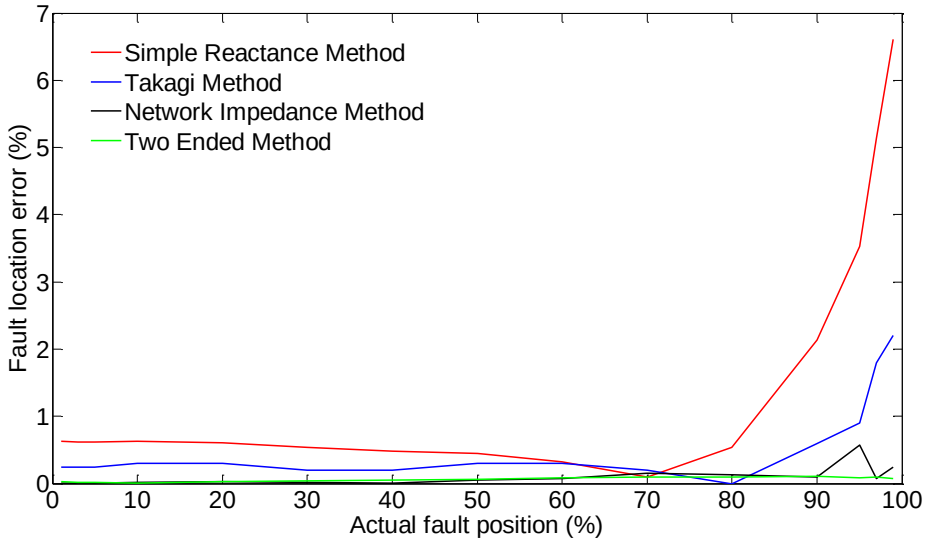

Figure 3.8. Effect of remote end short circuit level when *SCL2*=15GVA

	SCL2=5GVA	*SCL2*=10GVA	*SCL2*=15GVA
Simple Reactance method	1.92%	4.53%	6.61%
Takagi method	0.50%	1.60%	2.20%
Network Impedance method	0.48%	0.45%	0.58%
Two ended method	0.13%	0.14%	0.11%

Table 3.2. Maximum estimation error under different remote end short circuit level levels

Figure 3.6 to Figure 3.8 and Table 3.2 demonstrate the comparative performance of the different fault location algorithms. There are certain positions on the transmission line where the fault location error reaches minimum as the angle of current distribution factor reaches a minimum, which can be seen as an “equivalent point”.

From the figure, the "equivalent point" of both simple reactance method and Takagi method moves as the value of *SCL2* changes and maximum error occurs at furthest away point (99%) on the line. The maximum errors of both the simple reactance method and the Takagi method increase with *SCL2*. Results also prove that the estimation error of both the Network Impedance method and two ended method do not change as *SCL2*.

3.3.3 Effect of pre-fault loading angle

Recall the accuracy influencing element of the simple reactance method, $\frac{\Delta I_s R_f}{|C_m|e^{j\gamma}}$. Except R_f and C_m, the fault location accuracy is affected by the incremental current ΔI_s. ΔI_s is determined by the current during the fault and pre-fault current (3.3), and the pre-fault current depends on the pre-fault load angle. Thus, the accuracy of simple reactance method can be affected by the pre-fault load angle. Both the network impedance method and the two ended method obtain fault location by solving a set of equations. The pre-fault load angle does not have an impact on such equations.

In order to evaluate the effect of loading angle, both the remote end short circuit level and the fault resistance are kept constant and set to 30GVA and 5Ω respectively.

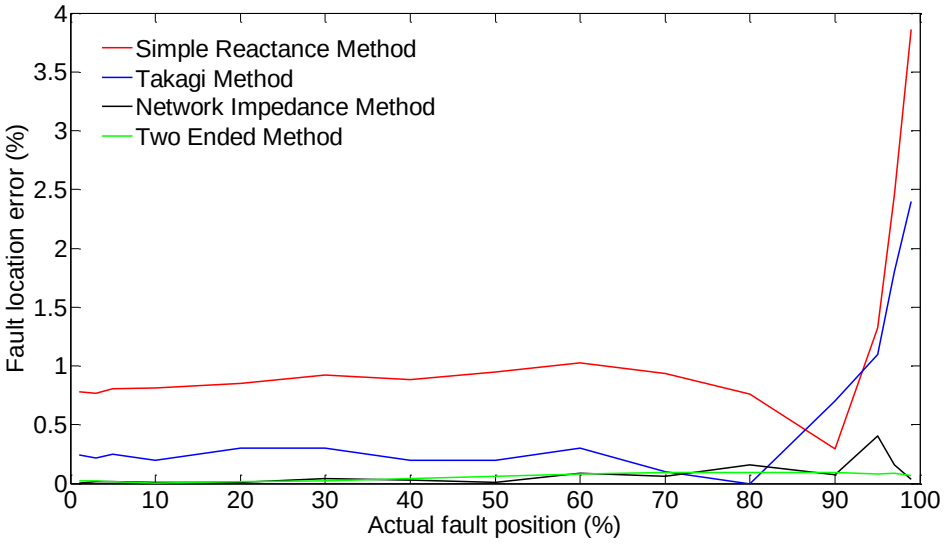

Figure 3.9. Effect of load angle with loading angle=1^{o}

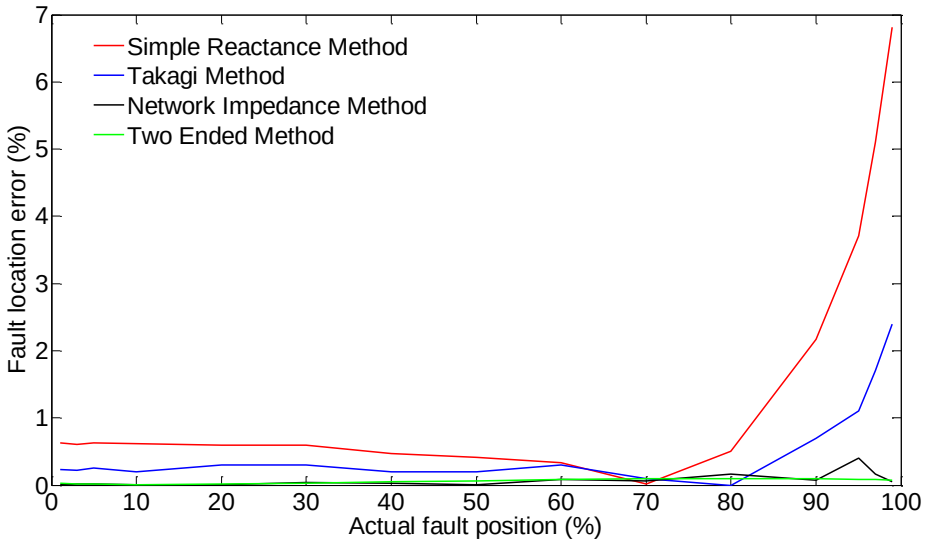

Figure 3.10. Effect of load angle with loading angle=3^{o}

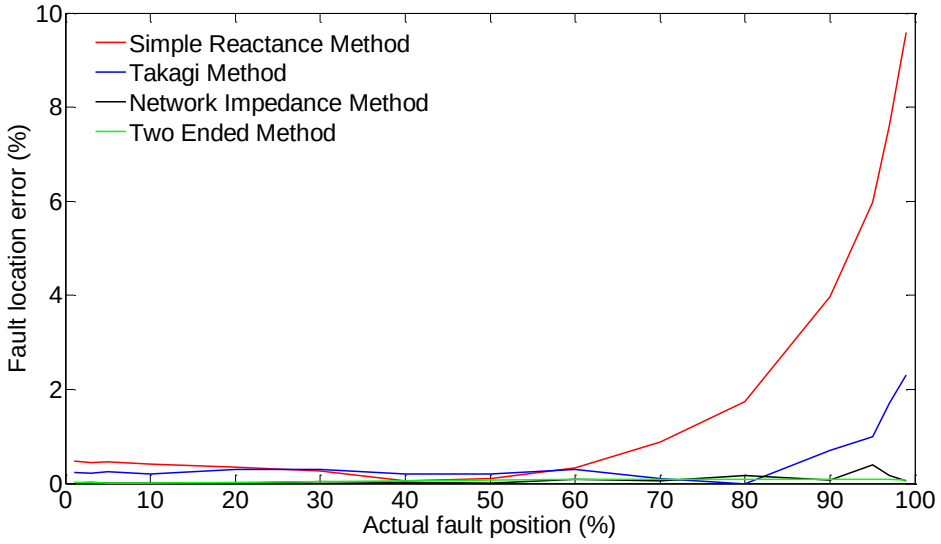

Figure 3.11. Effect of load angle with loading angle=5^{o}

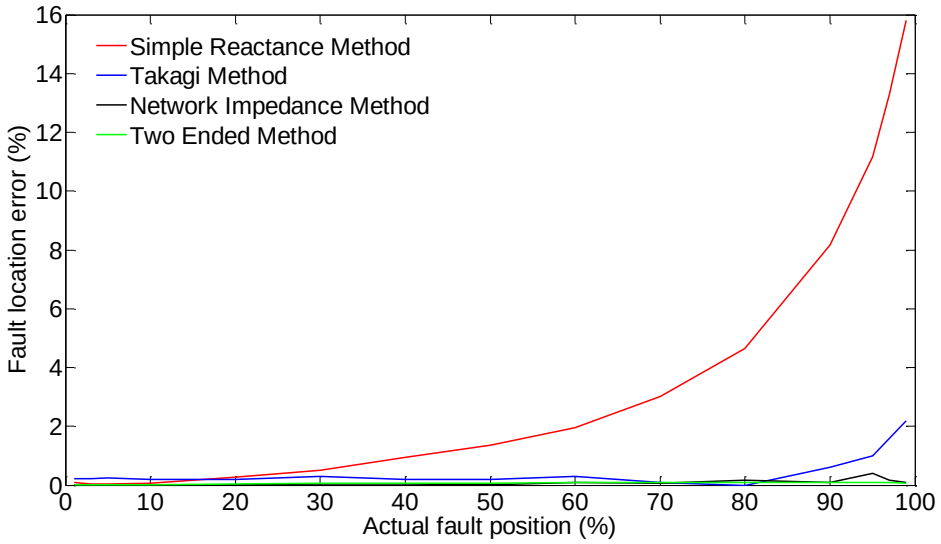

Figure 3.12. Effect of load angle with loading angle=10^{o}

Load angle	1	3	5	10
Simple Reactance method	3.86%	6.81%	9.58%	15.80%
Takagi method	2.40%	2.40%	2.39%	2.20%
Network Impedance method	0.41%	0.40%	0.40%	0.40%
Two ended method	0.10%	0.10%	0.09%	0.09%

Table 3.3. Maximum estimation error under different pre-fault loading conditions

Figure 3.9 to Figure 3.12 and Table 3.3 illustrate the performance of the alternative fault location algorithms under various load angle scenarios. It can be clearly seen that the accuracy of the simple reactance method suffers under increased pre-fault load angle. The maximum error reaches 15.8% when the load angle is 10 degrees. The other three techniques are immune to this factor, with the error levels remaining unchanged.

3.4 Conclusion

In this chapter, evaluation and comparative analysis of the Takagi method with three other phasor based methods, namely the simple reactance method, the network impedance method and the two ended method, have been presented.

The simple reactance method reduces the effect of fault resistance by using the imaginary part of calculated line impedance. Compared with the Takagi method, the simple reactance method has lower accuracy and it suffers from the effects of

varying remote end short circuit level and pre-fault load angle. The maximum error reaches 49.01% in the case where R_f=25Ω and n=99%. The simple reactance method is relatively simple to implement as only the during fault data is required.

Results illustrate that Takagi method has a comparatively good and consistent level of accuracy as it reduces the effect of fault resistance and pre-fault load angle compared with the simple reactance method. However, the fault location error increases with fault resistance. The maximum error reaches 8.4% when R_f increases to 25Ω. Both local and remote end short circuit level affects the fault current distribution factor C_m, the angle of which directly affects the fault location accuracy. The implementation cost of both Takagi method and simple reactance method is relatively low, as modern numerical protection relays used for distance protection already possess functionality to perform impedance calculation.

The network impedance improves the fault location accuracy significantly compared to the Takagi method by taking into account the known value of *SCL2*. The maximum error is only 0.76% for all evaluations. However, the value of *SCL2* is often uncertain and may vary with the changes in system configuration. It is also more expensive to implement compared to Takagi method and simple reactance method. A communication channel is required in cases where the instantaneous value of the remote end short circuit level is needed.

The two ended method provides the most accurate fault location which is less than 0.13% for all evaluations. It does not suffer from the effects of fault resistance, fault

distance, uncertain remote end short circuit level or pre-fault load angle. However, it is most expensive and may be difficult to implement, as communication and GPS technology may be required.

After comparative analysis of several typical impedance fault location methods, The Takagi method improves upon the accuracy of fault location of the simple reactance method, but with the similar requirements. Only local data is required, the numerical and computational complexity is moderate and it is relatively easy to implement on a modern numerical protection relay. Thus it is one of the most widely used fault location techniques in modern transmission/distribution system. Evaluation results prove that both the network impedance method and the two ended method can provide better accuracy than the Takagi method, especially in the cases of high fault resistance. However, for the network impedance method, the value of *SCL2* is required, which is not highly certain in power system. The two ended method is relatively expensive to implement as it requires extra devices such as communication channel and GPS facilities.

Due to these reasons, the novel impedance based fault location methods using local end data are developed and demonstrated as part of this PhD project. The target of these methods is to improve upon the existing impedance based single ended techniques in terms of accuracy, while maintaining low implementation cost and complexity (characteristic of impedance based techniques).

3.5 References

[1] E. O.Schweitzer, "A Review of Impedance-Based Fault LocatingExperience," presented at the Proceedings of the 15th Annual Western Protective Relay Conference, Spokane WA, 1988.

[2] L. Eriksson, *et al.*, "An Accurate Fault Locator With Compensation For Apparent Reactance In The Fault Resistance Resulting From Remore-End Infeed," *Power Apparatus and Systems, IEEE Transactions on,* vol. PAS-104, pp. 423-436, 1985.

[3] K. Zimmerman and D. Costello, "Impedance-Based Fault Location Experience," in *Rural Electric Power Conference, 2006 IEEE*, 2006, pp. 1-16.

[4] E. Rosołowski, *et al.*, "Adaptive measuring algorithm suppressing a decaying DC component for digital protective relays," *Electric Power Systems Research,* vol. 60, pp. 99-105, 2001.

[5] M. M. Saha and E.Rosolowski, *Fault Locaiton On Power Network*. Wrocloaw: Springer, 2011.

[6] T. Takagi, *et al.*, "Development of a New Type Fault Locator Using the One-Terminal Voltage and Current Data," *Power Apparatus and Systems, IEEE Transactions on,* vol. PAS-101, pp. 2892-2898, 1982.

[7] G. Yaozhong, *New techniques for protective relaying and fault location*. Xi'an China: Xi'an Jiaotong University Publisher, 2007.

[8] M. Sumner, *et al.*, "Impedance measurement for improved power quality-Part 1: the measurement technique," *Power Delivery, IEEE Transactions on,* vol.

19, pp. 1442-1448, 2004.

[9] K. Young-Jin, *et al.*, "A fault location algorithm using estimated local source impedance," in *Power Systems Conference and Exposition, 2009. PSCE '09. IEEE/PES*, 2009, pp. 1-5.

Chapter 4. Fault location through analysis of data from inter-pole states during circuit breaker operation

4.1 Introduction

As mentioned in Chapter 2, single ended impedance based fault location methods are relatively straightforward to implement in the field. A novel fault location method on this type is introduced in this chapter. While the implementation advantages of single-ended impedance based method are preserved by only requiring local end data, the accuracy has been greatly improved and the effects of the negative factors, in terms of R_f and *SCL2*, are significantly reduced.

To achieve improvements over existing techniques, the proposed technique utilises voltage and current data recorded during the various stages of circuit breaker operation until the final clearance of the fault is achieved. The fault clearing process of circuit breaker is separated into a number of individual states, termed interpole states [1, 2]. Recorded data is divided into appropriate intervals and analysed to

obtain individual current and voltage phasors during each state.

A fault location estimation system, based on modelling of these interpole states has been developed and showed improved accuracy. In the following sections of this chapter, a detailed description of the method based on circuit breaker interpole states is included, followed by the case study and systematic evaluation of the method's performance. Some challenges related to the implementation of the methods are also discussed.

4.2 Interpole states

4.2.1 Definitions

There are three possible circuit breaker opening sequences in transmission lines supplied from two ends: (a) local circuit breaker opens before remote end, (b) remote end circuit breaker opens before local end and, (c) two sides open simultaneously. The number of possible states depends on the opening sequence. For example, in sequence (a) 4 different states could arise, while in sequence (c) 7 different states are possible. All states can be modelled by using a superposition method, as described later in section 4.2.2. In this chapter, sequence (a) will be considered only. Other opening sequences result in analogous calculations.

During the opening operation of a three-phase circuit breaker, the individual phase currents are not interrupted simultaneously, as the current zero crossings of the

consecutive phases is displaced by 120°[1, 2]. Figure 4.1 presents this effect in an ideal system. In this case, the circuit breaker is set to initiate the opening operation at 100ms. The time interval between current zero crossings is 3.33ms in a 50Hz system.

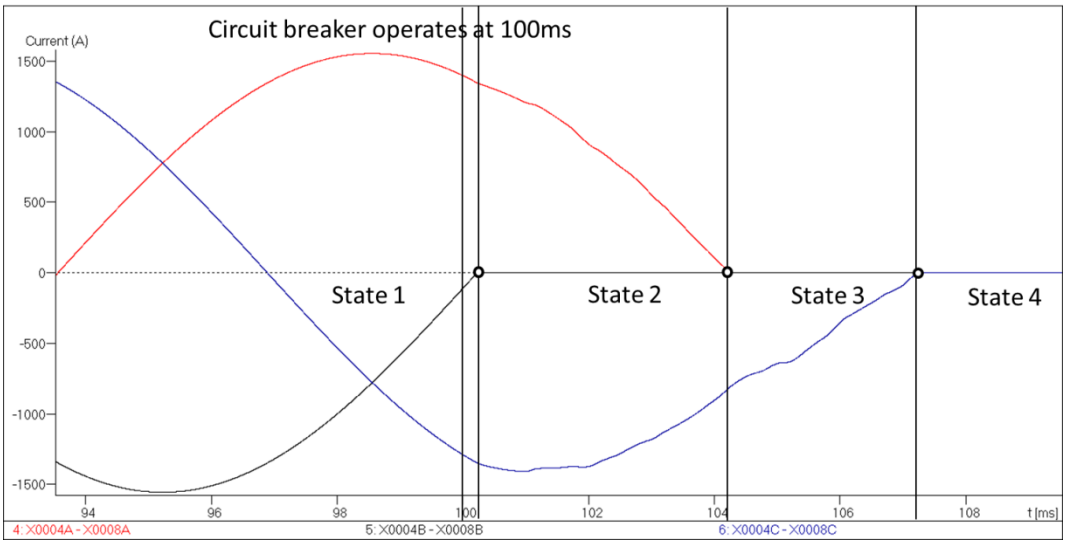

Figure 4.1.Circuit breaker operation (ideal theoretical case)

In reality, several factors, such as fault resistance, fault type and circuit breaker pole contact opening times, may impact on the duration of the interpole states. Figure 4.2 shows three phase current wave during the circuit breaker operation taken from EMTP/ATP simulation. A single phase to earth fault is simulated. The duration of state 2 and state 3 are 4.1ms and 1.1ms respectively.

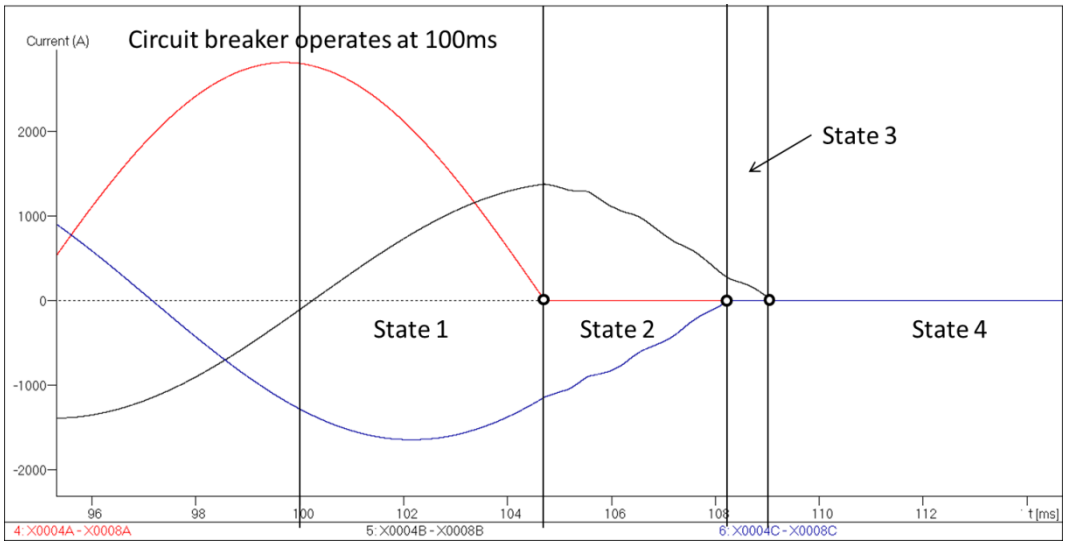

Figure 4.2 Circuit breaker operation (EMTP/ATP simulation)

According to the status of the individual circuit breaker poles, there are effectively four individual system states during the opening process, namely:

- state 1: All poles are closed (no contacts have separated);
- state 2: One pole is open, two poles are closed;
- state 3: Two poles are open, one pole is closed;
- state 4: All poles are open.

4.2.2 Modelling of interpole states

For the modelling of interpole states the superposition method has been applied. As the lumped R-L line model does not consider the effect of shunt capacitance, the accuracy of this model is not as high as distributed line model. However, for representing short length transmission lines, the effect of shunt capacitance can be easily neglected and such transmission lines can be modelled by lumped R-L models without significant loss of accuracy. In this thesis, two line models (lumped and

distributed) are used to represent 400kV, 100km transmission line interpole states. In fault location technique based on circuit breaker operation analysis (presented in this chapter), a lumped R-L type model has been considered, while in fault location technique based on auto reclose operation (presented in Chapter 5), a distributed line type model is considered.

The tripping sequence of three phases depends on pre-fault load flow, fault inception time, fault type and fault resistance. Considering the phase status, there are three possible contact opening sequences: F-H-H, H-F-H and H-H-F, where F and H denote faulty and healthy phase respectively.

Pre-fault data is required to facilitate the use of superposition. In this section, the F-H-H sequence is investigated. The details of H-F-H and H-H-F sequence calculations are introduced in Appendix B**.**

4.2.2.1 Modelling resistive fault on power lines using phase coordinates

In three phase power lines, the general short circuit fault resistance model **R**, as shown in Figure 4.3, can be represented using a 3×3 matrix [3-6] using phase coordinates.

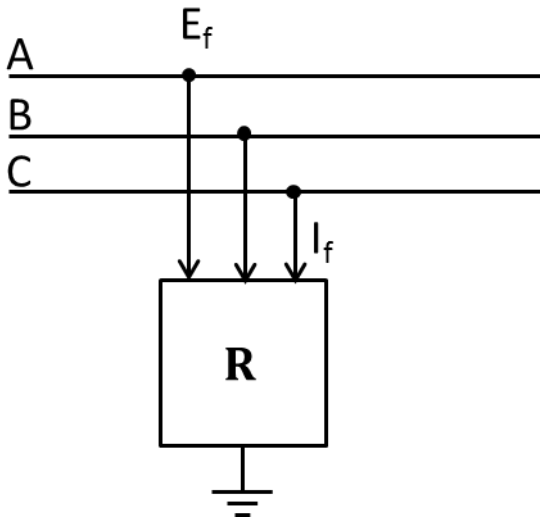

Figure 4.3.Fault resistance model

The three phase current through the fault resistance $\mathbf{I_f}$, is presented in (4.1).

$$\mathbf{I_f} = \mathbf{R^{-1}E_f} = \frac{1}{R_f}\mathbf{K} * \mathbf{E_f} \tag{4.1}$$

In equation (4.1), R_f is the fault resistance; $\mathbf{E_f}$ is the phase-earth voltage at the fault point. $\mathbf{K}$ is 3×3 fault matrix, which elements are depending on fault types

$$\mathbf{K} = \begin{bmatrix} K_{aa} & K_{ab} & K_{ac} \\ K_{ba} & K_{bb} & K_{bc} \\ K_{ca} & K_{cb} & K_{cc} \end{bmatrix} \tag{4.2}$$

The calculation of the fault matrix **K** can be divided into two steps:

1. Denote the phase(s) which is(are) involved in the fault

$$K_{ij} = \begin{cases} -1 & \text{if the phase is involved} \\ 0 & \text{if the phase is not invloved} \end{cases} \quad i,j = \text{a, b, c}$$

Note that i,j represent phases.

2. Replace the diagonal elements by the value calculated in the equation

$$K_{ii} = \sum_{j=a}^{j=c} \left| K_{ij} \right| \; i = a, b, c \tag{4.3}$$

Table 4.1 shows the values of **K** of all fault types [5].

In the modelling of interpole states, the resistive fault model will be used.

Fault types	**K**
a-e	$\begin{bmatrix}1 & 0 & 0\\0 & 0 & 0\\0 & 0 & 0\end{bmatrix}$
b-e	$\begin{bmatrix}0 & 0 & 0\\0 & 1 & 0\\0 & 0 & 0\end{bmatrix}$
c-e	$\begin{bmatrix}0 & 0 & 0\\0 & 0 & 0\\0 & 0 & 1\end{bmatrix}$
a-b	$\begin{bmatrix}1 & -1 & 0\\-1 & 1 & 0\\0 & 0 & 0\end{bmatrix}$
b-c	$\begin{bmatrix}0 & 0 & 0\\0 & 1 & -1\\0 & -1 & 1\end{bmatrix}$
c-a	$\begin{bmatrix}1 & 0 & -1\\0 & 0 & 0\\-1 & 0 & 1\end{bmatrix}$
a-b-e	$\begin{bmatrix}2 & -1 & 0\\-1 & 2 & 0\\0 & 0 & 0\end{bmatrix}$
b-c-e	$\begin{bmatrix}0 & 0 & 0\\0 & 2 & -1\\0 & -1 & 2\end{bmatrix}$
c-a-e	$\begin{bmatrix}2 & 0 & -1\\0 & 0 & 0\\-1 & 0 & 2\end{bmatrix}$
a-b-c	$\begin{bmatrix}2 & -1 & -1\\-1 & 2 & -1\\-1 & -1 & 2\end{bmatrix}$

Table 4.1. Fault matrix for different fault types

4.2.2.2 State 1

In state 1, all three poles of the circuit breaker are closed. According to the superposition method, the state 1 network can be seen as the sum of the pre-fault network and the state 1 superimposed network, which is shown in Figure 4.4.

In the superimposed network (Figure 4.4b), the value of $\mathbf{E_f}$ is equal to the voltage at the fault location in the pre-fault network (Figure 4.4a), which can be expressed as:

$$\mathbf{E_f} = \mathbf{V_L} - n\mathbf{Z_L}\mathbf{I_R} \tag{4.4}$$

Note that *n* denotes the fault location as a fraction of the line length.

Table 2.1 shows the statistical occurrence of different categories of short circuit faults [7]. From the table, it is clear that single phase to earth fault represents the vast majority of faults that are encountered on overhead systems. Therefore, in this section, the single phase to earth fault is incorporated. All fault types can be dealt with by changing the element of **K**, as shown in Table 4.1. Equation (4.5) represents the fault impedance matrix, where R_f is the fault/earth loop resistance. For a single phase to ground fault, **K** is represented by the matrix (4.6).

$$\mathbf{I_f} = \frac{1}{R_f}\mathbf{K}(-\mathbf{E_f} - \mathbf{V_f}) \tag{4.5}$$

$$\mathbf{K} = \begin{bmatrix} 1 & 0 & 0 \\ 0 & 0 & 0 \\ 0 & 0 & 0 \end{bmatrix} \tag{4.6}$$

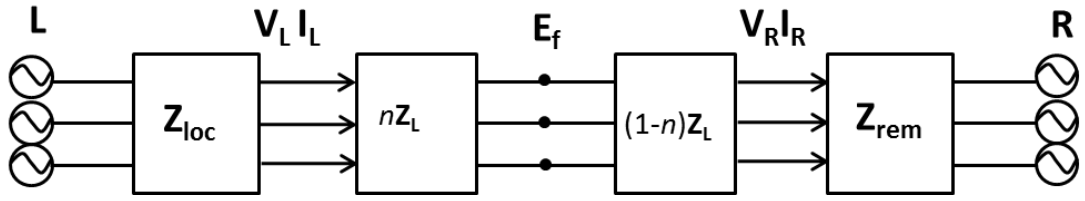

a) Pre-fault network

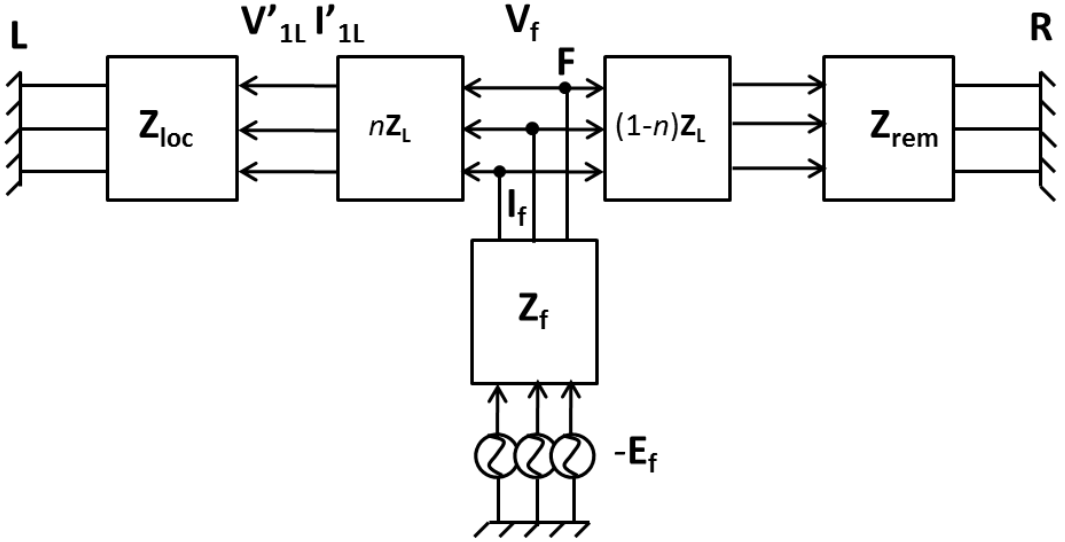

b) State 1 superimposed network

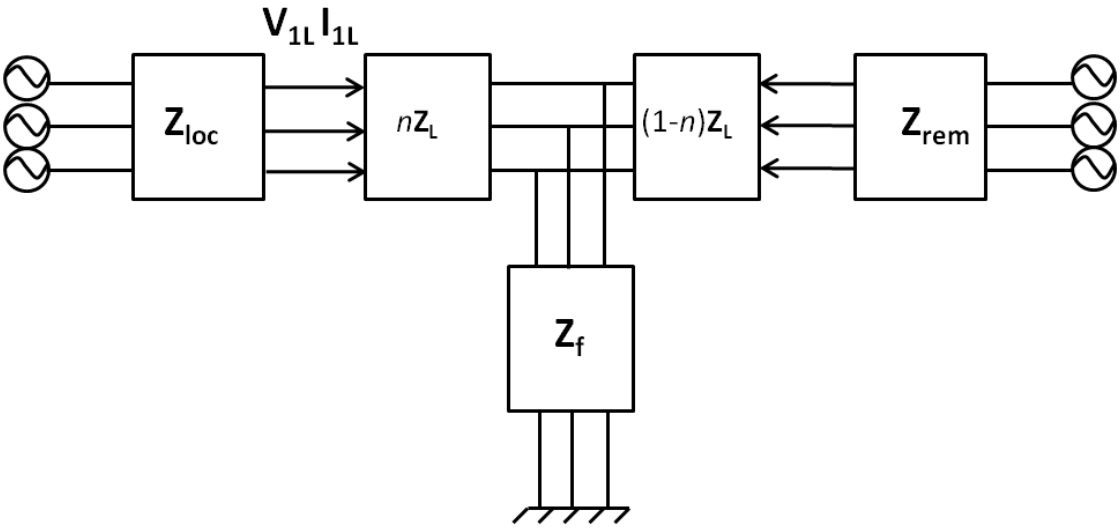

c) State 1 combined network

Figure 4.4. Superposition method in state 1

In the superimposed network (Figure 4.4b), the Thevenin equivalent impedance $\mathbf{Z_t}$ from the fault point F towards two ends (the total impedance of the parallel connection from **F** to **L** side and **F** to **R** side), can be calculated as:

$$\mathbf{Z_t} = \frac{(\mathbf{Z_{loc}} + n\mathbf{Z_L})(\mathbf{Z_{rem}} + (1-n)\mathbf{Z_L})}{\mathbf{Z_{loc}} + \mathbf{Z_{rem}} + \mathbf{Z_L}} \tag{4.7}$$

The fault current $\mathbf{I_f}$ in the superimposed network can also be obtained as:

$$\mathbf{I_f} = \frac{\mathbf{V_f}}{\mathbf{Z_t}} \tag{4.8}$$

Combining equations (4.5) and (4.8) gives:

$$\mathbf{V_f} = \frac{-\frac{1}{R_f}\mathbf{K}\mathbf{E_f}}{\frac{\mathbf{1}}{\mathbf{Z_t}} + \frac{1}{R_f}\mathbf{K}} \tag{4.9}$$

Consequently, the fault current $\mathbf{I_f}$ can be inherently obtained by (4.8). The sending-end current $\mathbf{I'_{1L}}$ in the superimposed network can be calculated using the principle of a current divider as:

$$\mathbf{I'_{1L}} = \mathbf{I_f} \times \frac{\mathbf{Z_{rem}} + (1-n)\mathbf{Z_L}}{\mathbf{Z_{loc}} + \mathbf{Z_{rem}} + \mathbf{Z_L}} \tag{4.10}$$

Then the sending-end voltage $\mathbf{V'_{1L}}$is:

$$\mathbf{V'_{1L}} = \mathbf{E_f} - \mathbf{I_f Z_f} - \mathbf{I'_{1L}} n\mathbf{Z_L} \tag{4.11}$$

According to the superposition theory, the local voltage $\mathbf{V_{1L}}$ and current $\mathbf{I_{1L}}$ in state 1 are:

$$\mathbf{V_{1L}} = \mathbf{V_L} + \mathbf{V'_{1L}} \tag{4.12}$$

$$\mathbf{I_{1L}} = \mathbf{I_L} + \mathbf{I'_{1L}} \tag{4.13}$$

4.2.2.3 State 2

In state 2, one pole of the circuit breaker is open. According to superposition theory, the state 2 network can be represented as the sum of the state 1 network (refer to Figure 4.4c) and the state 2 superimposed network, which is depicted in Figure 4.5a.

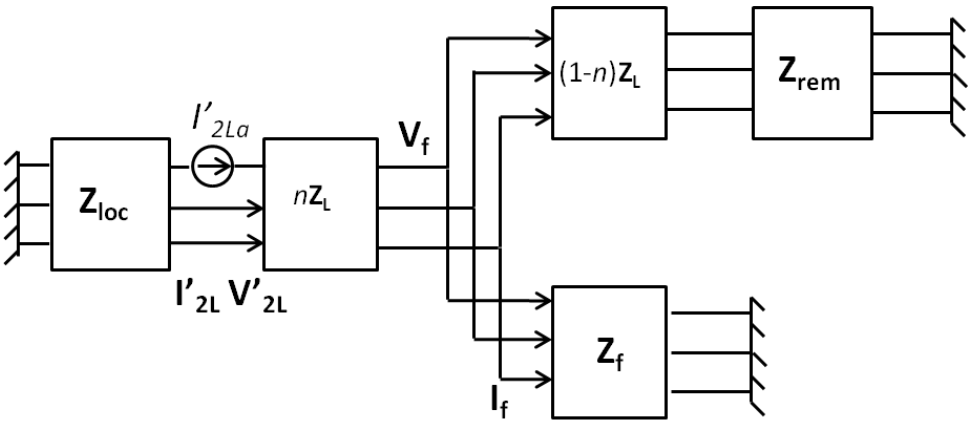

a). State 2 superimposed network

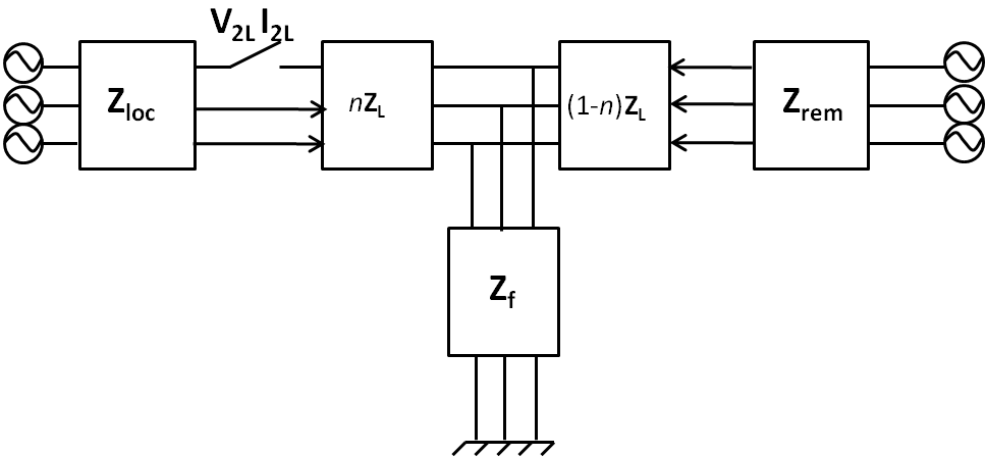

b). State 2 combined network

Figure 4.5. Superposition method in state 2

In the superimposed network (Figure 4.5a), the open phase is represented as a controlled current sourceI'_{2La}, which has the same amplitude as the fault current in state 1 but the opposite direction. Note that I_{1La} denotes the phase A current in state 1.

$$I'_{2La} = -I_{1La} \tag{4.14}$$

$$\mathbf{Y_f} = \frac{1}{R_f}\mathbf{K} \tag{4.15}$$

The Thevenin equivalent impedance $\mathbf{Z_{th}}$ on the right hand side of the circuit breaker can be calculated using simple principles of series and parallel connection of impedances as shown below:

$$\mathbf{Z_{th}} = \frac{\mathbf{1}}{\mathbf{Y_f} + \frac{\mathbf{1}}{\mathbf{Z_{rem}} + (\mathbf{1}-n)\mathbf{Z_L}}} + n\mathbf{Z_L} \tag{4.16}$$

The phase B and C superimposed voltages at the local end (V'_{2Lb}, V'_{2Lc}) can be calculated as follows:

$$V'_{2Lb} = Z_{th_{12}} I'_{2La} + Z_{th_{22}} I'_{2Lb} + Z_{th_{13}} I'_{2Lc} \tag{4.17}$$

$$V'_{2Lc} = Z_{th_{13}} I'_{2La} + Z_{th_{23}} I'_{2Lb} + Z_{th_{33}} I'_{2Lc} \tag{4.18}$$

$$V'_{2Lb} = Z_{sm} I'_{2La} + Z_{ss} I'_{2Lb} + Z_{sm} I'_{2Lc} \tag{4.19}$$

$$V'_{2Lc} = Z_{sm} I'_{2La} + Z_{sm} I'_{2Lb} + Z_{ss} I'_{2Lc} \tag{4.20}$$

Note that $Z_{th_{\mathrm{ij}}}$ are the element of $\mathbf{Z_{th}}$; Z_{sm} and Z_{ss} are the mutual and self-impedances of $\mathbf{Z_{loc}}$. After combining equations (4.17) to (4.20), the remaining parameters in the superimposed network can be calculated as:

$$\begin{bmatrix} I'_{2Lb} \\ I'_{2Lc} \end{bmatrix} = -I'_{2La} \times \begin{bmatrix} Z_{sm} + Z_{th_{12}} \\ Z_{sm} + Z_{th_{13}} \end{bmatrix} \times \begin{bmatrix} Z_{ss} + Z_{th_{22}} & Z_{sm} + Z_{th_{23}} \\ Z_{sm} + Z_{t_{23}} & Z_{ss} + Z_{th_{33}} \end{bmatrix} \tag{4.21}$$

$$\mathbf{I'_{2L}} = \begin{bmatrix} I'_{2La} \\ I'_{2Lb} \\ I'_{2Lc} \end{bmatrix} \tag{4.22}$$

$$\mathbf{V'_{2L}} = \mathbf{Z_{th}} \mathbf{I'_{2L}} \tag{4.23}$$

The pre-fault component of state 2 is effectively state 1. Thus, $\mathbf{V_{2L}}$ and $\mathbf{I_{2L}}$ are:

$$\mathbf{V_{2L}} = \mathbf{V_{1L}} + \mathbf{V'_{2L}} \tag{4.24}$$

$$\mathbf{I_{2L}} = \mathbf{I_{1L}} + \mathbf{I'_{2L}} \tag{4.25}$$

4.2.2.4 State 3

The calculations in state 3 are analogous to those in state 2. In this case two poles are open (refer to Figure 4.6). In the superimposed network, phase A pole remains open as in state 2 (current equals to 0) and since the pole of phase B has been tripped in this state, it is represented by a controlled current source. Note that I_{2Lb} denotes the phase B current of state 2.

$$I'_{3La} = 0 \tag{4.26}$$

$$I'_{3Lb} = -I_{2Lb} \tag{4.27}$$

The phase C superimposed voltage at the local end can be represented as:

$$V'_{3Lc} = Z_{th_{13}} I'_{3La} + Z_{th_{23}} I'_{3Lb} + Z_{th_{33}} I'_{3Lc} \tag{4.28}$$

$$V'_{3Lc} = Z_{sm} I'_{3La} + Z_{sm} I'_{3Lb} + Z_{ss} I'_{3Lc} \tag{4.29}$$

The phase C superimposed current is:

$$I'_{3Lc} = \frac{-I'_{3Lb}(Z_{sm} + Z_{th_{23}})}{Z_{ss} + Z_{th_{33}}} \tag{4.30}$$

Consequently, the local end currents of state 3 superimposed network are as follows:

$$\mathbf{I'_{3L}} = \begin{bmatrix} I'_{3La} \\ I'_{3Lb} \\ I'_{3Lc} \end{bmatrix} \tag{4.31}$$

$$\mathbf{V'_{3L}} = \mathbf{Z_{th}}\mathbf{I'_{3L}} \tag{4.32}$$

According to superposition theory, the voltage $\mathbf{V_{3L}}$ and current $\mathbf{I_{3L}}$ in state 3 can be calculated as:

$$\mathbf{V_{3L}} = \mathbf{V_{2L}} + \mathbf{V'_{3L}} \tag{4.33}$$

$$\mathbf{I_{3L}} = \mathbf{I_{2L}} + \mathbf{I'_{3L}} \tag{4.34}$$

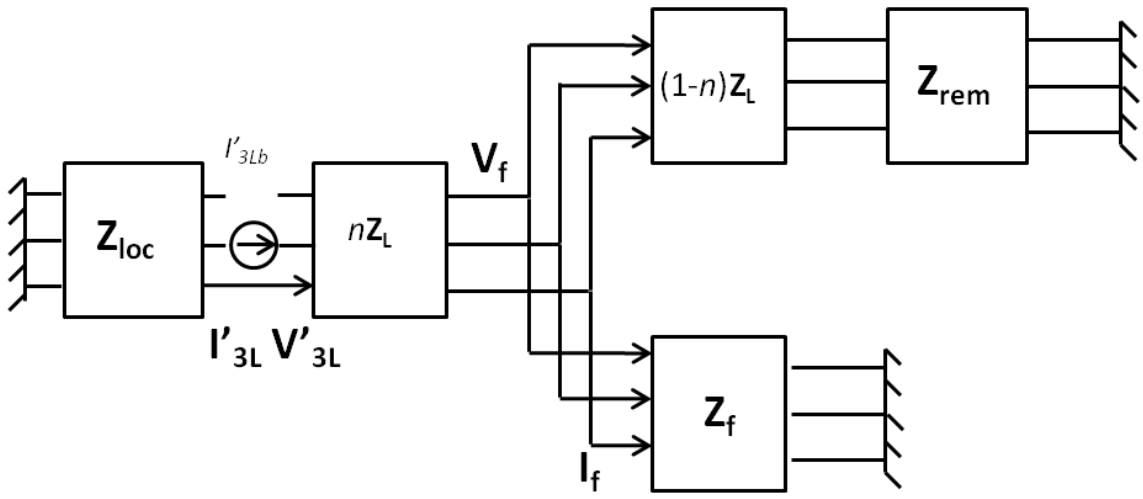

a) State 3 superimposed network

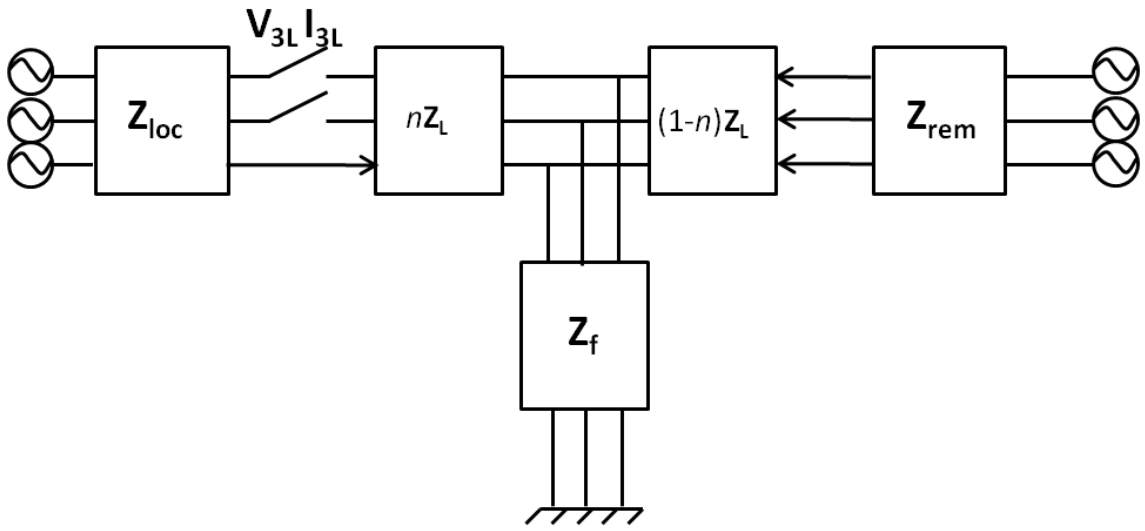

b) State 3 combined network

Figure 4.6. Superposition method in state 3

4.2.2.5 State 4

In state 4, all circuit breaker poles are open (as shown in Figure 4.7). In the superimposed network, the current of phase C is represented by a controlled source. The other two phases are already open. Consequently, the superimposed current and voltage are calculated from (4.35) - (4.39).

$$I'_{4La} = 0 \tag{4.35}$$

$$I'_{4Lb} = 0 \tag{4.36}$$

$$I'_{4Lc} = -I_{3Lc} \tag{4.37}$$

$$\mathbf{I'_{4L}} = \begin{bmatrix} I'_{4La} \\ I'_{4Lb} \\ I'_{4Lc} \end{bmatrix} \tag{4.38}$$

$$\mathbf{V'_{4L}} = \mathbf{Z_{th}}\mathbf{I'_{4L}} \tag{4.39}$$

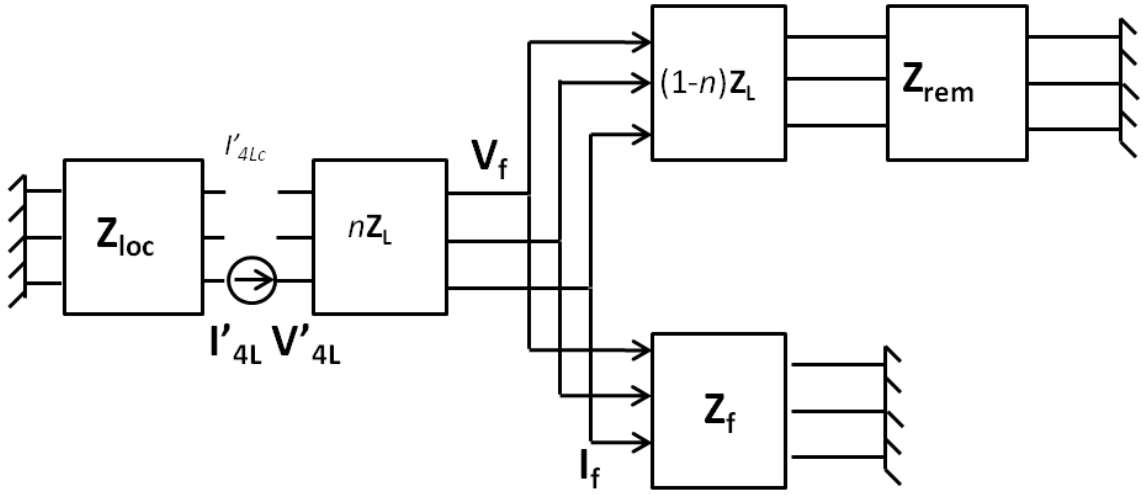

a). State 4 superimposed network

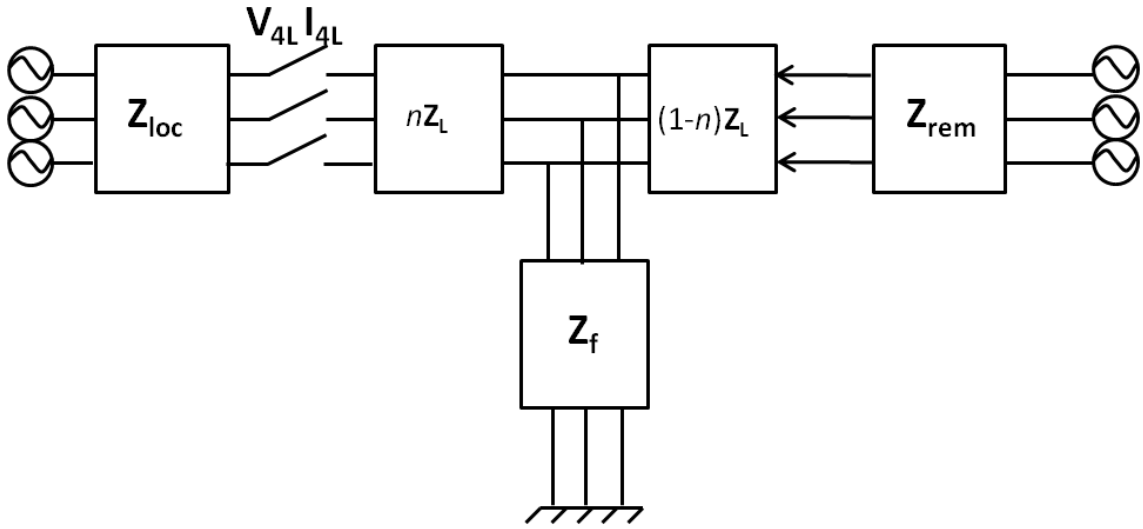

b). State 4 combined network

Figure 4.7. Superposition method in state 4

Thus, the voltage $\mathbf{V_{4L}}$ and current $\mathbf{I_{4L}}$ in state 4 can be obtained as below:

$$\mathbf{V_{4L}} = \mathbf{V_{3L}} + \mathbf{V'_{4L}} \tag{4.40}$$

$$\mathbf{I_{4L}} = \mathbf{I_{3L}} + \mathbf{I'_{4L}} \tag{4.41}$$

Source impedances $\mathbf{Z_{loc}}$ and $\mathbf{Z_{rem}}$ can be represented by *SCL1* and *SCL2*. $\mathbf{Z_L}$ and *SCL1* are assumed to be known in this method. Accordingly, the local voltages and currents during states 1, 2, 3 and 4 can be calculated if the remaining three parameters *n, R_f and SCL2* are established. Equation (4.5) represents the fault impedance and fault type which is expressed by fault resistance R_f and the fault matrix **K.** This enables the algorithm to deal with all fault types by changing the relevant elements in **K**.

4.3 Fault location algorithm

4.3.1 Basic principles

The basic concept of the fault location algorithm, which is illustrated in Figure 4.8, is to compare the calculated voltages and currents during the consecutive interpole states with simulated data, and to record the possible fault locations, fault resistances and remote end short circuit level. The number of possible solutions reduces as the analysis of interpole states progresses from states 1 through to 4. The fault location estimation system contains three sections:

- transmission line modelling;
- comparison;
- recording of candidate solution(s).

The transmission line modelling stage is based on the local voltage and current calculation using the impedance based algorithm as described in section 4.2.2. The transmission line modelling is used to iteratively calculate the voltage and current

data associated with the range of potential n, R_f and $SCL2$. The comparison section matches the voltage and current data calculated by the transmission line modelling with simulated data. If the matching process is successful, the recording section stores the corresponding values of n, R_f and $SCL2$. The three sections repeat until the assumed range of values for all three parameters is completed. After this iteration (for one of the interpole states), the new ranges for the three parameters are formed and the algorithm proceeds to the next interpole state. As progress through each of the interpole states is made, the possible range of values for each of the unknown parameters reduces and the final accurate solution is obtained including fault location, fault resistance and remote end short circuit level.

It should also be noted that in the comparison process, a certain tolerance has to be assumed which determines the range of possible solutions in subsequent stages. This will be discussed in more depth in the following sections.

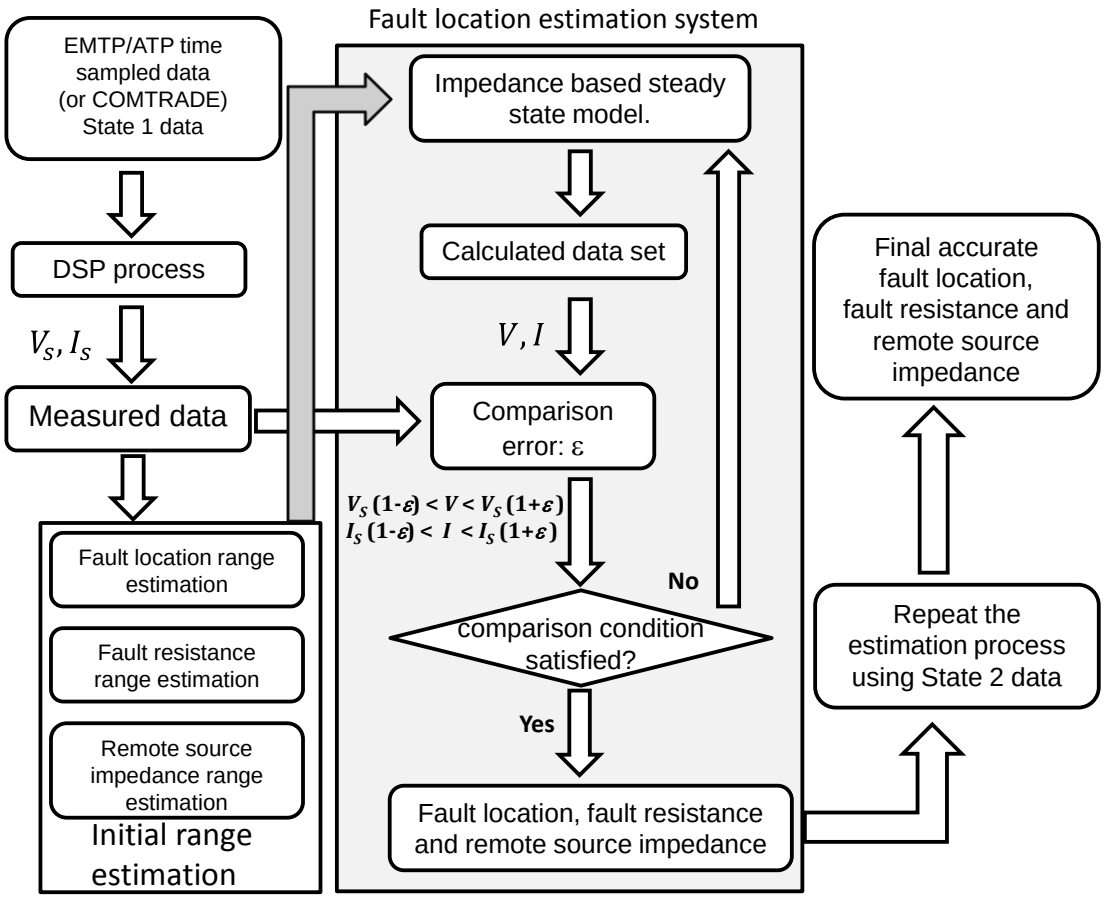

Figure 4.8. Fault location algorithm

4.3.2 Range pre-estimation

The main principle of the proposed fault location method is to compare the simulated data with the results of voltage and current phasor model-based computations, and to obtain the most likely combination of R_f, n and *SCL2*. Before state 1, the analysis of simulated data is used to initially limit the ranges of each variable using a conventional impedance-based fault location method (e.g. Takagi method can be used).

The range of *SCL2* in this study is assumed to be between 5GVA and 30GVA, which is assumed to be representative of most transmission system fault levels, but could be extended if required. The parameter *n* (fault location) pre-estimation range is calculated using the Takagi fault location algorithm [8] as shown in (4.42).

$$fl = \frac{Im(V_s I_{sup}^*)}{Im(I_s Z_l I_{sup}^*)} \tag{4.42}$$

Where, V_s and I_s are the faulty voltage and current. Z_l is the line impedance, and I_{sup} is the superimposed current, which is equal to fault current minus pre-fault current ($I_{sup} = I_{fault} - I_{pre-fault}$). I_{sup}^* is conjugate of I_{sup}

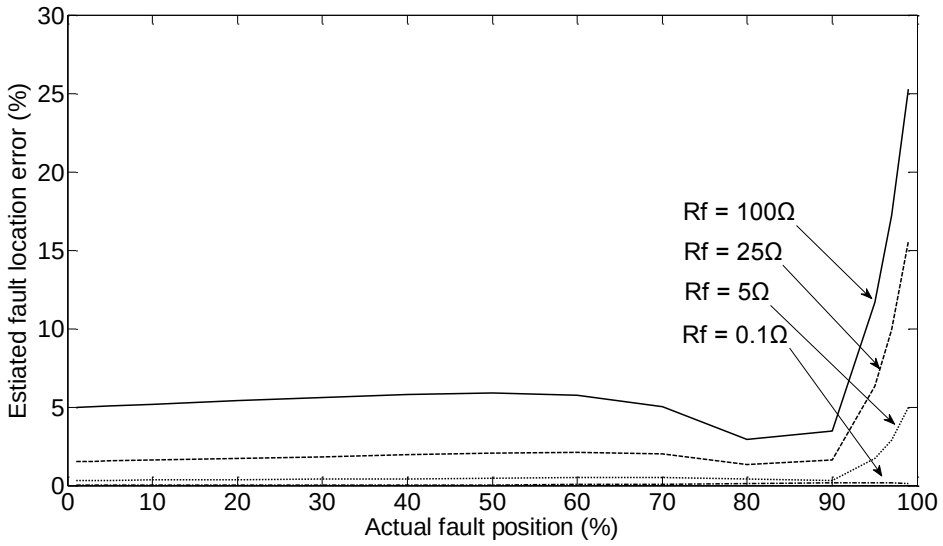

Figure 4.9. Accuracy of Takagi method for different values of fault location and resistance (*SCL2* 30GVA)

Figure 4.9 shows the accuracy of the Takagi method for various scenarios. In Chapter 3, the performance of Takagi method has been evaluated. The *SCL1* is set as

5GVA. Consequently, *SCL2* is set as 30GVA, which is the maximum value in *SCL2* range. It is found that in the majority of cases the accuracy is very high but the error can be significant for high resistive faults (e.g. 25.2% when R_f=100Ω). Consequently, the initial fault location pre-estimation range is set to $[fl - 25.2\%, fl + 25.2\%]$. Note that in cases where $fl - 25.2\% < 0\%$, the range is set to $[0\%, fl + 25.2\%]$, while in the case of $fl + 25.2\% > 100\%$, the range is set to $[fl - 25.2\%, 100\%]$.

To establish the initial range for R_f, the assumed minimum and maximum values for *n* and *SCL2* are used in conjunction with equations describing state 1 from (4.4) to (4.13) and measured values of voltage and current. For all four possible combinations of *n* and *SCL2* (i.e. *n_min*, *SCL2_min*; *n_min*, *SCL2_max; n_max*, *SCL2_min; n_max*, *SCL2_max*) four different R_f values are calculated and the minimum and maximum values of the four are used to form the boundaries of the initial R_f range.

4.3.3 Comparison

The fault location, fault resistance and remote end short circuit level are obtained once there is a match between the simulated data and calculated data. However, the calculated data based on the same settings of fault location, fault resistance and remote end short circuit level as the simulation model may not match the simulated data exactly due to the unexpected errors in simulated data (in terms of fundamental frequency phasor extraction, sensor/sampling error, etc.). Therefore, the comparison

tolerance (ε) is introduced. Both calculated data and simulated data are represented in the form of phasor which contains magnitude and angle. In the comparison, the angles and magnitude of both voltage and current are applied as to increase the certainty of the comparisons.

The criteria for the comparison of the simulated data and the output of the fault location estimation system are expressed by (4.43) and (4.44):

$$I_{m\_mag}(1-\varepsilon) < I_{c\_mag} < I_{m\_mag}(1+\varepsilon) \quad (4.43)$$

$$I_{m\_ang}(1-\varepsilon) < I_{c\_ang} < I_{m\_ang}(1+\varepsilon) \quad (4.44)$$

Where:

I_{m_mag}: Magnitude of measured current.
I_{m_ang}: Angle of measured current.
I_{c_mag}: Magnitude of calculated current.
I_{c_ang}: Angle of calculated current.
ε: Assumed comparison tolerance

Note that the voltage comparison takes the same principle as current.

In order to prove the concept of the proposed fault location technique, the simulated data has been obtained using steady state transmission line model calculations. For each result obtained from the fault location estimation system which matches the simulated data (taking into account the assumed tolerance ε), the three values *n, SCL2* and R_f are recorded as a potential correct solution (candidate). In reality the

measured phasors used in this method are obtained from the voltage and current time sampled values.

It is possible that more than one combination of R_f, *SCL2* and *n* could result in the same voltage values as the correct combination group in individual states. Fortunately, voltage and current calculations in each state are based on independent sets of equations, which mean that only a small set of candidates in the vicinity of the correct solution will proceed to the final state.

The comparison tolerance ε determines the amount of possible combinations of R_f, *SCL2* and *n* in each state. Higher value of comparison tolerance results in higher number of possible combination groups. Table 4.2 shows an example of the number of possible combination groups resulting from different comparison tolerances. In the example, a single phase to earth fault is assumed to have occurred in 400kV, 100km transmission line. The fault is located at midpoint of the line (50% of the total line length).

Number of possible groups	Comparison tolerance			
	1%	0.5%	0.3%	0.1%
State 1	8598	3079	715	190
State 2	1219	224	78	30
State 3	896	199	50	5
State 4	398	102	20	-

Table 4.2. Effect of comparison tolerance

It can be seen that higher value of comparison tolerance brings more possible combination groups at each state. Because the most probable combination groups should be identified only, the comparison tolerance should be relatively small. However, if the tolerance is too small, the match may fail. In the example shown in Table 4.2, the match of state 4 fails when tolerance is set as 0.1%. Therefore, in order to establish the optimal value, the tolerance is iteratively increased from an initially small value until the number of possible combination groups of each state is sufficient. Through large amount of simulation based tests, it was established that the method is most effective when the number of possible combinations in each of the four states are 200, 40, 20 and 10 respectively. This is achieved when the initial comparison tolerance set to 0.1%.

The number of possible combination groups of R_f, *SCL2* and *n* reduces as the fault location algorithm progresses through the various stages of operation. However, there may be still more than one candidate group in the final state (state 4) because of the non-zero value of comparison tolerance. In order to achieve the final most accurate value for fault location, an averaging method is incorporated to assist in the final fault location estimation. By listing the final range of fault locations, it is found that all individual estimates within the final range are concentrated around the actual fault location value; this has been verified through exhaustive testing. An example in the case study section will illustrate this comprehensively.

4.3.4 Summary of operation of the fault location system

The proposed fault location method can be summarised as follows:

1. Obtain state 1 simulated data from the record of the real event or CT/VT outputs in real time (fundamental frequency phasors from steady state transmission line model are used for development and testing as reported in this chapter).
2. Pre-estimate R_f, *SCL2* and *n* ranges using state 1 simulated data and the existing modified Takagi method.
3. Calculate the network voltages and currents in state 1 by using *n*, *SCL2* and R_f in pre-estimated range.
4. Compare calculated voltages and currents with simulated data and record the values of *n*, *SCL2* and R_f for results falling within the assumed comparison error ε in terms of 3-phase voltages and currents.
5. Iteratively repeat steps 2 and 3 until the whole pre-estimated range of *n*, *SCL2* and R_f is used.
6. Update ranges for *n*, *SCL2* and R_f based on all possible candidates recorded in stage 1.
7. Subsequently obtain simulated data for states 2, then 3 and 4, repeating steps 2-5 each time in an analogous way until the final set of candidate combinations of *n*, *SCL2* and R_f is obtained.
8. Obtain the final results by averaging all possible combinations of *n*, *SCL* and R_f resulting from state 4

Note:

1. It is assumed that the local source impedance is known. In practice, this could be calculated from the state 1 superimposed network.
2. The ranges of unknown parameters in step 4 are:
   - *n*: 0-100% of line length in steps of 0.1%
   - *SCL2*: 5-35 GVA in steps of 0.5 GVA (for 400kV application)
   - R_f : 0-100Ω in steps of 0.1Ω

4.4 Case study and performance comparisons

In order to assess the accuracy of the method, a steady state model of a 100km, 400kV double supplied transmission line with a single phase to ground fault has been simulated in MATLAB. The local short circuit level is 5GVA**.** The zero sequence line impedance Z_{L0}=0.108+*j*0.88 Ω/km and the positive sequence line impedance Z_{L1}=0.018+*j*0.31Ω/km.

In order to prove the concept of this novel fault location algorithm, the simulated data is obtained by the steady state simulation of interpole states. The amounts of possible combination groups are set as 200, 40, 20 and 10 for states 1 to 4 respectively. The final result is obtained by averaging the possible candidates remaining at state 4.

4.4.1 Case study

An example fault has been applied to test the performance of the proposed algorithm. The settings for the measured (in this case simulated) data are:

- fault location: 50km (50% of line length from measurement point)
- R_f: 5Ω (high resistive fault)
- *SCL1*: 5GVA
- *SCL2*: 30GVA
- load angle: 10^o

Table 4.3 shows the simulated data from the steady state transmission line model. From the table, it can be judged that the fault occurred in phase A; and the circuit breaker phase tripping sequence is A-B-C, i.e. Faulty-Healthy-Healthy (F-H-H).

	state 1	state 2	state 3	state 4
V_a[kV]	256.06 + 13.09i	42.60 – 64.68i	24.16 – 60.46i	14.64 – 54.13i
V_b[kV]	–130.06 – 308.56i	–132.79 – 307.41i	–255.51 – 305.46i	–272.61 – 297.57i
V_c[kV]	–212.34 + 251.23i	–215.07 + 252.38i	–218.38 + 252.70i	–272.30 + 273.07i
I_a[kA]	6.65 – *j*8.97	0	0	0
I_b[kA]	–0.4845 – 1.4572i	0.2164 – 2.9177i	0	0
I_c[kA]	–1.0171 + 1.1453i	–0.3162 – 0.3152i	–0.3139 – 1.1995i	0

Table 4.3. Simulated voltage and current phasor data

The simulated data is achieved through the steady state modelling of interpole states. Table 4.3 shows the simulated data of the example case. The pre-estimation ranges of *n*, R_f and *SCL2* are established using the simulated data, which have been shown in Table 4.5.

Unknown parameters	Pre-estimated range
Fault location (n)	24.6% – 75.0%
Fault resistance (R_f)	0.5Ω – 30Ω
Remote end short circuit level ($SCL2$)	5GVA – 35GVA

Table 4.4 Pre-estimation ranges of n, R_f and $SCL2$

The interpole state model generates voltage and current by assuming different values of n, R_f and $SCL2$ iteratively within the pre-estimated ranges. The generated data is then compared with the simulated data. The possible values of such three parameters are recorded when the match is found (i.e. current and voltage phasors are within certain assumed tolerance). After the iterations from the pre-estimated ranges are complete, new ranges are established for state 2. The above actions are subsequently repeated until the final state is reached. The ranges of each state have been shown in Table 4.5. As expected, the number of candidates is gradually reduced and the values of n, $SCL2$ and R_f gravitate towards the correct solution as the calculation progresses from state 1 to state 4.

	Number of Candidates	n (km)	R_f (Ω)	$SCL2$ (GVA)
state 1	224	46.7 –52.7	4–7	29–31
state 2	60	48.9–51.1	5–5	29–31
state 3	25	49.0–51.0	5–5	29–30
state 4	11	49.5–50.5	5–5	30
Final result	1	50	5	30

Table 4.5. Results of fault location estimation system

In the final state, 11 possible fault locations remain, and the final result is obtained by the averaging method. A very accurate result has been achieved in this example as the simulated data has been achieved from the simplified steady state transmission line modelling, which does not contain any errors, resulting from measurement or sensor/sampling. In practical implementations, the fault location accuracy is likely to be influenced by these factors but this, to higher or lesser degree, applies to all impedance based fault location methods.

4.4.2 Performance comparison of the proposed method with selected conventional algorithms

Table 4.6 and Table 4.5 shows the performances under varying parameters *n*, *SCL2* and R_f for the Takagi method (A), Network Impedance method (B) and the proposed method (C). Chapter 3 has evaluated the performance of both Takagi and Network Impedance methods. For ease of comparison these results are brought into the combined Table 4.6 (single phase-to-earth fault) and Table 4.5 (phase-to-phase-to-earth fault). The results demonstrate clearly that the proposed method provides the highest accuracy among the three algorithms. It is also not influenced by fault resistance or remote end short circuit level. In case of single phase to earth fault, the maximum error is less 0.08% when R_f=100Ω, and *SCL2*=5GVA. In case of double phase to earth fault, the maximum error is less 0.11% when R_f=100Ω, and *SCL2*=15GVA. The proposed method improves the fault location accuracy significantly compared with Takagi method, especially when R_f increases to 100Ω. The maximum error of network impedance based method is under

0.90% and 0.94% when R_f reaches 100Ω. However, the proposed method does not require the value of *SCL2* as input.

Simulation settings			Maximum estimated error (%)		
Rf (Ω)	*SCL2*(GVA)	*n* (%)	A	B	C
0.1	5	0–100	0.22	0.25	0.01
0.1	15	0–100	0.18	0.24	0.02
0.1	30	0–100	0.17	0.20	0.01
5	5	0–100	1.02	0.26	0.01
5	15	0–100	2.98	0.30	0.04
5	30	0–100	4.95	0.60	0.04
25	5	0–100	5.40	0.28	0.02
25	15	0–100	11.6	0.50	0.00
25	30	0–100	15.54	0.79	0.02
100	5	0–100	15.53	0.39	0.08
100	15	0–100	23.20	0.60	0.02
100	30	0–100	25.20	0.90	0.03

Table 4.6. Performance comparison results of single phase–to–earth fault

Simulation settings			Maximum estimated error (%)		
Rf (Ω)	*SCL2*(GVA)	*n* (%)	A	B	C
0.1	5	0–100	0.47	0.42	0.02
0.1	15	0–100	0.74	0.75	0.03
0.1	30	0–100	0.78	0.79	0.04
5	5	0–100	3.70	0.46	0.01
5	15	0–100	2.60	0.49	0.05
5	30	0–100	2.89	0.77	0.02
25	5	0–100	6.25	0.79	0.03
25	15	0–100	7.86	0.69	0.02
25	30	0–100	8.99	0.68	0.03
100	5	0–100	12.90	0.69	0.06
100	15	0–100	16.70	0.88	0.11
100	30	0–100	21.18	0.94	0.03

Table 4.7. Performance comparison results of phase-to-phase-to-earth fault

4.5 Limitations of the proposed method

As stated in section 4.2.1, the time interval between interpole states is theoretically 3.33ms in 50Hz system, which is 1/6 of the fundamental cycle. If there are no errors (i.e. non-fundamental frequency components, DC offset, unexpected high frequency oscillations) in the waveform, then the extraction of accurate phasor data from such a short time period of data should not be a problem. Sinusoidal wave based algorithms [9-11], which calculate fundamental phasors using a small number of samples, can be used in such circumstances. However, the natural response of the power system may produce imperfections such that errors in extracted waveforms when only a small portion of the cycle is available will be introduced. Conventional phasor extraction technique (DFT) [12] may reduce such errors, however, typically one full fundamental cycle is required for such algorithms to complete the extraction of the data. During the interpole states, the time window of 1/6 cycle is still a significant challenge for existing techniques; the location scheme based on analysis of auto-reclose schemes reported in the next chapter helps to address any potential shortcomings associated with phasor extraction. Recently, a number of algorithms have been investigated and proposed that attempt to reduce the time window required. [13] has reported upon techniques which apply the direct quadrature transformation. These techniques reduce the time for phasor extraction to 1/3 of a cycle of data. [14] reports upon a technique which applies short window orthogonal filters. The minimum time window required is a quarter of a cycle. Using these techniques, it is believed that this problem can be addressed in the near future.

4.6 Conclusion

A new fault location algorithm, which analyses the interpole states of circuit breakers during fault clearing operation, has been developed. It compares calculated data with simulated data; once a match is found within a specified tolerance error, all possible fault locations, fault resistances and remote end short circuit level are recorded. The ranges of all possible values are reduced through the analysis of the consecutive interpole stages. Accurate fault location is obtained after the final state. The algorithm is based on single ended data. Furthermore, it not only eliminates but also quantifies the negative effects of conventional single ended methods. It is relatively economical to implement. Only local end data is needed. Results show that the algorithm is capable of accurate fault location in situations where the remote source impedance and fault resistance are unknown. This chapter includes am example case study, demonstrating the theoretically ideal accuracy of the method. It compares very favourably against two well-established (and used in practice) fault location methods, and therefore, displays good promise of achieving very high accuracy, which can be implemented at low cost.

4.7 References

[1] P. J. Moore, "Radiometric measurement of Circuit Breaker interpole switching times," *Power Delivery, IEEE Transactions on*, vol. 19, pp. 987-992, 2004.

[2] P. J. Moore and V. S. H. Chong, "Analysis of the radiated electromagnetic field generated by a 132 kV, SF6 circuit breaker," in *Electrical Insulation and Dielectric Phenomena, 2002 Annual Report Conference on*, 2002, pp. 134-137.

[3] M. M. Saha, *et al.*, "Fault location in uncompensated and series-compensated parallel lines," in *Power Engineering Society Winter Meeting, 2000. IEEE*, 2000, pp. 2431-2436 vol.4.

[4] M. M. Saha, *et al.*, "New concept for fault location in series-compensated parallel lines," in *Power Engineering Society Winter Meeting, 2001. IEEE*, 2001, pp. 769-774 vol.2.

[5] M. M. Saha and E.Rosolowski, *Fault Locaiton On Power Network*. Wrocloaw: Springer, 2011.

[6] M. M. Saha, *et al.*, "A new accurate fault locating algorithm for series compensated lines," *Power Delivery, IEEE Transactions on*, vol. 14, pp. 789-797, 1999.

[7] G. Yaozhong, *New techniques for protective relaying and fault location*. Xi'an China: Xi'an Jiaotong University Publisher, 2007.

[8] T. Takagi, *et al.*, "Development of a New Type Fault Locator Using the One-Terminal Voltage and Current Data," *Power Apparatus and Systems, IEEE Transactions on*, vol. PAS-101, pp. 2892-2898, 1982.

[9] B. J. Mann and I. F. Morrison, "Digital Calculation of Impedance for Transmission Line Protection," *Power Apparatus and Systems, IEEE Transactions on*, vol. PAS-90, pp. 270-279, 1971.

[10] B. J. Mann and I. F. Morrison, "Relaying a Three Phase Transmission Line with a Digital Computer," *Power Apparatus and Systems, IEEE Transactions on*, vol. PAS-90, pp. 742-750, 1971.

[11] J. G. Gilbert and R. J. Shovlin, "High speed transmission line fault impedance calculation using a dedicated minicomputer," *Power Apparatus and Systems, IEEE Transactions on*, vol. 94, pp. 872-883, 1975.

[12] A. T. Johns and S. K. Salman, *Digital Protection For Power System*. London, United Kingdom: Peter Peregrinus 1985.

[13] Y. Ziwen, "Fundamental Phasor Calculation With Short Delay," *Power Delivery, IEEE Transactions on*, vol. 23, pp. 1280-1287, 2008.

[14] D. Finney, *et al.*, "Ultra fast distance protection," in *Developments in Power System Protection (DPSP 2010). Managing the Change, 10th IET International Conference on*, 2010, pp. 1-5.

Chapter 5. Fault location through analysis of data from auto-reclose operations

5.1 Introduction

An improved fault location method based on the analysis of circuit breaker operation has been presented in Chapter 4. The performance of the method has been verified using a steady state transmission line model representation [1]. However, the interval between interpole state transitions is typically of the order of 3.33ms in a 50Hz system (this time could vary depending on the individual fault conditions and on circuit breaker performance). It is difficult to extract fundamental frequency phasors from such a short time window and the effectiveness of the proposed method may therefore be questionable in real-world applications, which has been highlighted in Chapter 4, although short-time phasor extraction techniques continue to improve, as was also highlighted in the previous chapter.

Accordingly, in this chapter, it is proposed to enhance and extend the proposed method using data recorded during the auto-reclose sequences. For permanent faults on overhead systems (which are of most interest from a fault location perspective),

auto-reclose data will provide more information related to the fault and thus improving the fault location accuracy. Reclosing onto the same fault provides a number of additional cycles of current and voltage waveforms during the fault and during the subsequent opening sequence after the failed reclose.

Auto-reclose schemes applied to transmission lines are effective in terms of improving the availability of the power system. Single phase auto-reclose scheme (SPAR) and three phase auto-reclose scheme (TPAR) have been widely implemented in many parts of the world [2-8]. The overall fault clearing process can be viewed as being separated into a number of discrete states, governed and demarcated by the activities of the protection, switchgear and auto-reclose schemes. In this chapter, the development and testing of a fault location technique based on the analysis of data from the auto-reclose operations is reported. Both TPAR and SPAR schemes are investigated.

5.2 Overview of auto-reclose scheme operation

Auto-reclose schemes applied to transmission line system are effective in terms of improving the availability of the power system [9, 10]. Generally, three types of faults can occur in a transmission line, namely: transient faults, semi-transient faults and permanent faults [6-8]. Transient faults are most common, occupying over 90% of all faults in an overhead system [11]. The prevailing cause of transient faults is atmospheric lightning. The insulator strings are normally flashed over through lightning induced over voltages that form an arc, usually over deliberately designed weak-points (or “arcing horns”) in the insulation – normally connected in parallel

with the insulator string. The arc is seldom extinguished by itself. This type of transient fault must be cleared by tripping the line temporarily to de-ionise the fault path. In the majority of cases the line can be energised again without the fault recurring. A semi-transient fault requires more than one de-energised interval. Permanent faults account for only about 5% of all faults in practice and normally require time-consuming (and costly) repair work [11].

Due to the fact that over 90% faults are transient and most transient faults can be cleared by the tripping action only, auto-reclose scheme provide significant advantages in terms of system availability and avoidance of unnecessary maintenance and fault finding activities. It minimises the outage time and maintenance cost so as to improve system reliability. The choice of single phase or three phase reclosing depends on many factors. In this thesis, both reclosing practices are investigated.

5.2.1 Auto-reclosing mechanism

The transient fault is cleared by tripping the line to de-ionise the arc path. De-ionising time of the fault path depends on several factors, such as fault duration, fault current magnitude, wind speed, air humidity and pressure, circuit voltage, capacitive coupling to adjacent conductors, etc. Among these factors, the circuit voltage is the predominant factor influencing de-ionising time. In order to ensure that the fault path is thoroughly de-ionised, auto reclosing requires a dead time, which must exceed the de-ionising time.

Figure 5.1 illustrates the individual processes involved in an individual auto reclosing action following a fault [12]. A system fault is induced at time t_1. The line relay detects the fault and begins to operate. The circuit breaker receives the tripping command from relay at time t_2 and starts to clear the fault by opening the contacts and thus interrupting the fault path and CB is completely tripped at t_3. At time t_4, the line relay is reset and the auto-reclosing device begins to operate. There is a delay before the circuit breaker begins to reclose to ensure the dead time exceeds the de-ionising time. At time t_5, circuit breaker begins to reclose and at time t_6, the contacts of the circuit breaker are fully closed. After t_6, the system is restored back to nominal operation if the fault was transient. In the case of a permanent fault, the line relay will detect the fault again and open the circuit breaker permanently.

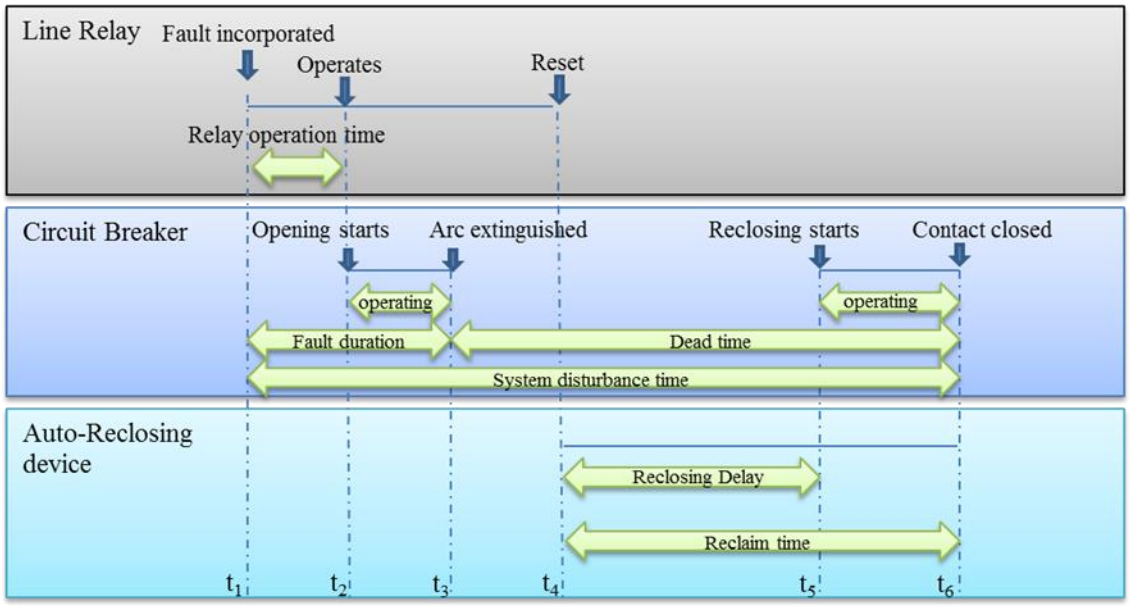

Figure 5.1.Progress of auto-reclosing action

5.2.2 Single phase auto-reclose scheme (SPAR)

In SPAR schemes, only the faulted phase is tripped [13], as the majority of faults in transmission systems are single phase to earth faults. In a transmission line with infeed sources at both ends, which is a typical situation, the circuit breaker poles corresponding to the faulted phase should theoretically open and reclose simultaneously at both ends of the circuit (for both transient and permanent faults). However, in the case of a permanent fault, the measurement devices, protection relays and circuit breakers will suffer stress at least on two occasions (in some cases more, when multiple reclosing is attempted). With the assistance of communications facilities, Guo [14] proposed a modified SPAR scheme, which recloses one side of the protected transmission line first. If the reclosed side protection device judges the fault to be permanent, the circuit breaker of the reclosing side will be tripped and the reclosing attempt at the opposite end will be prevented using the communication channel. Otherwise, the remote circuit breaker will be permitted to reclose if it is detected that the fault is transient in nature and the local end circuit breaker had reclosed successfully. Following Guo's modified scheme, the SPAR operation practice ensures that there is an interval between the reclosing attempts of the circuit breakers at the opposite ends of the protected line. This interval can be assumed to be sufficiently long to enable extraction of the fundamental frequency component from the waveform during fault conditions.

Figure 5.2 and Figure 5.3 illustrate the local-end currents as observed during operation of the SPAR scheme. Figure 5.2 presents the situation where the local

circuit breaker is first to reclose, while Figure 5.3 shows the situation where the remote circuit breaker is first to reclose. Both figures depict a permanent fault scenario. The various states (A to E) in the figures will be described the following section.

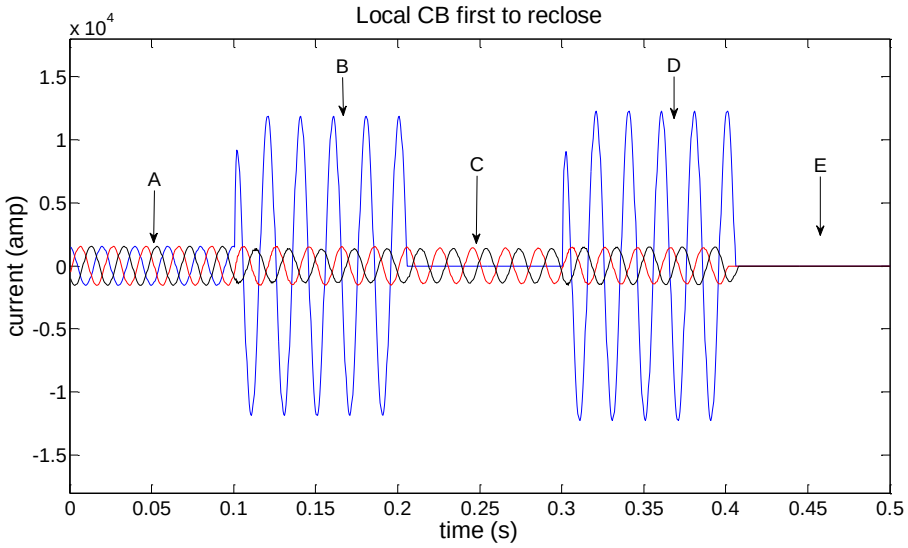

Figure 5.2. Currents for local CB reclosing first for a permanent fault scenario (SPAR)

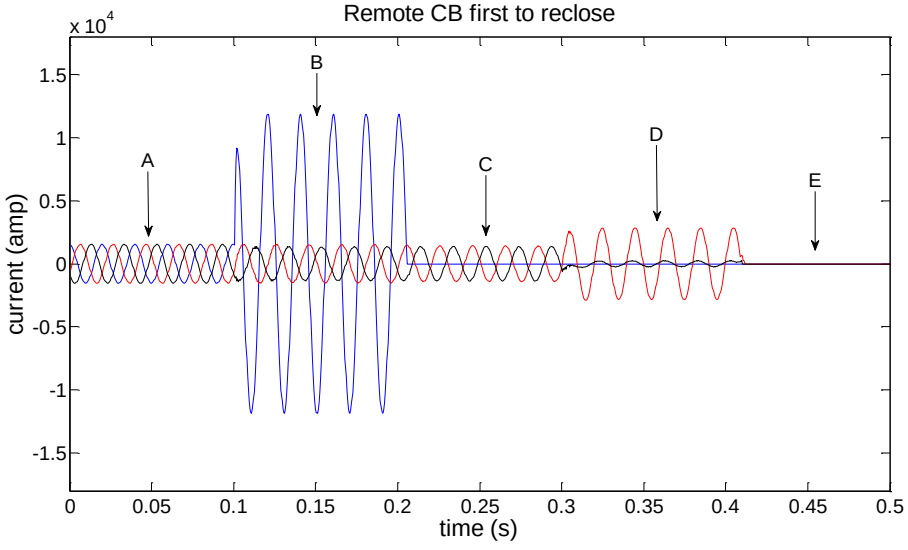

Figure 5.3. Currents for remote CB reclosing first for a permanent fault scenario (SPAR)

5.2.3 Three Phase Auto- Reclose Scheme (TPAR)

In TPAR schemes, all three phases are always tripped regardless of the type of fault. In a transmission line with infeed sources at both ends, and for similar reasons as explained earlier relating to SPAR schemes, the circuit breakers at both ends do not reclose simultaneously. In the case of an intermittent fault, one circuit breaker recloses first, followed by a synchronism check and reclose of the second circuit breaker. In the case of a permanent fault, the first reclosed circuit breaker trips again to clear the fault and the other circuit breaker remains open. Figure 5.4 and Figure 5.5 show the local currents as measured throughout the entire process of a TPAR operation for a permanent fault. Figure 5.4 presents the situation where the local circuit breaker is first to reclose , while Figure 5.5 illustrates the situation where the remote circuit breaker is first to reclose.

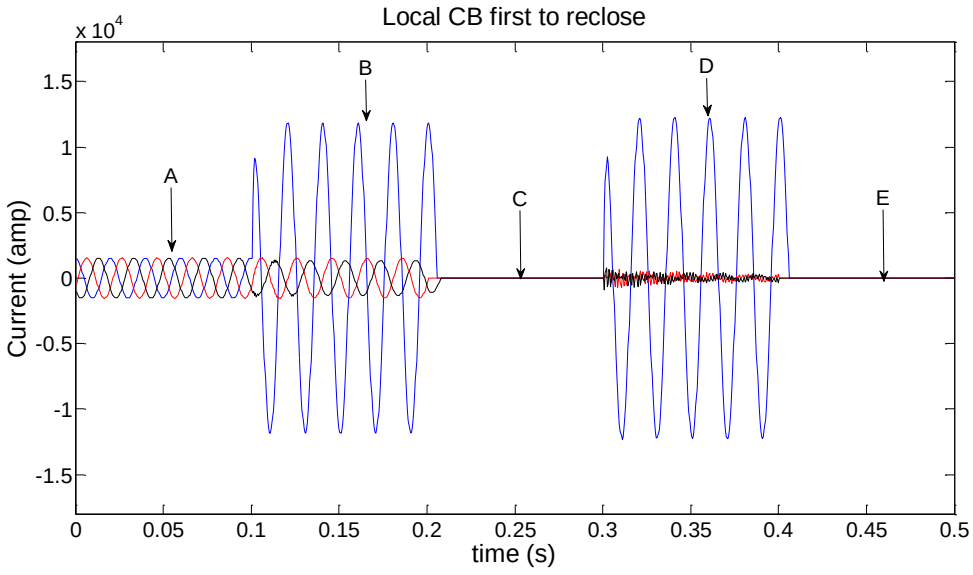

Figure 5.4. Currents for local CB reclosing first for permanent fault (TPAR)

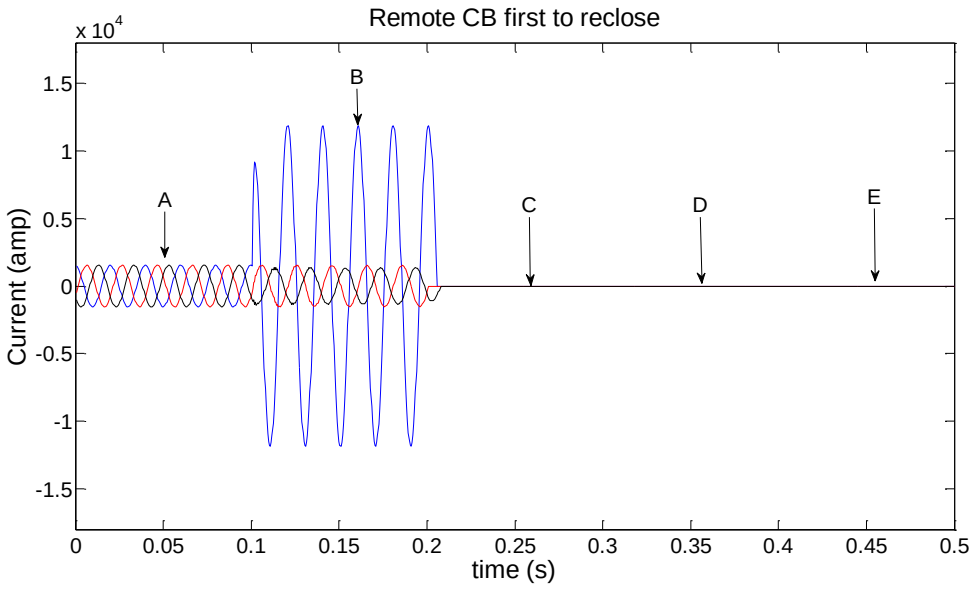

Figure 5.5. Currents for remote CB reclosing first for permanent fault (TPAR)

In both SPAR and TPAR schemes (refer to Figures 5.2 to 5.5), there are effectively five individual system states for a permanent fault scenario, as follows:

- State A: Pre-fault, both line end circuit breakers closed
- State B: During fault state, both circuit breakers remain closed
- State C: Isolation, both circuit breakers opened, fault cleared
- State D: One circuit breaker reclosed, other remains open ("dead-line charging state").
- State E: Isolation, the reclosed circuit breaker trips again in response to the presence of a permanent fault.

States A, B and D are the most interesting states from the perspective of the developed fault location algorithm. Consequently, it is proposed to simplify the fault location system and only analyse states A, B and D, which are re-denoted as the

pre-fault state, state 1 and state 2. During operation of the auto-reclose scheme, state 2 can differ because of the different possible operation sequences of the circuit breakers.

5.3 Transmission line model for auto-reclose scheme operation

The proposed fault location algorithm described in this chapter is designed for a double-ended transmission line, which is representative of the vast majority of interconnected transmission system applications. The superposition method has been applied in both state 1 and state 2 calculations. The calculation approach used for the auto reclosing states is analogous to the interpole state analysis presented earlier in chapter 4. However, in order to improve the accuracy of transmission line modelling, the distributed line model has been used instead of a lumped line model in this section. The method is applicable for all fault types by changing the elements of the fault matrix **K**, which has been introduced in section 4.2.2.1. As for the previous chapter, operation for a single phase to earth fault is presented as an example, as this is the predominant type of fault in overhead lines. The performance of the method for other fault types will be presented and evaluated in Chapter 6. As before, the method relies on the comparison of calculated states (based on the impedance model) with actual measurements taken during each state. This section describes how the various system states are modelled.

5.3.1 State 1 calculation

There are four different situations that must be considered for the operation of an auto-reclose scheme on a transmission line (as depicted in Figure 5.2 to Figure 5.5). In state 1, circuit breakers at both ends remain closed. Thus, the state 1 simulation for all situations is identical.

According to superposition theory, the state 1 network (during fault state) can be represented as the sum of the pre-fault state network and the superimposed network, as shown in Figure 5.6. In the pre-fault network, $\mathbf{V_L}$ and $\mathbf{V_R}$ are the local and remote end voltages. Using the equations (5.1) and (5.2), $\mathbf{V_R}$ and $\mathbf{I_R}$ can be determined. $\mathbf{Z_c}$ and $\boldsymbol{\gamma}$ are the surge impedance and the propagation constant of the transmission line and *d* is length of the transmission line.

$$\mathbf{V_L} = \mathbf{A}\mathbf{V_R} + \mathbf{B}\mathbf{I_R} \tag{5.1}$$

$$\mathbf{I_L} = \mathbf{C}\mathbf{V_R} + \mathbf{D}\mathbf{I_R} \tag{5.2}$$

Where, $\mathbf{A} = \mathbf{D} = \mathbf{cosh}\,\boldsymbol{\gamma} d\,, \mathbf{B} = \mathbf{Z_c} \cdot \mathbf{sinh}\,\boldsymbol{\gamma} d\,, \mathbf{C} = \frac{\mathbf{1}}{\mathbf{Zc}}\mathbf{sinh}\,\boldsymbol{\gamma} d$

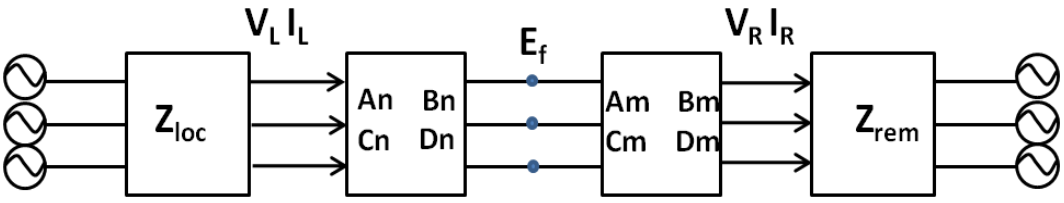

a). pre-fault network

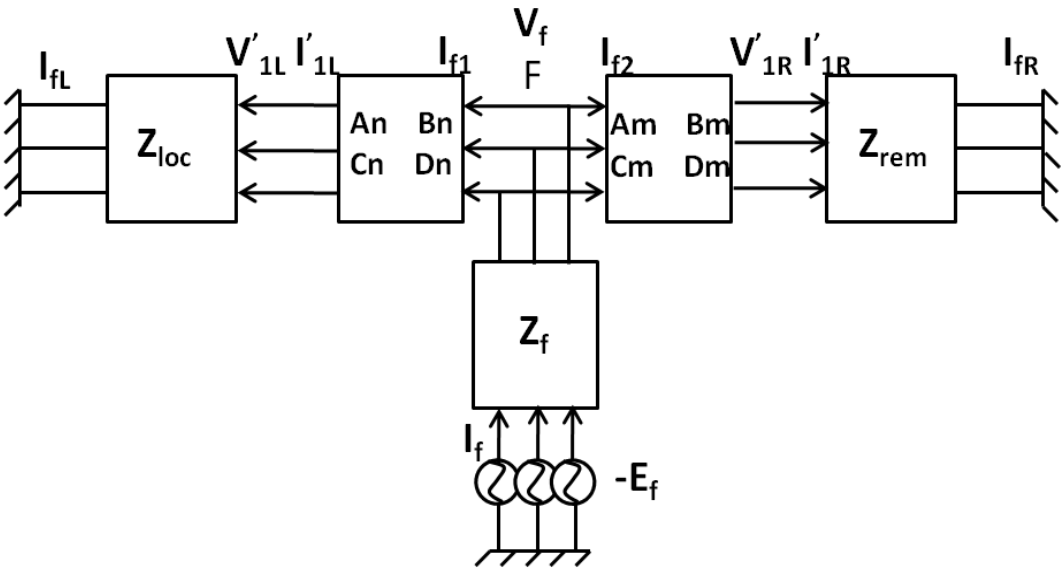

b). superimposed network

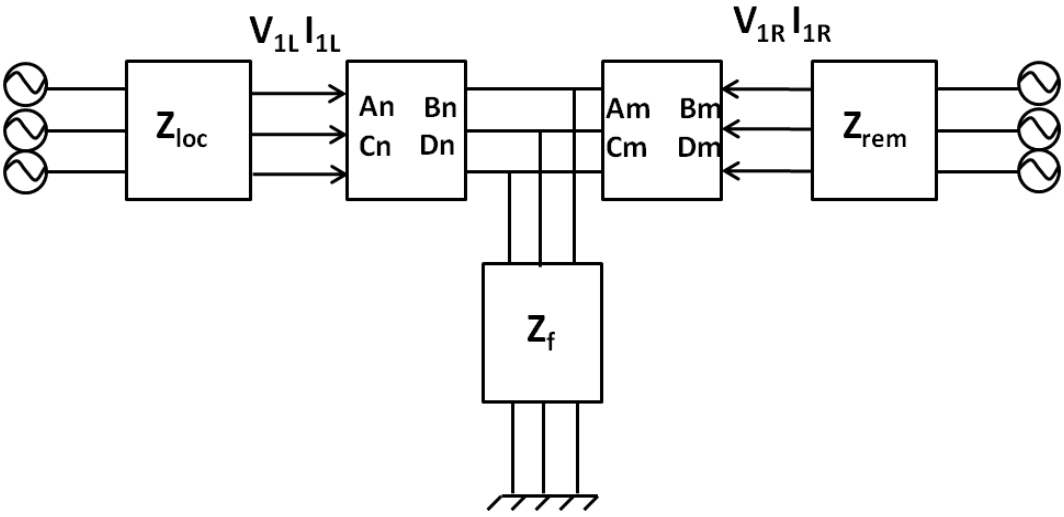

c). Faulted network

Figure 5.6. State 1 calculation using superposition theory

The pre-fault network is separated into two sections at the fault point, which are:

- the local end to fault point section $\begin{bmatrix} \mathbf{A_n} & \mathbf{B_n} \\ \mathbf{C_n} & \mathbf{D_n} \end{bmatrix}$ and;
- fault point to remote end section $\begin{bmatrix} \mathbf{A_m} & \mathbf{B_m} \\ \mathbf{C_m} & \mathbf{D_m} \end{bmatrix}$.

Where, $\mathbf{A_n} = \mathbf{D_n} = \mathbf{cosh}\,\boldsymbol{\gamma} nd;$

$\mathbf{B_n} = \mathbf{Z_c} \cdot \mathbf{sinh}\,\boldsymbol{\gamma} nd \ \ \Omega;$

$\mathbf{C_n} = \frac{\mathbf{1}}{\mathbf{Zc}} \mathbf{sinh}\,\boldsymbol{\gamma} nd \ \ \Omega^{-1};$

$\mathbf{A_m} = \mathbf{D_m} = \mathbf{cosh}\,\boldsymbol{\gamma}(1-n)d \ \ ;$

$\mathbf{B_m} = \mathbf{Z_c} \cdot \mathbf{sinh}\,\boldsymbol{\gamma}(1-n)d \ \ \Omega;$

$\mathbf{C_m} = \frac{\mathbf{1}}{\mathbf{Zc}} \mathbf{sinh}\,\boldsymbol{\gamma}(1-n)d \ \ \Omega^{-1};$

n is the fault location as a fraction of the total line length.

$\mathbf{E_f}$ is the voltage at the fault point in pre-fault network, which is equal to:

$$\mathbf{E_f} = \mathbf{A_n V_L} - \mathbf{B_n I_L} \tag{5.3}$$

In the superposition network (Figure 5.6b), the local end and remote end voltages are zero. Considering the distributed network from the fault point to both local and remote ends, the following relationships (5.4) and (5.5) may be obtained:

$$\begin{bmatrix} \mathbf{V_f} \\ \mathbf{I_{f1}} \end{bmatrix} = \begin{bmatrix} \mathbf{A_L} & \mathbf{B_L} \\ \mathbf{C_L} & \mathbf{D_L} \end{bmatrix} \begin{bmatrix} \mathbf{0} \\ \mathbf{I_{fL}} \end{bmatrix} \tag{5.4}$$

$$\begin{bmatrix} \mathbf{V_f} \\ \mathbf{I_{f2}} \end{bmatrix} = \begin{bmatrix} \mathbf{A_R} & \mathbf{B_R} \\ \mathbf{C_R} & \mathbf{D_R} \end{bmatrix} \begin{bmatrix} \mathbf{0} \\ \mathbf{I_{fR}} \end{bmatrix} \tag{5.5}$$

Where: $\mathbf{A_L} = \mathbf{A_n}$,

$\mathbf{B_L} = \mathbf{A_n} + \mathbf{Z_{loc}}\mathbf{B_n}$,

$\mathbf{C_L} = \mathbf{C_n}$,

$\mathbf{D_L} = \mathbf{C_n} + \mathbf{Z_{loc}}\mathbf{D_n}$,

$\mathbf{A_R} = \mathbf{A_m}$,

$\mathbf{B_R} = \mathbf{A_m} + \mathbf{Z_{rem}}\mathbf{B_m}$,

$\mathbf{C_R} = \mathbf{C_m}$,

$\mathbf{D_R} = \mathbf{C_m} + \mathbf{Z_{rem}}\mathbf{D_m}$

From (5.4) and (5.5), $\mathbf{I_{f1}}$ and $\mathbf{I_{f2}}$ can be expressed as a function of $\mathbf{V_f}$

$$\mathbf{I_{f1}} = \mathbf{B_L}^{-1}\mathbf{D_L}\mathbf{V_f} \tag{5.6}$$

$$\mathbf{I_{f2}} = \mathbf{B_R}^{-1}\mathbf{D_R}\mathbf{V_f} \tag{5.7}$$

Considering the path from the fault point to earth we can derive:

$$\mathbf{I_f} = \mathbf{Y_f}(-\mathbf{E_f} - \mathbf{V_f}) \tag{5.8}$$

$$\mathbf{I_f} = \mathbf{I_{f1}} + \mathbf{I_{f2}} \tag{5.9}$$

$$\mathbf{Y_f} = R_f^{-1}\mathbf{K} \tag{5.10}$$

By combining the above equations (5.6) to (5.10), $\mathbf{V_f}$ and $\mathbf{I_{f1}}$ can be resolved. Consequently, the local end voltage and current in the superimposed network are:

$$\begin{bmatrix} \mathbf{V'_{1L}} \\ \mathbf{I'_{1L}} \end{bmatrix} = \begin{bmatrix} \mathbf{A_n} & \mathbf{B_n} \\ \mathbf{C_n} & \mathbf{D_n} \end{bmatrix} \begin{bmatrix} \mathbf{V_f} \\ -\mathbf{I_{f1}} \end{bmatrix} \tag{5.11}$$

The remote end voltage and current in the superimposed network are:

$$\begin{bmatrix} \mathbf{V'_{1R}} \\ \mathbf{I'_{1R}} \end{bmatrix} = \begin{bmatrix} \mathbf{A_m} & \mathbf{B_m} \\ \mathbf{C_m} & \mathbf{D_m} \end{bmatrix} \begin{bmatrix} \mathbf{V_f} \\ -\mathbf{I_{f2}} \end{bmatrix} \tag{5.12}$$

According to the superposition theory, the local voltage $\mathbf{V_{1L}}$ and current $\mathbf{I_{1L}}$ in state 1 are:

$$\mathbf{V_{1L}} = \mathbf{V_L} + \mathbf{V'_{1L}} \tag{5.13}$$

$$\mathbf{I_{1L}} = \mathbf{I_L} + \mathbf{I'_{1L}} \tag{5.14}$$

The remote voltage $\mathbf{V_{1R}}$ and current $\mathbf{I_{1R}}$ in state 1 are:

$$\mathbf{V_{1R}} = \mathbf{V_R} + \mathbf{V'_{1R}} \tag{5.15}$$

$$\mathbf{I_{1R}} = \mathbf{I_R} + \mathbf{I'_{1R}} \tag{5.16}$$

5.3.2 State 2 calculation

In state 2, both SPAR and TPAR schemes have two possible situations depending on which of the line end circuit breakers recloses first. In summary, there are four possible scenarios that may occur in state 2, which are categorised as A, B, C and D scenarios, as follows:

A. SPAR local end recloses first;

B. SPAR remote end recloses first;

C. TPAR local end recloses first;

D. TPAR remote end recloses first.

5.3.2.1 SPAR with local end CB reclosing first

In this scenario, the faulty phase of the remote circuit breaker is open and the local circuit breaker remains closed (after reclosing). Superposition theory has been applied in this situation. As shown in Figure 5.7, the state 2 network is the sum of state 1 and state 2 superimposed networks.

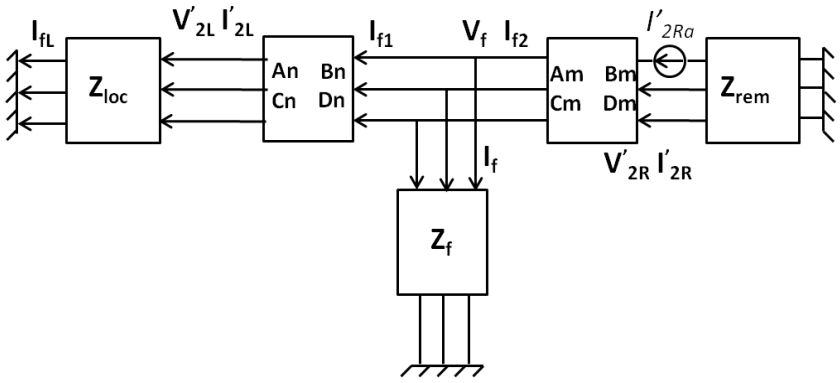

a) State 2 superimposed network

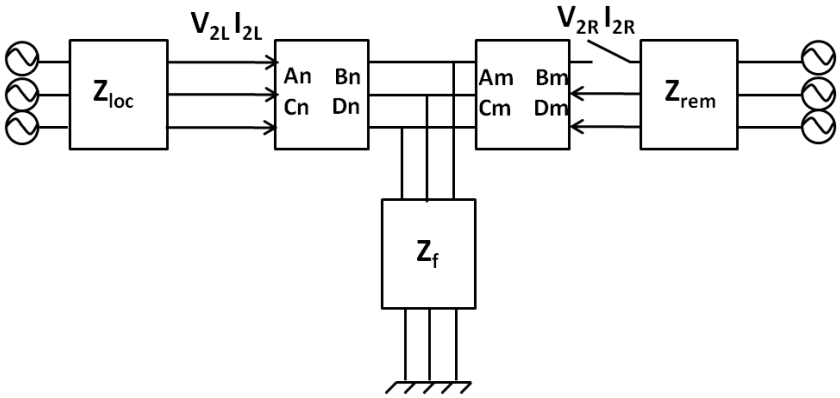

b) State 2 network during reclose

Figure 5.7. Scenario of SPAR with local CB reclosing first

In the state 2 superimposed network, the tripped pole of the circuit breaker is represented as a controlled current source, with the current equal to:

$$\mathbf{I'_{2R}}(1) = -I_{1Ra} \tag{5.17}$$

In Figure 5.7a, the distributed network section from the fault point to the local end is represented as:

$$\begin{bmatrix} \mathbf{V_f} \\ \mathbf{I_{f1}} \end{bmatrix} = \begin{bmatrix} \mathbf{A_L} & \mathbf{B_L} \\ \mathbf{C_L} & \mathbf{D_L} \end{bmatrix} \begin{bmatrix} \mathbf{0} \\ \mathbf{I_{FL}} \end{bmatrix} \tag{5.18}$$

Where, $\mathbf{A_L} = \mathbf{A_n}$,

$\mathbf{B_L} = \mathbf{A_n} + \mathbf{Z_{loc}}\mathbf{B_n}$,

$\mathbf{C_L} = \mathbf{C_n}$,

$\mathbf{D_L} = \mathbf{C_n} + \mathbf{Z_{loc}}\mathbf{D_n}$

The fault path from the fault point to earth is represented as:

$$\mathbf{I_f} = \mathbf{Y_f}\mathbf{V_f} = R_f^{-1}\mathbf{K}\mathbf{V_f} \tag{5.19}$$

$$\mathbf{I_{f1}} = \mathbf{D_L}\mathbf{B_L^{-1}}\mathbf{V_f} \tag{5.20}$$

From (5.19) and (5.20) we can obtain:

$$\mathbf{I_{f2}} = \mathbf{I_{f1}} + \mathbf{I_f} = \left(R_f^{-1}\mathbf{K} + \mathbf{D_L}\mathbf{B_L^{-1}}\right)\mathbf{V_f} \tag{5.21}$$

The network section from the remote relay point to the fault point is represented as:

$$\mathbf{V'_{2R}} = \mathbf{A_m V_f} + \mathbf{B_m I_{f2}} \tag{5.22}$$

$$\mathbf{I'_{2R}} = \mathbf{C_m V_f} + \mathbf{D_m I_{f2}} \tag{5.23}$$

Eliminating $\mathbf{V_f}$ from (5.22) and (5.23) and using (5.21) gives:

$$\mathbf{V'_{2R}} = \mathbf{X}\,\mathbf{I_{f2}} \tag{5.24}$$

$$\mathbf{I'_{2R}} = \mathbf{Y}\,\mathbf{I_{f2}} \tag{5.25}$$

Where, $\mathbf{I_{f2}}$ is 3×1 matrix and **X, Y** are 3×3 matrixes, represented as:

$$\mathbf{X} = [{R_f}^{-1}\mathbf{K} + \mathbf{D_L}\mathbf{B_L}^{-1}]^{-1}\mathbf{A_m} + \mathbf{B_m} \tag{5.26}$$

$$\mathbf{Y} = [{R_f}^{-1}\mathbf{K} + \mathbf{D_L}\mathbf{B_L}^{-1}]^{-1}\mathbf{C_m} + \mathbf{D_m} \tag{5.27}$$

X and **Y** depend on *n*, R_f and $\mathbf{Z_{rem.}}$ Note that $\mathbf{Z_{rem}}$ is the remote end source impedance which can be calculated from *SCL2*. Assuming *n*, R_f and $\mathbf{Z_{rem}}$ are known, $\mathbf{V_f}$ can be solved using equations (5.17), (5.21), (5.24) to (5.27).

In the superimposed network, the network section from the fault point to the local end can be represented as:

$$\begin{bmatrix}\mathbf{V_f}\\ \mathbf{I_{f1}}\end{bmatrix} = \begin{bmatrix}\mathbf{A_L} & \mathbf{B_L}\\ \mathbf{C_L} & \mathbf{D_L}\end{bmatrix}\begin{bmatrix}\mathbf{0}\\ \mathbf{I'_{2L}}\end{bmatrix} \tag{5.28}$$

It is assumed that $\mathbf{I'_{2L}} = \mathbf{I_{fL}}$. Equation (5.28) can be solved for $\mathbf{I'_{2L}}$, and

consequently, $\mathbf{V'_{2L}} = \mathbf{Z_{loc}}\mathbf{I'_{2L}}$. According to superposition theory, the local voltage $\mathbf{V_{2L}}$ and current $\mathbf{I_{2L}}$ in state 2 are:

$$\mathbf{V_{2L}} = \mathbf{V_{1L}} + \mathbf{V'_{2L}} \tag{5.29}$$

$$\mathbf{I_{2L}} = \mathbf{I_{1L}} + \mathbf{I'_{2L}} \tag{5.30}$$

5.3.2.2 Situations B, C and D

The calculation of situation A, which is SPAR with local end CB reclosing first, has been introduced. The calculations used in other situations (B, C and D) are similar to situation A. Open CBs are represented as current sources and the superposition method is applied to derive the voltage and current phasors. The detailed solutions for situation B, C and D are included in Appendix C.

Accordingly, the local voltage and current during both states 1 and 2 can be estimated assuming the values of n, R_f and *SCL2* are known. This is the basis of the novel fault location method; when the local voltages and currents match the model-estimated values, then the corresponding n, R_f and *SCL2* can be estimated with high accuracy. Analogous calculations are also possible for all fault types by changing the elements in fault matrix **K** (4.2).

5.4 Fault location process and algorithm

5.4.1 Basic principle

There are three main elements within the algorithm: fault data processing; initial range estimation; and final fault location estimation. As the basic concept of this method is similar to the fault location technique based on interopole states, the algorithm has been shown in Figure 4.8.

The fault data processing element extracts the fundamental frequency phasor from the actual sampled fault recorder data. In this research, the frequency phasor is extracted by applying the weighted LSM method [15], which is explained in Appendix A2.

The initial range estimation element which narrows down the search space by establishing initial ranges of n, R_f and $SCL2$ using simulated data, has been utilised in this algorithm. The details of initial range estimation have been introduced in section 4.3.2. This reduces the computational burden of the method.

Similar to the fault location algorithm based on interpole states, the fault location element itself comprises three main stages of operation, which are transmission line modelling, comparison and storing of interim outputs for use in the following states. Transmission line modelling has been described in section 5.3, which estimates local voltage and current for various combination groups of n, R_f *and* $SCL2$.

Both voltage and current are used for comparison between simulated data and algorithm-calculated phasor data. This comparison is applied separately to magnitude and angle of the complex phasors, which has been shown in (4.43) and (4.44). The tolerance used in the comparison determines the number of candidate solutions (each solution comprising a value for R_f, *SCL2* and *n*). Greater tolerances will result in a greater number of candidate solutions. The tolerance is iteratively increased from an initial setting value until the number of candidate solutions at each state is greater than a certain value. In the following case study, the initial comparison tolerance is set to 0.1% and the minimum number of candidate solutions for state 1 and state 2 are 100 and 10 respectively.

The modelling, comparison and storing stages are repeated until the solution is found and the comparison condition is satisfied. As progress through each of the states is made, the possible ranges of locations reduce and the final accurate fault location is obtained.

In the initial fault location technique developed through this research, which analysed only initial circuit breaker opening with no consideration of auto-reclose states (introduced in chapter 4), the final result is obtained by applying an averaging method of the candidates remaining after the final state, and the accurate results from numerous evaluations have proven the effectiveness of the method. In this method reported in this chapter, which extends analysis to include auto reclose operations, the results are again obtained by averaging the values remaining at the final state.

5.4.2 Summary of operation of the fault location estimation system

The operation of the fault location system which includes analysis of auto reclose operational states can be summarised as follows:

1. Obtain state 1 simulated data from a record of the actual event or CT/VT outputs in real time (during development and systematic performance assessment, EMTP/ATP simulated results are used at this stage).
2. Pre-estimate R_f, *SCL2* and *n* ranges using state 1 simulated data.
3. Select the corresponding situation according to auto-reclose scheme operation – in practical implementation this information could be derived by the protection relay algorithm or else from external indications (e.g. circuit breaker status).
4. Simulate the network in state 1 using the impedance-based model applying systematically *n*, *SCL2* and R_f values from the pre-estimated ranges.
5. Compare the simulation outputs with the calculated data and record the values of *n*, *SCL* and R_f if the result falls within the assumed comparison error.
6. Repeat steps 4 and 5 until the whole range of *n*, *SCL* and R_f have been covered.
7. Obtain updated ranges which cover all possible values for *n*, *SCL* and R_f.
8. Obtain simulated data for state 2 and repeat steps 4-6 until the final possible ranges of fault location *n*, *SCL2* and R_f generated by step 7 have been covered.
9. Update the ranges of *n*, *SCL2* and R_f.
10. Through application of the averaging process, the final values of *n*, *SCL2* and R_f are obtained

Note:

- *SCL1*is assumed to be a known input parameter in the transmission line modelling process used by the developed method. The influence of inaccurate *SCL1* will be discussed in Chapter 6.
- The ranges and increment settings of *n, SCL2* and R_f are currently set as listed:
    - Fault position *n*: 0-100% of line length in steps of 0.1%
    - Remote source short circuit level *SCL*: 5-30 GVA in steps of 0.5GVA
    - Fault resistance R_f : 0.1Ω. The selections of the increment settings will be discussed in Chapter 6.

5.5 Case study

In this section, ATP simulated data is used to evaluate the performance of the proposed fault location algorithm. A modified Least Squared Method introduced in chapter 2 is applied to extract the fundamental frequency phasors from the EMTP/ATP generated waveforms.

A double supplied transmission line model has been utilised. The voltage level is 400kV; the length is 100km; *SCL1* is set as 5GVA and the X/R ratio of both local and remote ends is 30**.** The zero sequence line impedance Z_{L0}=(0.10+*j*0.76)Ω/km and the positive sequence line impedance is Z_{L1}=(0.02+*j*0.25)Ω/km. The zero shunt capacitance is Y_{L0}=(0+*j*2.5) μS/km and positive shunt capacitance is Y_{L1}=(0+*j*4.7) μS/km. The model is similar to the one in section 4.4, but utilises the distributed line model which covers the effect of shunt capacitance.

5.5.1 Example fault location estimation

In the example, the fault position is assumed at 50km (50% of line length from measurement point), the fault resistance R_f is set as 5Ω, the remote end short circuit level is set as 15GVA and load angle is 10^o. In this example, the increments of n, R_f and *SCL2* are 0.1km, 0.1Ω and 0.5GVA respectively. The example is based on an SPAR scheme, assuming that the local end recloses first. Figure 5.8 illustrates the local three phase current produced by the ATP simulation.

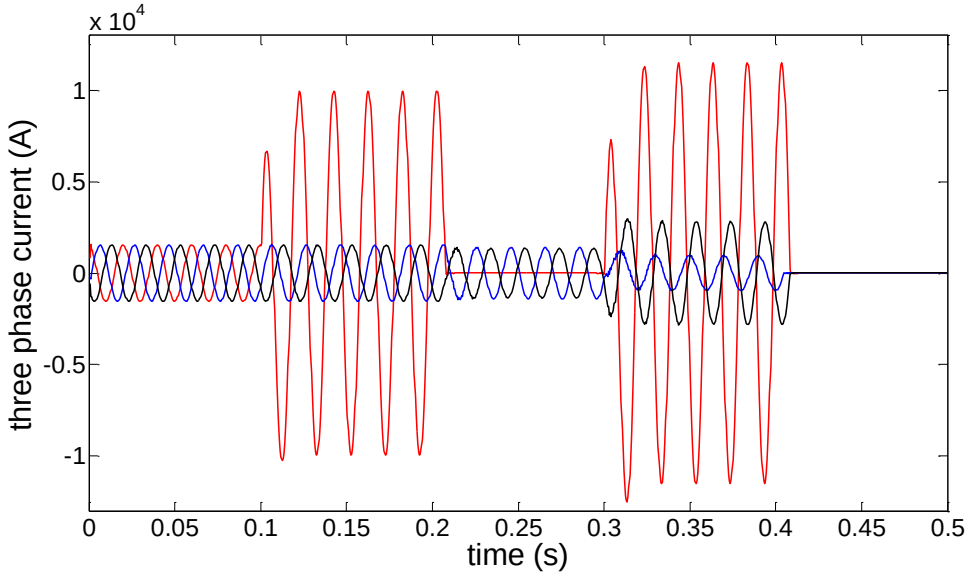

Figure 5.8. Three phase currents for auto-reclose example

Table 5.1 presents the progression and convergence of the estimated ranges of values during the state-by-state estimation process.

	Pre-estimated range	State 1 range	State 2 range	Averaged value
n (%)	25.10–75.10	44.30–57.20	49.40–50.50	44.95
R_f (Ω)	3–7	3.7–6.3	4.8–5.3	4.90
SCL2 (GVA)	5–30	12–20	15–15	15.0

Table 5.1. Results of fault location estimation system

It is clear that each progression produces a drastic reduction in the number of candidates. In this example, the final output value is computed by averaging the 11 candidates from state 2.

5.5.2 Systematic performance evaluation

In order to systematically assess the performance of the proposed auto-reclose based fault location method, all possible auto-reclose scheme scenarios have been simulated (i.e. SPAR LOCAL, SPAR REMOTE, TPAR LOCAL, and TPAR REMOTE - note that, for example, SPAR LOCAL denotes a SPAR scheme where the local end CB recloses first). In each auto-reclose scheme all possible fault positions (from 0%-100% of protected line) and fault resistances (from 0-100Ω) were considered. *SCL2* is set as 15GVA in the simulation in this section. In theory, the varying of *SCL2* does not affect the fault location accuracy of the proposed method. The evaluations of varying the values of *SCL2* are carried out in Chapter 6. The estimated fault location errors used in this chapter are defined as

$$Error = \frac{estimated\ fault\ location - actual\ fault\ location}{line\ length} \times 100\% \qquad (5.31)$$

Figure 5.9 to Figure 5.12 illustrates the performance for all considered cases and Takagi method. It is clear that the proposed method can achieve very high accuracy in the majority of situations, with average error being well under 1% (often under 0.1%) in all cases. It is only in scenarios where R_f and n are high (representative of high resistance faults close to the remote end of the line) that relatively larger errors (up to 1%) are encountered. In Chapter 6, evaluations of possible negative factors, in terms variations of R_f and *SCL2*, inaccurate *SCL1* settings and measurement error, will be carried out.

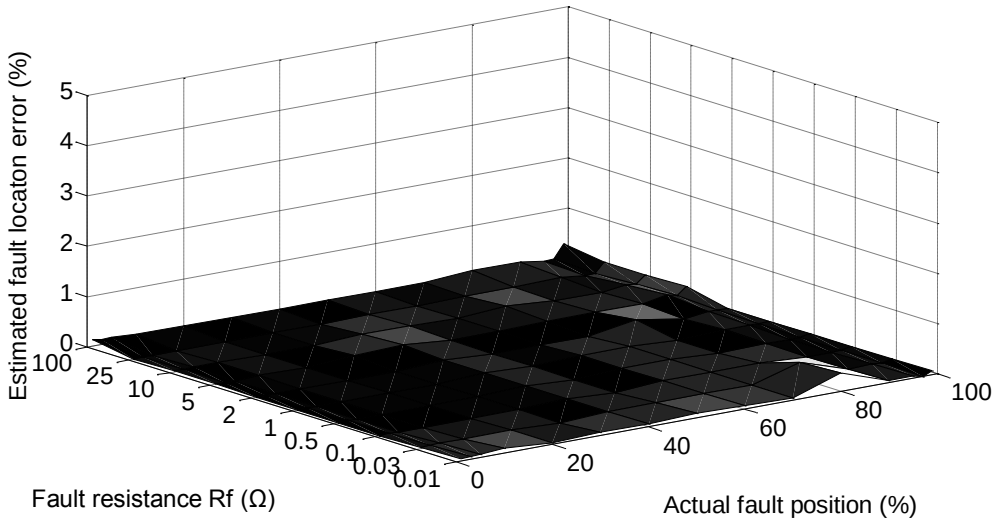

Figure 5.9. Results of SPAR local

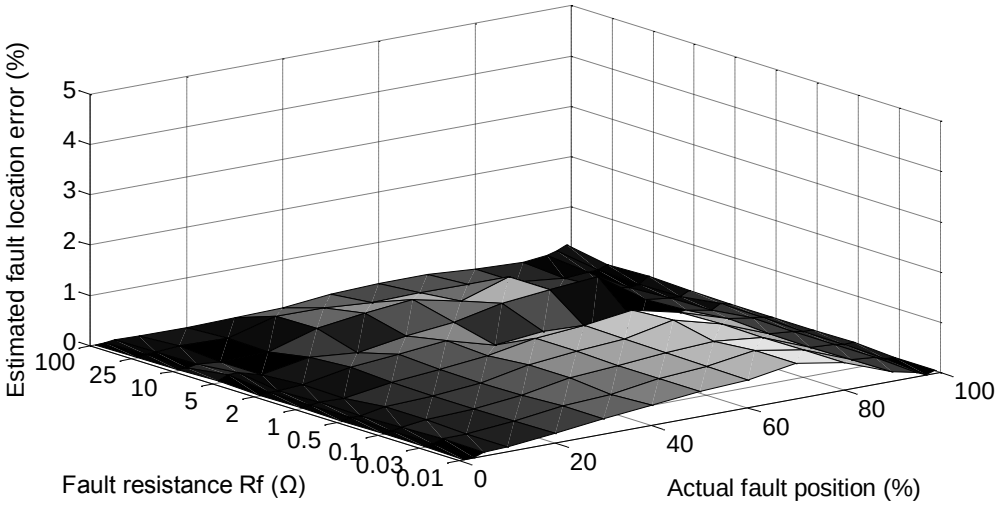

Figure 5.10. Results of SPAR remote

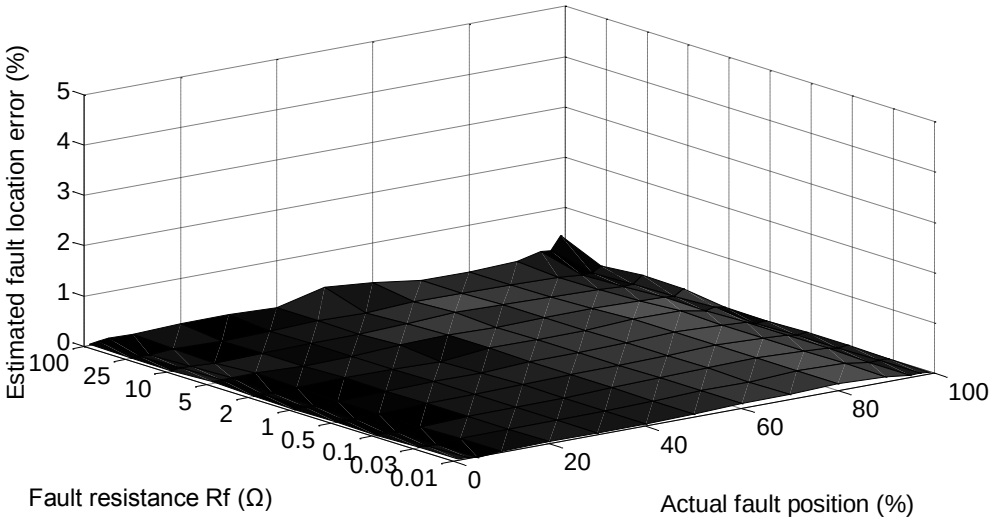

Figure 5.11. Results of TPAR local

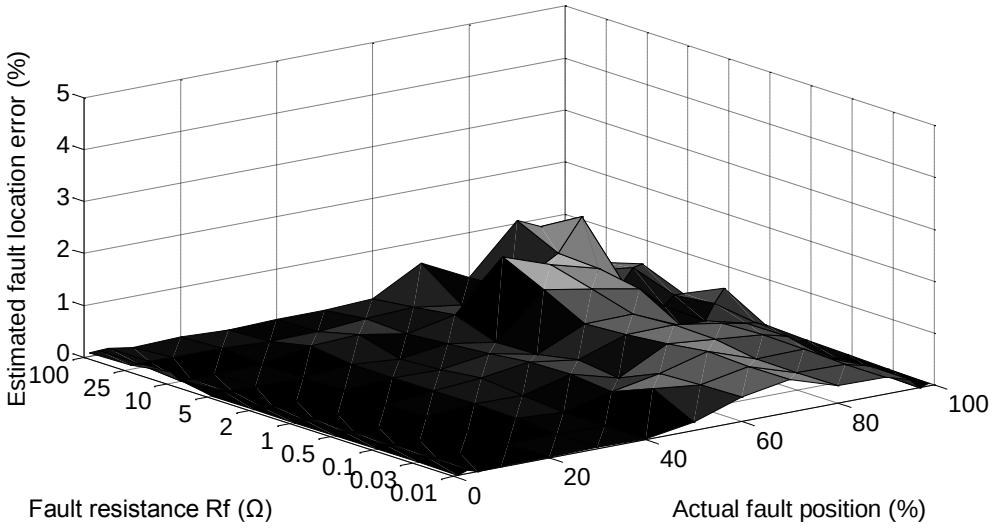

Figure 5.12. Results of TPAR remote

5.6 Conclusion

A novel fault location algorithm, which analyses the different states arising during the operation of the auto-reclose schemes, has been developed. It compares calculated data with simulated data and iteratively proceeds until a match is found within a specified tolerance error. The ranges of all possible values are reduced through the analysis of the consecutive auto-reclose scheme stages. When a match is found within the specified tolerance, all possible fault locations, fault resistances and remote source impedances are recorded. The most possible fault positions are obtained at the final state and an averaging technique is used to select the final output value. The algorithm is based on a single ended data and can not only eliminate, but also quantify, the negative effects of conventional single ended methods.

5.7 Reference

[1] J. L, *et al.*, "Improving fault location by analysis of electric parameters during circuit breaker operation," presented at the PSCC, Stockholm Sweden, 2011.

[2] A. I. Megahed, *et al.*, "Development of an adaptive single-pole auto-reclosure scheme for Alexandria HV transmission system," in *Transmission and Distribution Conference and Exposition, 2003 IEEE PES*, 2003, pp. 309-314 Vol.1.

[3] A. T. Johns and A. M. Al-Rawi, "Digital simulation of EHV systems under secondary arcing conditions associated with single-pole autoreclosure," *Generation, Transmission and Distribution, IEE Proceedings C*, vol. 129, pp. 49-58, 1982.

[4] G. Yaozhong, *et al.*, "Prediction methods for preventing single-phase reclosing on permanent fault," *Power Delivery, IEEE Transactions on*, vol. 4, pp. 114-121, 1989.

[5] A. Halim, *et al.*, "Auto-reclose performance on 275 kV and 132 kV transmission line in Malaysia," in *Transmission and Distribution Conference and Exhibition 2002: Asia Pacific. IEEE/PES*, 2002, pp. 603-608 vol.1.

[6] I. P. S. R. Committee, "Automatic Reclosing of Transmission Lines," *Power Apparatus and Systems, IEEE Transactions on*, vol. PAS-103, pp. 234-245, 1984.

[7] G. Ban, *et al.*, "Automatic reclosing of compact and uprated transmission lines," in *Electrotechnical Conference, 1998. MELECON 98., 9th Mediterranean*, 1998, pp. 954-958 vol.2.

[8] "IEEE Guide for Automatic Reclosing of Line Circuit Breakers for Ac Distribution and Transmission Lines," *IEEE Std C37.104-2002,* p. 0_1, 2003.

[9] R. Aggarwal, "Experience with advanced adaptive auto-control techniques for EHV transmission systems," in *HV Measurements, Condition Monitoring and Associated Database Handling Strategies (Ref. No. 1998/448), IEE Colloquium on*, 1998, pp. 6/1-6/4.

[10] "Single phase tripping and auto reclosing of transmission lines-IEEE Committee Report," *Power Delivery, IEEE Transactions on,* vol. 7, pp. 182-192, 1992.

[11] G. Yaozhong, *New techniques for protective relaying and fault location*. Xi'an China: Xi'an Jiaotong University Publisher, 2007.

[12] R. Nylen, "Auto-Reclosing," vol. Pamphlet RK85-201E Edition 1, 1979.

[13] A. Sang-Pil, *et al.*, "An alternative approach to adaptive single pole auto-reclosing in high voltage transmission systems based on variable dead time control," *Power Delivery, IEEE Transactions on*, vol. 16, pp. 676-686, 2001.

[14] F. GUO, *et al.*, "Time integrating improvement of Single Phase Reclose Scheme using Fiber-optic current differential protection," *Shanxi Electric Power*, vol. No.5(Ser. 141), pp. pp 15-17, 2007.

[15] E. Rosołowski, *et al.*, "Adaptive measuring algorithm suppressing a decaying DC component for digital protective relays," *Electric Power Systems Research*, vol. 60, pp. 99-105, 2001.

Chapter 6. Evaluation of sensitivity of auto-reclose based location to variations in input parameters

6.1 Introduction

A novel fault location algorithm, which analyses the different states arising during the operation of auto-reclose schemes, has been introduced in Chapter 5. It obtains fault location using only local end data. It is immune to changes in fault resistance and uncertainty and variability in remote end short circuit level. A number of case studies have illustrated the performance and accuracy of the method. As the the accuracy evaluation is carried out to assess the impact (possibly negative) of various primary system related factors, simulated data has been processed as from a perfect measurement instrument (i.e. sensor/sampling errors have not been included).

The increments of n, R_f and *SCL2* within the ranges used for these parameters obviously influences the accuracy of fault location error. All values in the ranges are multiple of the corresponding increments. However, the real values of each of the three target parameters may not be exact multiples of the increments, which causes a mismatch between the values of possible elements in the ranges and the actual values.

This can contribute to an error in the overall fault location accuracy. The selections of increments will be made by considering this effect in this chapter.

In this chapter, the performance of the proposed algorithm is evaluated in order to investigate the impact of factors that usually are detrimental to conventional single ended methods. These include variations in R_f and variations in *SCL2*. Comparisons between the Takagi method, the network impedance method and the proposed method will be carried out to show the improvements of the proposed method over both of the other methods.

*SCL1*is assumed to be a known input parameter in the transmission line modelling process used by the developed method, and this can be measured at the local end (or the data can be estimated using techniques reported in [1-3], or made available from the utility company). Inaccurate estimates of *SCL1* will introduce an error to the voltage and current calculations in the transmission line modelling stage. Additionally, the instrument transformers (CTs and VTs) are likely to introduce errors. The proposed fault location algorithm relies on the comparison of calculated voltage and current phasors (obtained from a transmission line impedance model) with the phasors extracted from the simulated waveforms. Therefore, the effects of both inaccurate *SCL1* and errors from measurement devices are investigated and quantified in this chapter.

The transmission line model used in Chapter 5 will be utilised in the evaluations in this chapter. The possible fault location in the simulation is from 0-100%. The value

of *SCL1* is required as a known input parameter to this algorithm; the value is set as 5GVA in all simulations of this chapter. The weighted least squares method [4] is applied to extract the fundamental frequency component from the EMTP/ATP generated waveforms. The details of this extraction algorithm are shown in Appendix A.

As all possible situations of auto-reclose scheme (i.e. SPAR LOCAL, SPAR REMOTE, TPAR LOCAL and TPAR REMOTE) are based on the same fault location principle and the single phase to earth fault is the most-likely fault type in practice the SPAR LOCAL is employed as the default situation in all evaluations reported in this chapter. The estimated fault location errors used in this chapter are defined as:

$$Error = \frac{(estimated\ fault\ location - actual\ fault\ location)}{line\ length} \times 100\% \qquad (6.1)$$

6.2 Selecting the increment values in the algorithm

As already stated, a mismatch between the values of possible elements in the ranges and in the actual values may lead to a fault location error and this is determined by the value of increment that is used. The value of maximum mismatch can reach half of the incremental value. In theory, smaller incremental values will result in higher fault location accuracy by reducing the magnitude of mismatch. However, the use of smaller incremental values for the possible locations of the fault will lead to longer

algorithm execution times. The selection of the value of the increment must, therefore, consider a trade-off between the algorithm execution time and accuracy.

6.2.1 Selecting the fault location increment value

It is clear that the value chosen for the fault location increment will directly determine the accuracy level of the results. Therefore, the optimal value of the fault position increment has been established through systematic simulation. The possible incremental value candidates of *n* were set to 1%, 0.5%, 0.1% and 0.01%. In order to quantify the effect of these increments on fault location accuracy, the value of *n,* which causes the maximum mismatch between the estimated and actual fault position, was used in the simulation (i.e. fault position was set in the midpoint between two adjacent increments). Table 6.1 presents various assumed incremental values and corresponding assumed faults positions along the line. In all simulations, R_f is set to 5Ω and *SCL2* is set to 15GVA.

	***n* increment (%)**			
	1%	**0.5%**	**0.1%**	**0.01%**
Simulated fault location (%)	1.5	1.25	1.05	1.005
	10.5	10.25	10.05	10.005
	35.5	35.25	35.05	35.005
	50.5	50.25	50.05	50.005
	75.5	75.25	75.05	75.005
	90.5	90.25	90.05	90.005
	99.5	99.25	99.05	99.005

Table 6.1 Simulation settings for the evaluations of *n* increment

Figure 6.1 shows the estimated fault location errors for the assumed values of *n* and its increment. In general, the results illustrate that the estimated fault location error increases as the increment setting increases. By summarising the performance for different incremental values, the maximum errors associated with increments of 1% and 0.5% are 1.35% and 0.87% respectively. Comparatively, the cases where the increments are 0.1% and 0.01% deliver much better fault location accuracy; the maximum errors in this case are 0.27% and 0.20% respectively. In the evaluation, as expected, the 0.01% case delivers the best results. However, the algorithm execution time for an incremental value of 0.01% case can be up to 10 times longer than the execution time for an incremental value of 0.1% (as the number of potential candidates to analyse increases by the same factor). At the same time the differences in the maximum error for these two cases are not significant enough to justify potential tenfold deterioration in calculation speed. Therefore, by considering both speed and accuracy of the proposed method, the increment of 0.1% was considered to achieve the optimal trade-off.

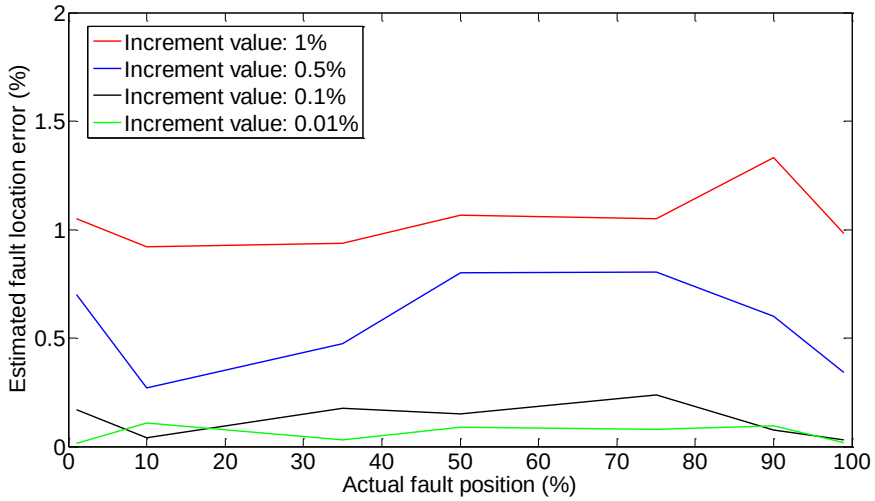

Figure 6.1 Impact of different *n* increments on the method accuracy

6.2.2 Selecting the fault resistance increment value

The possible incremental value candidates of R_f are set to 0.01Ω, 0.1Ω, 0.5Ω and 1Ω. In order to quantify the maximum effects on fault location accuracy that is introduced by these increments, the value of R_f, which causes the maximum mismatch is used in the simulation.

Table 6.2 presents incremental values and corresponding R_f settings in the simulation. The values R_f used in the simulation are categorised into three groups: groups A, B and C. As *SCL2* is an unknown parameter in the algorithm and the initial range is set from 5-30GVA, the investigation of the R_f increment will be executed for different *SCL2* values of 5GVA, 15GVA and 30GVA in the simulation.

Increment values (Ω)	R_f in simulation (Ω)		
	Group A	Group B	Group C
0.01	0.005	5.005	99.995
0.1	0.05	5.05	99.95
0.5	0.25	5.25	99.75
1	0.5	5.5	99.5

Table 6.2. Simulation settings for the evaluations of R_f increment

Figure 6.2 to Figure 6.4 show the estimated fault location errors of each group for different values of *SCL2*. Table 6.3 summarises the results in terms of maximum error. In general, both the figures and table illustrate that the estimated fault location error increases as the increment setting increases. Groups A, B and C represent different fault resistance levels. By summarising the performances fir different incremental values, the maximum errors associated with increments of 0.5Ω and 1Ω are 1.05% and 2.55% for all groups. Comparatively, the cases where the increments are 0.01Ω and 0.1Ω deliver relatively good fault location accuracy; the maximum errors of which are less than 0.27% and 0.36% for all groups. In the evaluation, the 0.01Ω case causes the minimum mismatch and delivers the best results. However, the algorithm execution times for an incremental value of 0.01Ω case can be up to 10 times the execution time for an incremental value of 0.1Ω, while there are no notable changes in the maximum errors for these two cases. Therefore, by considering both efficiency and accuracy of the proposed method, the R_f increment is set as 0.1Ω.

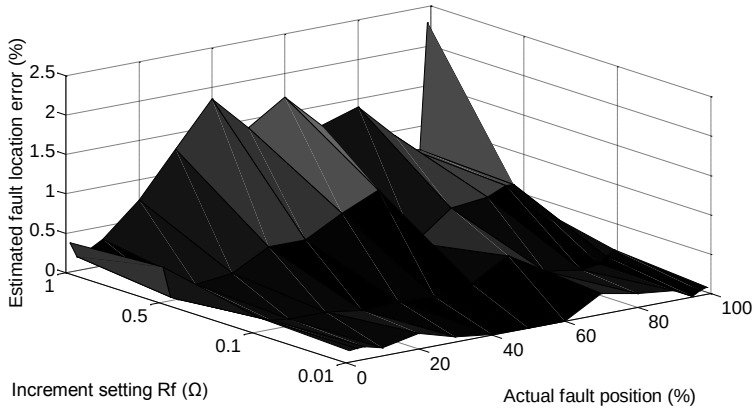

SCL2 = 5GVA

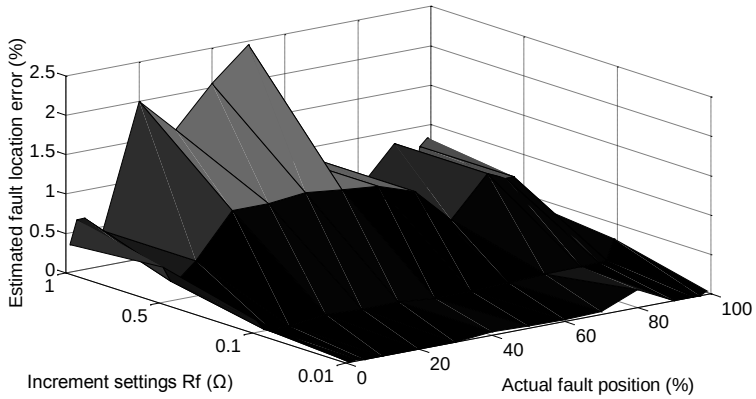

SCL2 = 15GVA

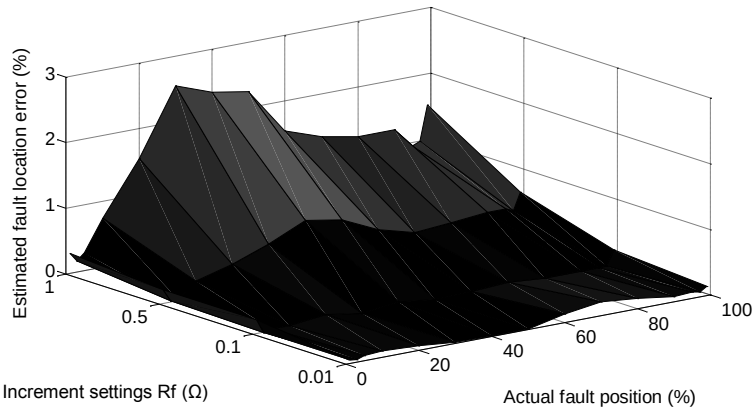

SCL2 = 30 GVA

Figure 6.2. Impact of different R_f increment on Group A

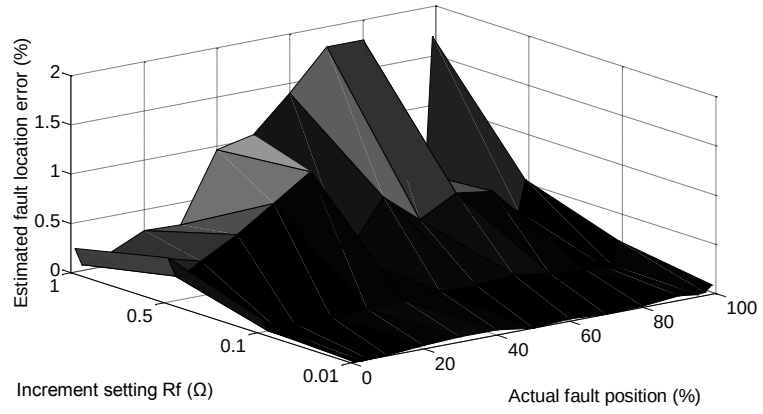

SCL2 = 5GVA

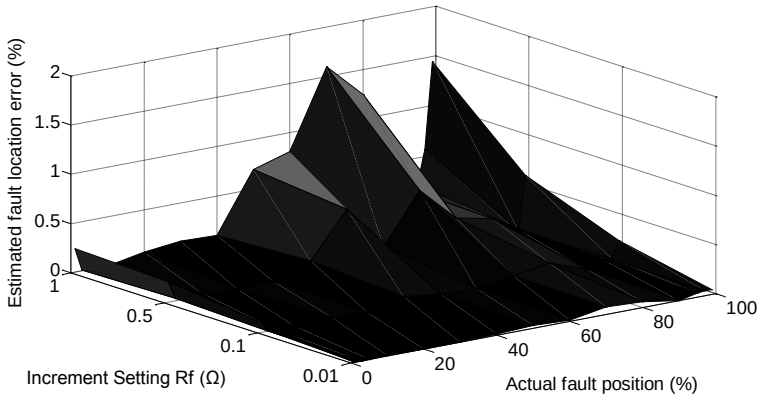

SCL2 = 15GVA

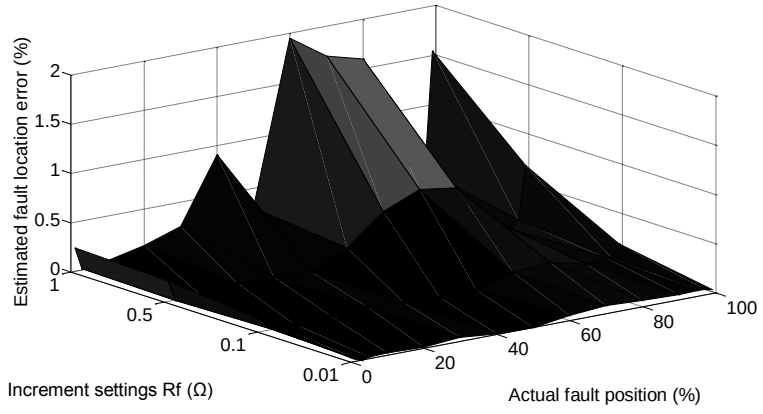

SCL2 = 30GVA

Figure 6.3. Impact of different R_f increment on Group B

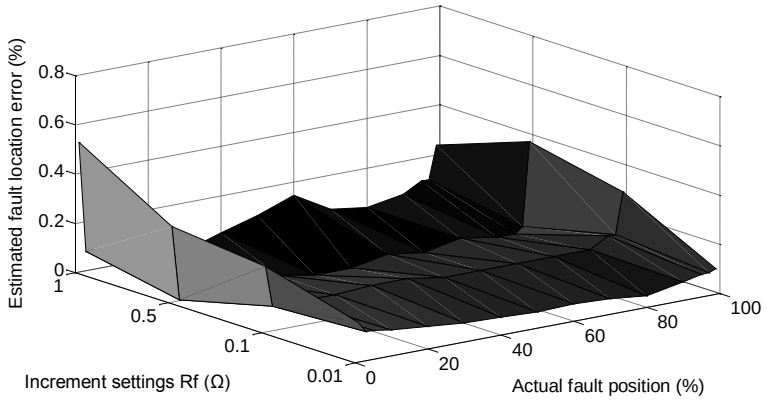

SCL2 = 5GVA

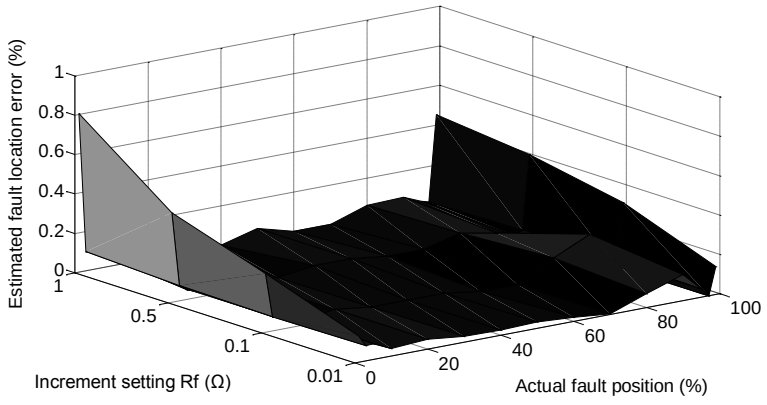

SCL2 = 15GVA

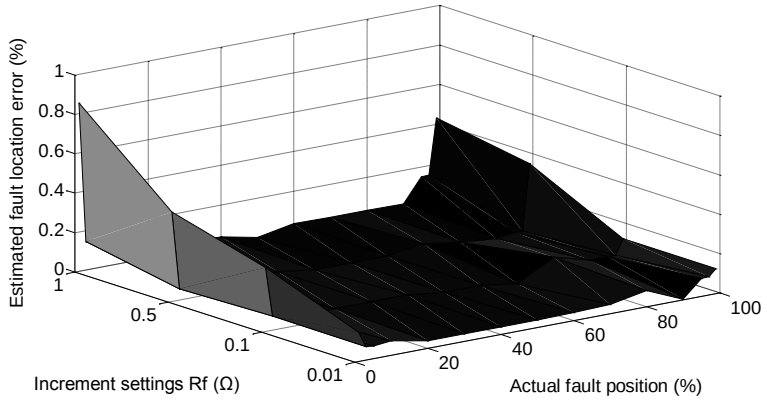

SCL2 = 30GVA

Figure 6.4. Impact of different R_f increment on Group C

Increment (Ω)	Maximum errors (%)								
	Group A			Group B			Group C		
	5 GVA	15 GVA	30 GVA	5 GVA	15 GVA	30 GVA	5 GVA	15 GVA	30 GVA
0.01	0.27	0.22	0.21	0.1	0.08	0.08	0.16	0.14	0.13
0.1	0.34	0.32	0.24	0.24	0.24	0.20	0.32	0.30	0.31
0.5	0.9	1.05	0.85	0.85	0.65	0.69	0.50	0.45	0.45
1	2.35	2.45	2.55	1.8	1.60	1.85	0.52	0.81	0.85

Table 6.3. Results of R_f increment evaluation

6.2.3 Selecting the remote end short circuit level increment value

It is clear that the *SCL2* increment may influence the results of the proposed method. To investigate this, the possible increment candidates of *SCL2* are set as 0.25GVA, 0.5GVA, 1GVA and 2GVA. In order to achieve the maximum effect on fault location accuracy introduced by increments, the value of *SCL2* which is associated with the maximum mismatches will be used in the simulation.

Table 6.4 presents the list of incremental values and corresponding possible *SCL2* settings in the simulation. The *SCL2* values used in the simulation are also categorised into three groups: A, B and C. The initial range of *SCL2* is 5-30GVA.

The investigation of the impact of the incremental value of *SCL2* is carried out for different values of R_f: 0.1Ω, 5Ω and 100Ω in each group.

Increments (GVA)	*SCL2* in simulation		
	Group A	Group B	Group C
0.25	5.125	15.125	29.125
0.5	5.25	15.25	29.25
1	5.5	15.5	29.5
2	6	16	30

Table 6.4. Simulation settings for the evaluations of *SCL2* increment

Figure 6.5 to Figure 6.7 show the estimated fault location errors for each group with different R_f values. Table 6.5 summarises the results by using the maximum error. In general, both the figures and table illustrate that the estimated fault location error increases with the magnitude of increment values. Group A, B and C represents different remote end short circuit level levels. The maximum errors brought by 1GVA and 2GVA are 5.33% and 8.00% for all groups. Comparatively, the increment setting of 0.25GVA and 0.5GVA delivers good results, the maximum fault location errors are less than 0.50% and 0.57% for all groups. In the evaluation, the 0.25GVA increment causes the minimum mismatch and brings the best results. However, the algorithm executing time of 0.25GVA case can be double that of 0.5GVA, while

there are no significant changes of errors brought by such two cases. Therefore, by considering both efficiency and accuracy of the proposed method, the *SCL2* increment is set as 0.5GVA.

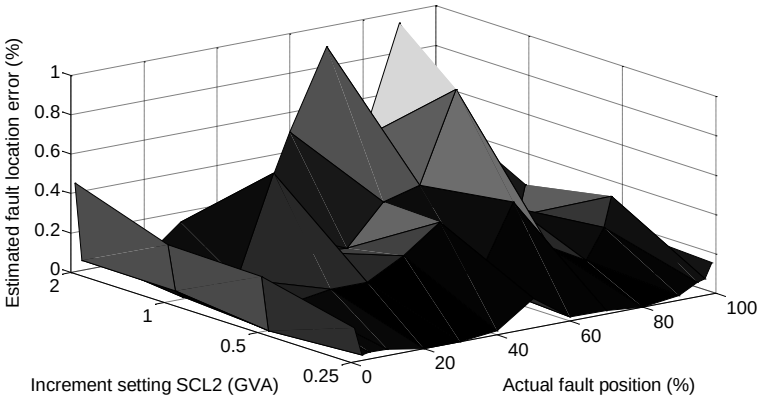

R_f=0.1Ω

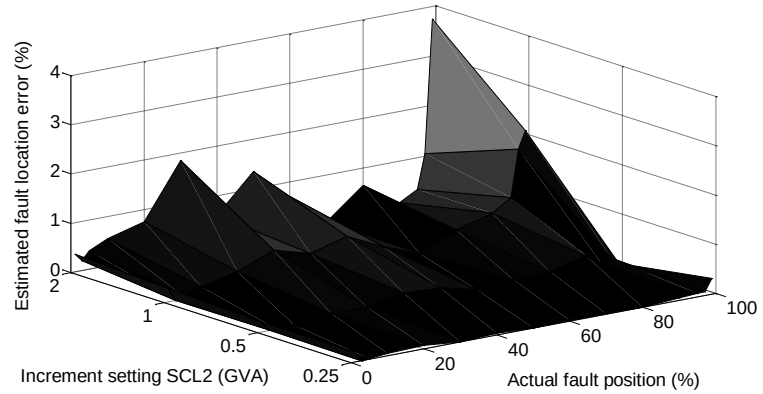

R_f=5Ω

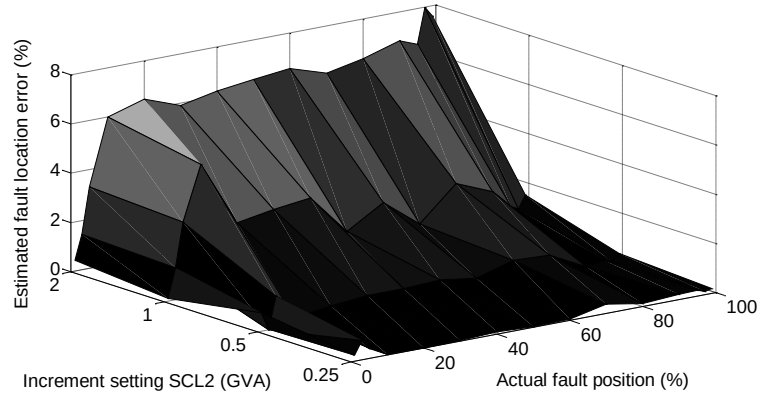

R_f=100Ω

Figure 6.5. Impact of different *SCL2* increment on Group A

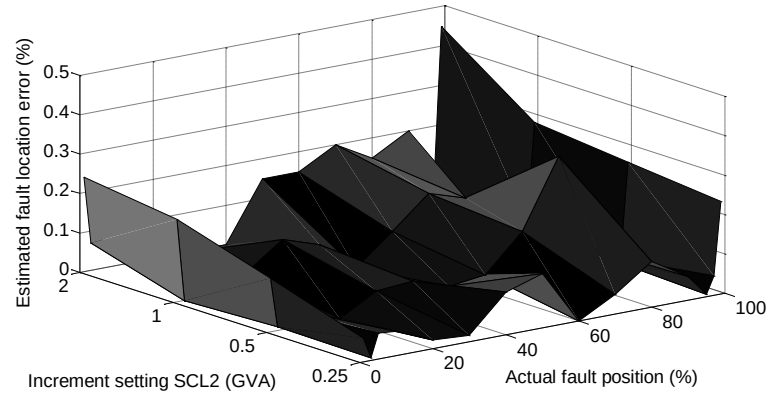

R_f=0.1Ω

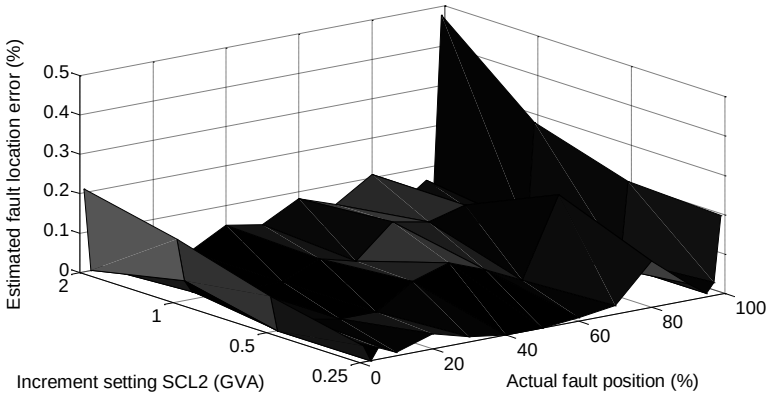

R_f=5Ω

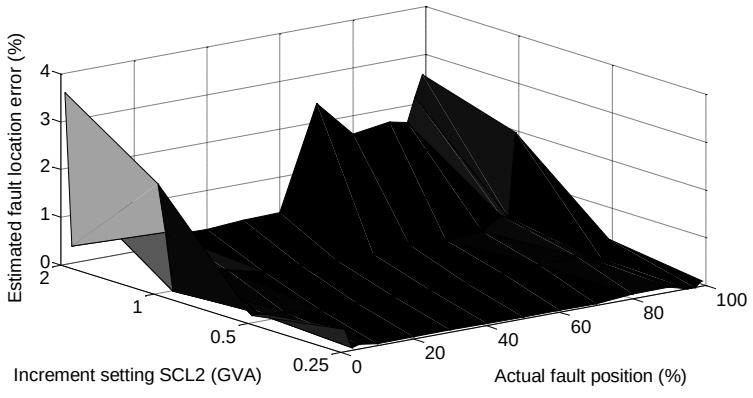

R_f=5Ω

Figure 6.6. Impact of different *SCL2* increment on Group B

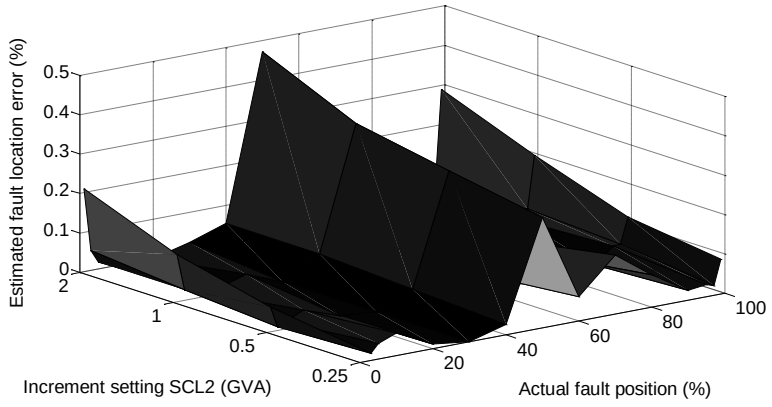

R_f=0.1Ω

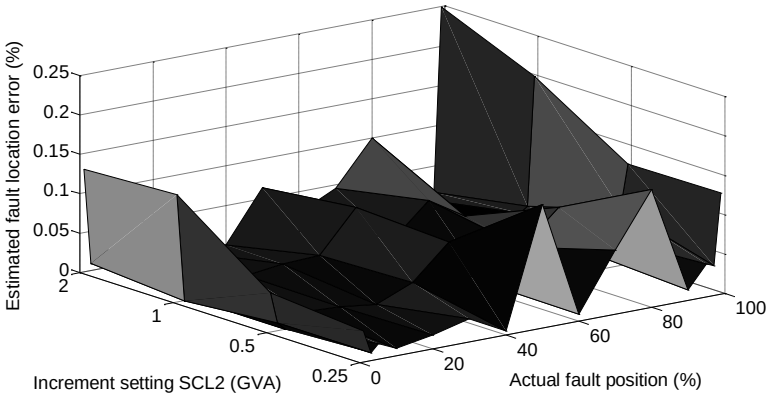

R_f=0.1Ω

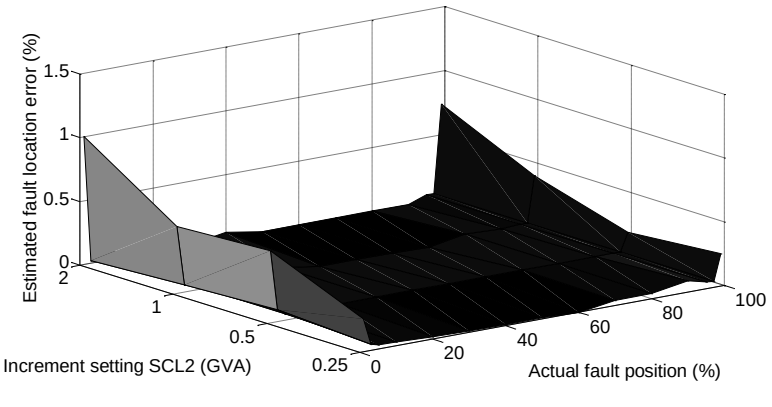

R_f=100Ω

Figure 6.7. Impact of different *SCL2* increment on Group C

Increment (GVA)	Maximum errors (%)								
	Group A			Group B			Group C		
	0.1Ω	5Ω	100Ω	0.1Ω	5Ω	100Ω	0.1Ω	5Ω	100Ω
0.25	0.17	0.32	0.50	0.23	0.20	0.37	0.28	0.13	0.26
0.5	0.35	0.35	0.57	0.30	0.21	0.47	0.32	0.15	0.56
1	0.80	2.10	5.33	0.31	0.28	2.30	0.36	0.2	0.57
2	0.95	3.75	8.00	0.45	0.48	3.60	0.47	0.25	1.00

Table 6.5. Results of *SCL2* increment evaluation

6.3 Evaluations of the effects of fault resistance and uncertain remote end short circuit level

As introduced in Chapter 3, single ended impedance based methods may suffer from variability in resistance and uncertainty relating to both end short circuit level. *SCL1* can be calculated/measured by using local end data. Some single end methods can avoid this effect but requiring extra information, i.e. *SCL2*. As introduced in Chapter 5, the proposed fault location algorithm, based on analysis of data from auto-reclose operations, only requires local end data, and does not suffer from the negative effects, in terms of R_f and uncertain *SCL2*. Moreover, the impact of such effects can be fully quantified for the proposed method. In this section, the effects of varying *SCL2* and varying R_f will be evaluated for the proposed method; and the impacts are quantified.

6.3.1 Effect of varying remote end short circuit level and fault resistance

In order to investigate and prove that success the proposed method is immune to the change of R_f and *SCL2*, the effects of varying *SCL2* and R_f will be carried out in this section. In the simulation, the range of R_f is set from 0.01Ω-100Ω. The values of *SCL2* are set as 5GVA, 15GVA and 30GVA respectively.

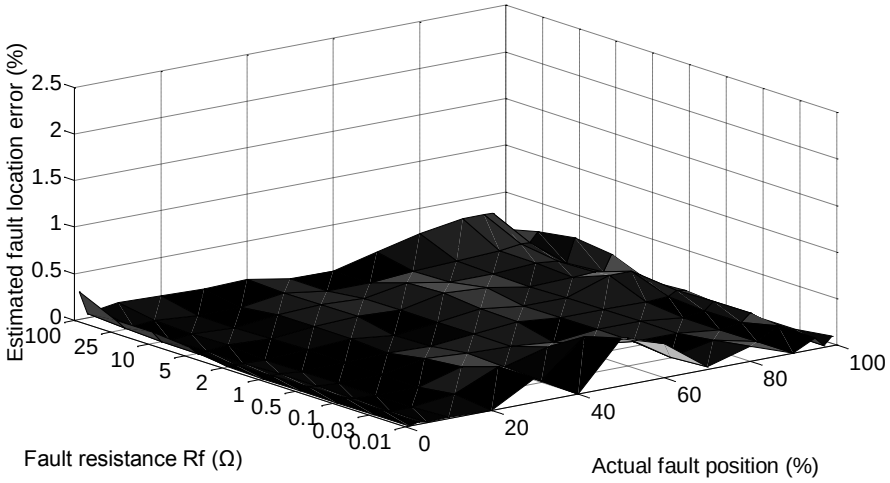

Figure 6.8. Evaluation results of *SCL2* = 5GVA

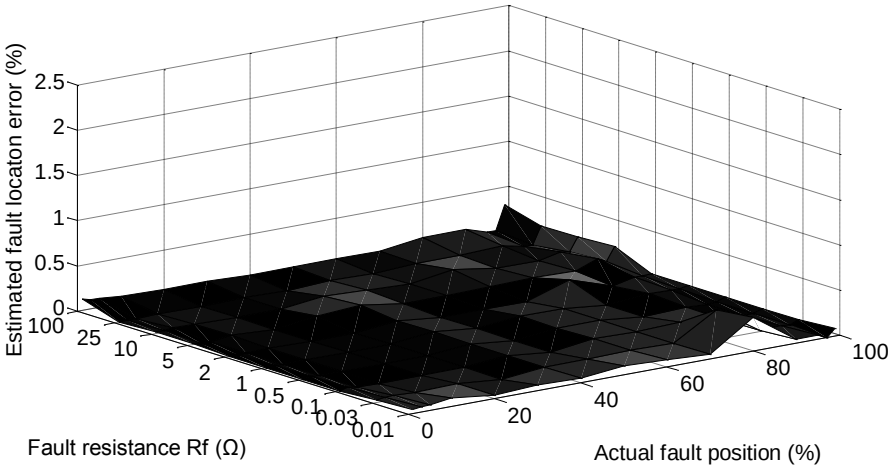

Figure 6.9. Evaluation results of *SCL2* = 15GVA

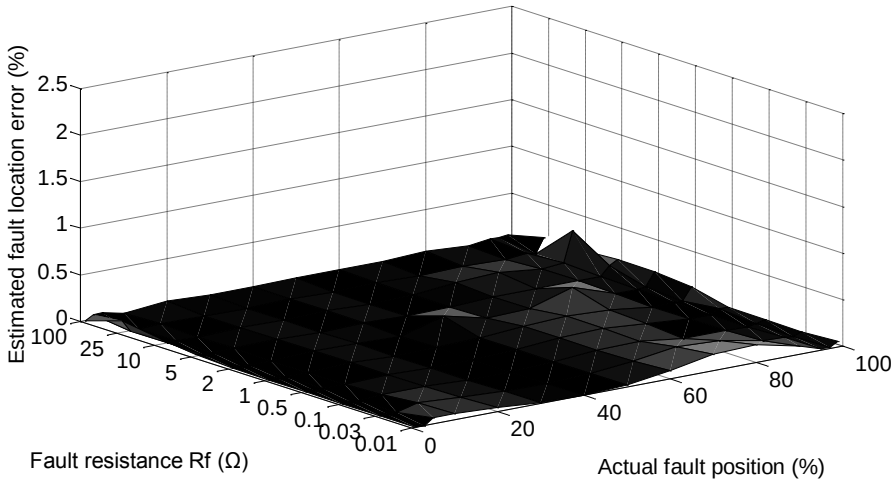

Figure 6.10. Evaluation results of *SCL2* = 30GVA

R_f (Ω)	Maximum estimated fault location error (%)		
	SCL2=5GVA	*SCL2*=15GVA	*SCL2*=30GVA
0.01	0.50	0.50	0.30
0.03	0.45	0.43	0.20
0.1	0.17	0.16	0.07
0.5	0.11	0.25	0.07
1	0.10	0.05	0.14
2	0.20	0.22	0.18
5	0.22	0.21	0.18
10	0.27	0.20	0.37
25	0.21	0.20	0.12
100	0.30	0.30	0.10

Table 6.6. Summary of the performances with the effect of varying *SCL2* and R_f

Figure 6.8 to Figure 6.10 show the estimated fault location errors with different values of *SCL2* and R_f and Table 6.6 summarises the evaluation results by using maximum estimated fault location errors. Note that the maximum estimated fault location error is the maximum value of the errors of possible fault positions (0%-100%) based on each *SCL2* and R_f settings. The evaluation results illustrate that the change of R_f does not influences the estimated fault location error significantly. The maximum change of the error based on different R_f values are less than 0.45% when *SCL2* = 15GVA. Similarly, the results illustrates that the change of *SCL2* does not influences the estimated fault location error significantly as well. The maximum change of the error based on different values of *SCL2* is less than 0.25% when R_f=0.03Ω. The evaluation results show that the varying *SCL2* and R_f do not influences the performance of the proposed method.

6.3.2 Estimation of remote end short circuit level and fault resistance

This proposed method improves fault location accuracy by eliminating the effects of R_f and unknown *SCL2*. Furthermore, it can actually provide an estimate for these parameters based upon the observed data. The estimation error of these parameters are defined as follows:

$$Error = \frac{(estimated\ value - actual\ value)}{actual\ value} \times 100\% \tag{6.2}$$

Table 6.7 summarises the maximum estimation errors of R_f and *SCL2*. The error of R_f

estimation varies in different fault conditions. Results show that the *SCL2* can be accurately estimated, the maximum error of which is less than 1.2%. The error of R_f estimation differs from the actual fault resistance level.

In general, small change of R_f may not bring notable change of calculated voltage and current used for comparison, which will result an error in R_f estimation. According to equation (6.2), low actual values of fault resistance may result in a high estimation error when expressed as percentage, but the absolute error may still be relatively low. In low fault resistance conditions, the maximum of which can reach 20%. As the actual fault resistance increases, the error decreases. When R_f value increases to 100Ω, the maximum error decreases to 0.08%. It should be noted that the primary target of the algorithm is fault location, the ability to estimate R_f and *SCL2* are merely by-products of the algorithm.

Simulation settings			Maximum Estimation Error		
R_f (Ω)	*SCL2* (GVA)	*n* (%)	R_f (%)	*SCL2* (%)	*n* (%)
0.1	5	0-100	20	0	0.17
0.1	15	0-100	16	0.5	0.16
0.1	30	0-100	12	1.2	0.07
5	5	0-100	3	0	0.20
5	15	0-100	2.8	0.6	0.21
5	30	0-100	2.8	0.6	0.18
25	5	0-100	0.12	0	0.20
25	15	0-100	0.12	0	0.21
25	30	0-100	0.12	1.2	0.18
100	5	0-100	0.06	0	0.30
100	15	0-100	0.02	0	0.30
100	30	0-100	0.08	0.7	0.10

Table 6.7. Estimation of R_f and *SCL2*

6.4 Comparison with conventional single end impedance based methods

Chapter 3 has comparatively analysis the performances of conventional impedance based method. The success of Takagi method is that it improves fault location accuracy by reducing the effect of fault resistance significantly. The network impedance method improves the fault location accuracy by requiring *SCL2* as known input. In this section, the comparison among Takagi method, the network impedance method and proposed method will be carried out.

Table 6.8 and Table 6.9 show the comparison results of Takagi method (denoted A in the table), network impedance method (B) and proposed method (C) by using the maximum and average estimated fault location error. The results illustrate that all methods have good accuracy in low fault resistance conditions (R_f=0.1Ω), the maximum error of which are less than 0.28%, 0.24% and 0.17% and the average error of which are less than 0.07%, 0.07% and 0.05%. The errors of Takagi method increase as the values of R_f. The worst case occurs when R_f =100Ω and *SCL2* = 30GVA, the maximum value of error reaches 25.2%. With the same case, the maximum errors of proposed method and network impedance method are only 0.10% and 0.90%. Results illustrate that the proposed method improves the fault location accuracy over Takagi method significantly. The proposed method has great accuracy level, the average errors of all simulated cases is 0.05% while the average error of Takagi method is 2.50%. The network impedance method has good accuracy level; the average error of all cases is 0.18%. Comparatively, the proposed method locates

the fault only with local end data, while the network impedance requires known *SCL2* as extra condition.

Simulation settings			Maximum Estimated error (%)		
Rf (Ω)	*SCL2*(GVA)	*n* (%)	A	B	C
0.1	5	0-100	0.20	0.20	0.17
0.1	15	0-100	0.28	0.24	0.16
0.1	30	0-100	0.17	0.20	0.07
5	5	0-100	1.12	0.26	0.20
5	15	0-100	2.78	0.30	0.21
5	30	0-100	5.45	0.60	0.18
25	5	0-100	5.50	0.28	0.20
25	15	0-100	11.3	0.50	0.21
25	30	0-100	15.64	0.79	0.18
100	5	0-100	16.3	0.39	0.30
100	15	0-100	21.20	0.89	0.30
100	30	0-100	25.20	0.90	0.10

Table 6.8. Comparison among Takagi method, network impedance method and proposed method: maximum error

Simulation settings			Average Estimated error (%)		
Rf (Ω)	*SCL2*(GVA)	*n* (%)	A	B	C
0.1	5	0-100	0.07	0.07	0.05
0.1	15	0-100	0.06	0.07	0.02
0.1	30	0-100	0.06	0.07	0.01
5	5	0-100	0.31	0.08	0.06
5	15	0-100	0.70	0.09	0.05
5	30	0-100	0.95	0.11	0.03
25	5	0-100	1.69	0.09	0.06
25	15	0-100	2.93	0.12	0.03
25	30	0-100	3.50	0.30	0.02
100	5	0-100	5.15	0.35	0.14
100	15	0-100	7.04	0.40	0.09
100	30	0-100	7.60	0.40	0.03
Average error of all cases			2.50	0.18	0.05

Table 6.9. Comparison among Takagi method, network impedance method and proposed method: average error

6.5 Effect of variations local end short circuit level

Local end short circuit level (*SCL1*) is assumed to be a known parameter that can be input to the developed fault location algorithm. The accuracy of the *SCL1* data is important and impacts upon the final result of the new method. In this section, the performance of the proposed method when there are inaccuracies in *SCL1* is investigated. To facilitate this investigation, defined errors set of 1%, 3%, 5% and 10% in the calculated/estimated values of *SCL1* are used.

In the simulation, the *SCL2* level is set to 15GVA, the range of fault distances is set from 0% to 100% and the range of R_f is set from 0.01Ω to 100Ω. Figure 6.11 to

Figure 6.14 show the results of the proposed algorithm when three different levels of inaccuracy are introduced to the *SCL1* input data. The corresponding maximum estimated fault location errors for each of these three scenarios are 0.63%, 1.17%, 2.4% and 4.75%; the average estimated fault location errors are 0.15%, 0.23%, 0.46% and 0.76%. This data is also contained in Table 6.10. Results illustrate that the estimated fault location error increases as the error in the *SCL1*. A number of techniques [1-3] have been developed that strive to estimate the infeed level. It is believed that the accuracy of the local end short circuit level data input to the fault locator can be improved in the future. Recently, [5] has reported a technique that measures the infeed level by using digital signal processing chip, the maximum error of which is less than 5% through massive tests. Also, investigation on accurately estimating (or measuring) local end short circuit level can be carried out as future work leading on from this project.

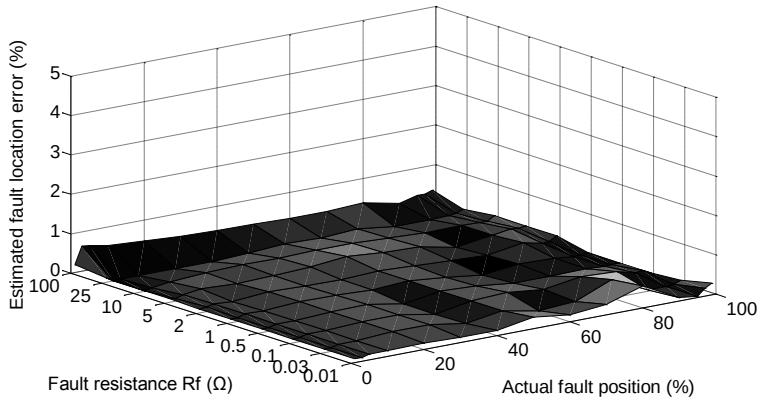

Figure 6.11. Inaccurate *SCL1* estimation error of 1%

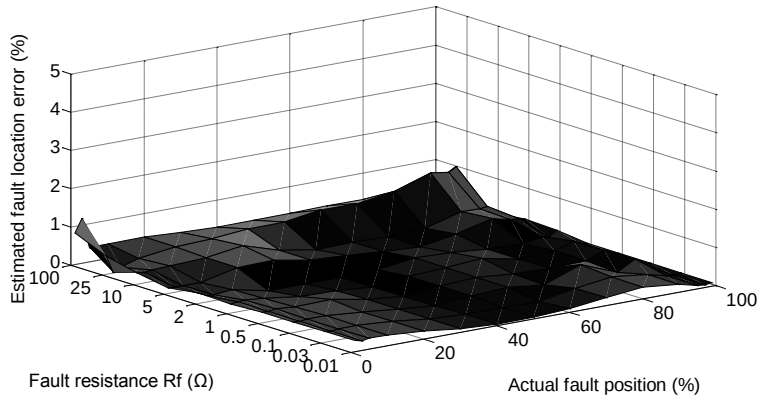

Figure 6.12. Inaccurate *SCL1* estimation error of 3%

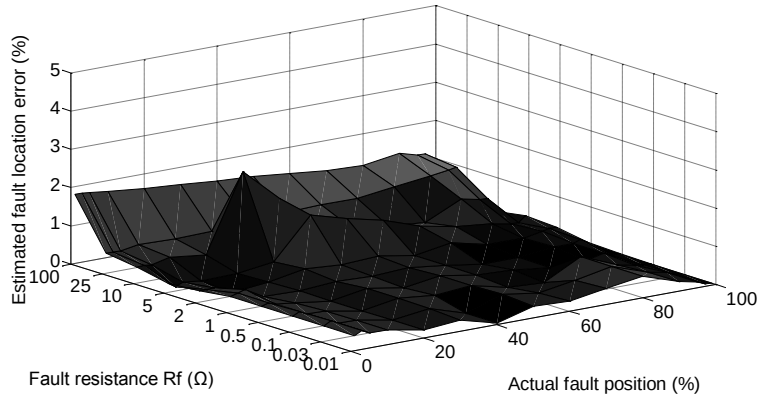

Figure 6.13. Inaccurate *SCL1* estimation error of 5%

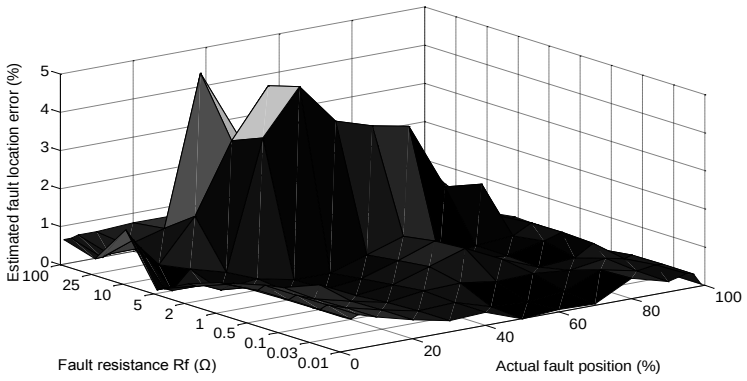

Figure 6.14. Inaccurate *SCL1* estimation error of 10%

SCL1 error	Maximum Estimated Error	Average Estimated Error
1%	0.63%	0.15%
3%	1.17%	0.25%
5%	2.40%	0.47%
10%	4.75%	0.76%

Table 6.10. Summary of the effect of inaccurate *SCL1* estimation

6.6 Effect of measurement error

The errors associated with current transformers (CT) and voltage transformers (VT) will directly pollute the measured current and voltage. The accuracy of majority impedance based fault location techniques can't avoid this effect. In this section, the evaluation of the effect of measurement errors is carried out. The measurement errors for both voltage and current are set to 1%, 3% and 5% [6, 7]. Note that the results are obtained by applying the worse cases that polarity of CT and VT errors is opposite (i.e. CT: 5%, VT: -5%). In the simulation, *SCL2* is set as 15GVA and the range of R_f is set from 0.01Ω to 100Ω.

Figure 6.15 to Figure 6.17 present the evaluation results and Table 6.11 shows the maximum and average error in location for each of the defined measurement errors. As expected, both maximum and average fault location estimation errors increase as the measurement errors increase, value of which reaches 8.5% and 2.24% when the error of CT and VT reaches 5% and the value of R_f reaches 100Ω. The measurement error is the negative factor to majority existing impedance based fault location methods. The proposed method can't overcome this weakness. However, new

measurement transducers, often using optical and other non-conventional techniques, are continually being developed and implemented [8-10] recently. It is believed that the negative effect can be reduced as the development of measurement instrument.

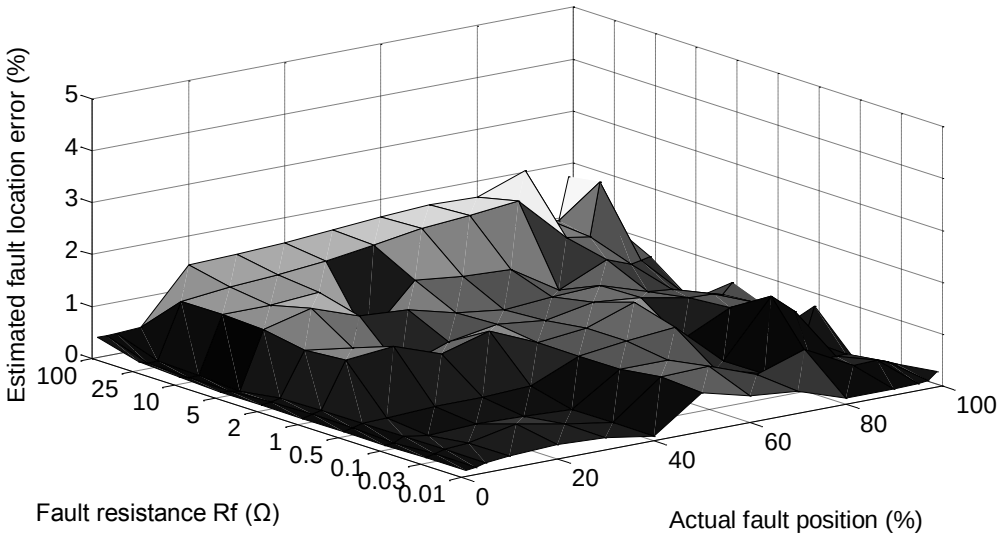

Figure 6.15. Measurement error of 1%

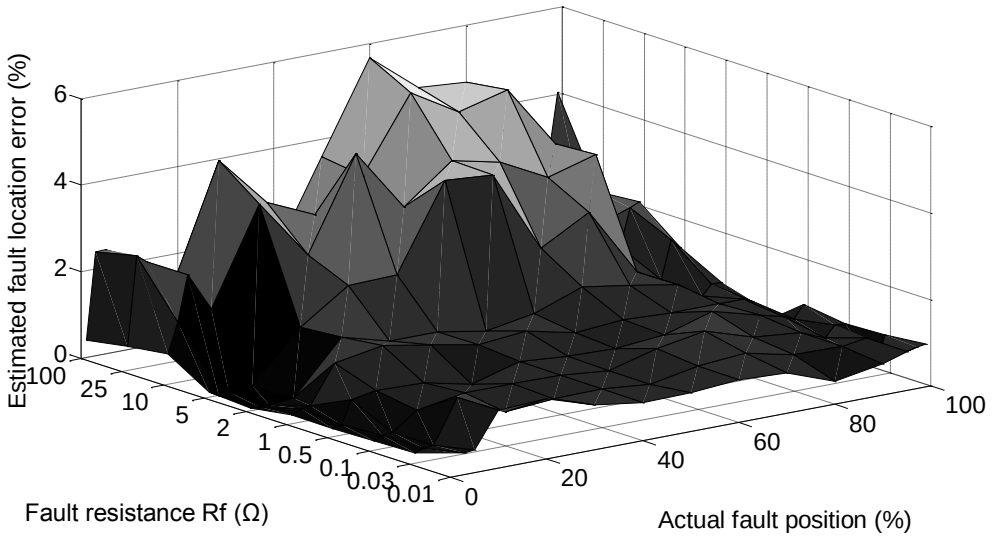

Figure 6.16. Measurement error of 3%

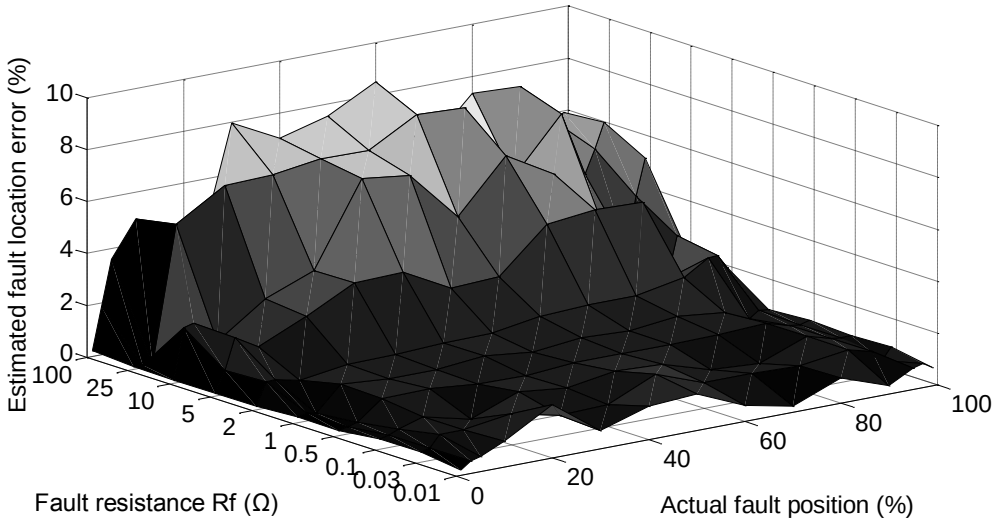

Figure 6.17. Measurement error of 5%

Measurement error	Maximum Estimated Error	Average Estimated Error
1%	2.04%	0.62%
3%	5.61%	1.46%
5%	8.5%	2.20%

Table 6.11. Summary of the effect of measurement error

6.7 Evaluation of fault location performance for all fault types

Section 4.2.2.1 described the modeling of resistive faults on transmission lines, which makes it possible to create a transmission line model for all fault types. Recall that the basic principle of the proposed method is to compare the computed voltage and current with the actual fault data. The single phase to earth fault is the most-likely happened in the system and has been widely evaluated in above sections.

However, the proposed method is capable of performing location for all fault types. In this section, phase-phase, phase-phase to earth and three-phases to earth faults will be evaluated. Consequently, only the TPAR LOCAL scenario is used in this section. Moreover, as it has been proven in the previous section, that the level of *SCL2* does not influence the performance of the proposed method; accordingly, *SCL2* is set to a value of 15GVA in the simulations.

Figure 6.18 to Figure 6.20 show the fault location results for a number of possible fault locations and fault resistance. Table 6.12 summaries the performances of the possible fault types by using maximum and average errors. Note that PP, PPE and TPE denote phase-phase fault, phase-phase to earth fault and three-phases to earth fault in the table. In general, good accuracy of fault location can be achieved for all fault types, the maximum errors of PP, PPE and TPE are less than 0.46%, 0.44% and 0.35%, and the average errors of PP, PPE and TPE are less than 0.20%, 0.18% and 0.09% respectively. To conclude, the proposed method is capable of accurate fault location for all fault types.

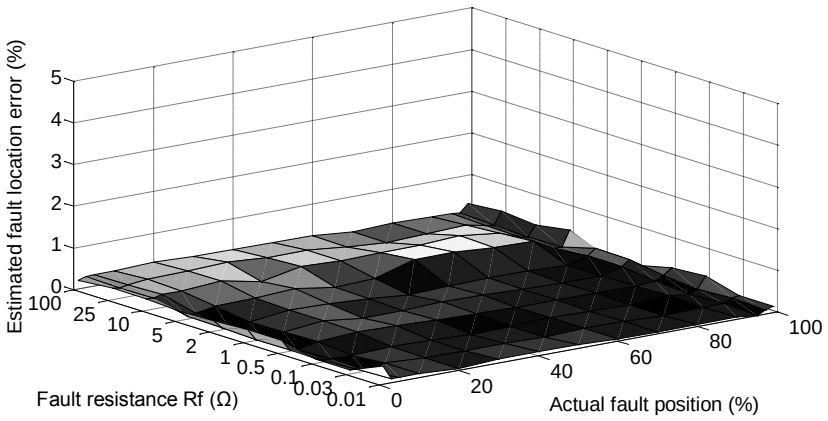

Figure 6.18. Estimated fault location errors of phase-phase fault

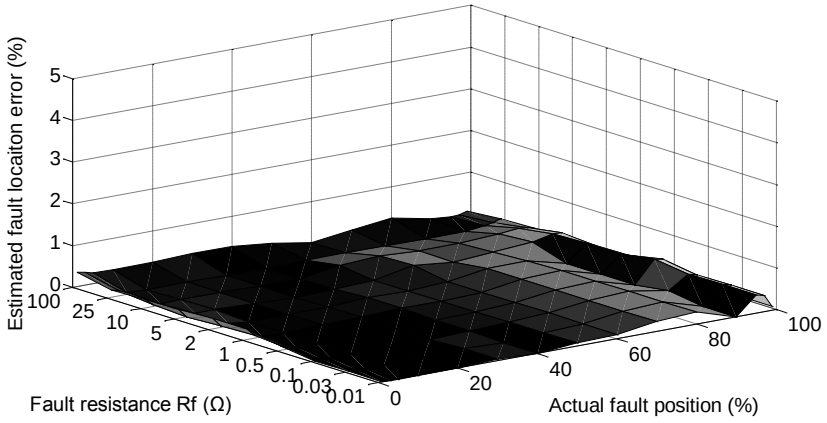

Figure 6.19. Estimated fault location errors of phase-phase to earth fault

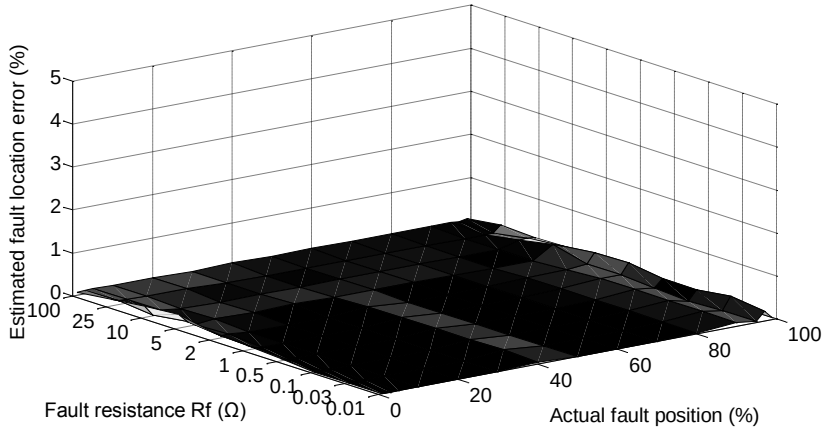

Figure 6.20. Estimated fault location errors of three phases to earth fault

R_f (Ω)	Maximum Error (%)			Average Error (%)		
	PP	PPE	TPE	PP	PPE	TPE
0.01Ω	0.45	0.44	0.23	0.10	0.11	0.05
0.03Ω	0.26	0.43	0.33	0.06	0.11	0.04
0.1Ω	0.38	0.42	0.23	0.07	0.12	0.03
0.5Ω	0.32	0.53	0.23	0.10	0.10	0.04
1Ω	0.30	0.40	0.35	0.10	0.11	0.06
2Ω	0.31	0.41	0.32	0.11	0.13	0.06
5Ω	0.46	0.37	0.32	0.16	0.1	0.09
10Ω	0.40	0.25	0.25	0.20	0.12	0.07
25Ω	0.42	0.17	0.17	0.16	0.06	0.05
100Ω	0.32	0.34	0.12	0.15	0.18	0.05

Table 6.12. Summary of all fault types

6.8 Conclusion

The incremental values that are selected as the basis for the ranges of *n*, R_f and *SCL2* obviously influence the accuracy of the fault location and the magnitude of the errors that may be produced. Accordingly, the influence of these incremental values on fault location accuracy has been evaluated in this chapter. The evaluation results have shown that, as one would expect, selecting smaller incremental values produces more accurate results, but also leads to longer algorithm execution times. After considering both aspects (accuracy and processing time), the increments for of *n*, *SCL2* and R_f have been selected as 0.1%, 0.5GVA and 0.1Ω respectively. The

maximum estimated error based the settings is less than 0.57%, and the execution time, based on a PC platform (with Matlab 2009 running on Intel core i7 processor @ 2.66Hz with 3G RAM) is less than 15 minutes. All other evaluations in this chapter are based on these incremental settings.

The performance of the proposed method has also been compared with conventional fault location methods (Takagi method and network impedance method). Results illustrate that the proposed method improves the accuracy significantly over the Takagi method. Compared to the network impedance method, the proposed method has similar accuracy level; however, the value of *SCL2* does not need to be known.

Inaccurate input values for *SCL1* introduce errors within the voltage and current calculations used in the transmission line modelling elements of the process, as the basic principle of the proposed method is to compare the calculated data with simulated data. A number of evaluations have been carried out to quantify the impact of errors between the assumed input values of *SCL1* and its actual prevailing value when the fault occurs. Investigations into accurate local end short circuit level estimation should be carried out as future work to reduce this negative effect and work is also being carried out into this by other researchers [1-3, 5].

The measurement devices (CT and VT) may also introduce errors. In this chapter, the effects of measurement error has been evaluated and the results shown the error of the proposed method increases with measurement error, again as one would expect. It is believed that the negative factor influences all impedance based fault location

techniques, and that no impedance based methods of fault location is immune to this weakness. Steps to improve the accuracy of measurement transducers should assist in reducing such errors and new devices, often using optical and other non-conventional techniques, are continually being developed and implemented [8-10].

6.9 References

[1] K. Young-Jin, *et al.*, "A fault location algorithm using estimated local source impedance," in *Power Systems Conference and Exposition, 2009. PSCE '09. IEEE/PES*, 2009, pp. 1-5.

[2] M. Sumner, *et al.*, "Impedance measurement for improved power quality-Part 1: the measurement technique," *Power Delivery, IEEE Transactions on,* vol. 19, pp. 1442-1448, 2004.

[3] M. Sumner, *et al.*, "A technique for power supply harmonic impedance estimation using a controlled voltage disturbance," *Power Electronics, IEEE Transactions on,* vol. 17, pp. 207-215, 2002.

[4] E. Rosołowski, *et al.*, "Adaptive measuring algorithm suppressing a decaying DC component for digital protective relays," *Electric Power Systems Research*, vol. 60, pp. 99-105, 2001.

[5] D. McIlvenna and A. Cruden, "Implementation of a fault level meter using a digital signal processing chip," in *Universities Power Engineering Conference (UPEC), 2010 45th International*, 2010, pp. 1-5.

[6] "IEEE Standard Requirements for Instrument Transformers," *ANSI/IEEE Std C57.13-1978,* p. 0_1, 1978.

[7] " Instrument transformers Part 1: Current transformers," *NTERNATIONAL*

STANDARD IEC60044-1, 2003.

[8] Orr P*, et al.*, "Flexible protection architectures using distributed optical sensors," presented at the Developments in Power Systems Protection, 2012, 2012.

[9] P. Orr, *et al.*, "FBG-based fibre-optic current sensors for power systems protection: Laboratory evaluation," in *Universities Power Engineering Conference (UPEC), 2009 Proceedings of the 44th International*, 2009, pp. 1-5.

[10] J. Hoark and J. Hrabliuk. *Current transformer errors and transformer inrush as measured by magnetic, optical and other unconventional CTs*.

Chapter 7. Conclusions and future work

7.1 Conclusions

This dissertation has presented new techniques for location of faults in transmission lines. It has been presented in the context of a detailed review of travelling wave and impedance based fault location methods, which are the main fault location techniques that have been implemented in practice.

The travelling wave based method, estimates fault distance by detecting and analysing the relative times of arrival of various high frequency travelling wave signals and reflections that are initiated by faults. It has been demonstrated to possess great accuracy in certain applications, but may be expensive and can sometimes be difficult to install or retrofit within existing substations. Impedance based methods do not possess the high levels of accuracy associated with travelling wave based techniques. However, they can be relatively efficient from an economic perspective and are easier to implement (often embedded within manufacturers' relays or fault recorder devices). Such methods estimate the distance to faults using only fundamental current and voltage phasor data. A large number of impedance based techniques have been developed to improve upon accuracy and mitigate the impact

of negative effects on the location process.

Several existing impedance based fault location techniques have been presented and reviewed in this dissertation. The Takagi method provides very good performance in the majority of situations; it is relatively economical and easy to implement within modern numerical protection relays and fault recorders. However, its accuracy is compromised by a number factors, including uncertainty associated with the assumed both ends short circuit level, varying performance as the distance to fault varies and degradations to performance caused by certain ranges of values of fault resistance. The network impedance method can improves upon the performance in these respects. It does not suffer from the change of fault resistance and both end short circuit level. However, the value of remote end short circuit level, which does not have a high certainty (if not measured and communicated during the fault), is required as a known input. The performances of Takagi and network impedance method are used to compare with the novel fault location techniques introduced in this dissertation.

The novel single ended fault location algorithm presented in this dissertation analyses the interpole states of circuit breakers during fault clearing operation (on both first clearance and subsequent clearance during circuit breaker operations). It has been shown how it compares calculated data with simulated data from the initial "during fault" state prior to the beginning of interruption in order to establish a range of possible fault locations (and supplementary estimations of remote end short circuit level and fault resistance). When a match is found within a specified tolerance error

from analysis of the initial "during fault" state, the range of corresponding possible fault locations, fault resistances and remote source impedances are recorded. The ranges of all possible values are subsequently reduced through analysis of the consecutive interpole stages as each pole of the circuit breaker opens consecutively to finally interrupt the flow of current in all three phases. The final, most accurate, fault location is obtained following on from analysis of the final state. The method also has been extended to analyse reclose and subsequent clearances in order to further improve the accuracy of location. The new method not only eliminates but also quantifies the negative effects of conventional single ended methods. Furthermore, it inherits the advantages of conventional single ended fault location method, in that it is relatively economical to implement. Only local end data is needed.

Case studies were included and excellent levels of accuracy have been obtained. Furthermore, a large number of results have been shown to compare favourably against both the Takagi and the network impedance based methods, with tests carried out for many locations and different values of R_f and *SCL2*. Accordingly it is claimed that the developed technique exhibits the potential for achieving a very high accuracy of location, which can be implemented at low cost.

However, it is acknowledge that there remain challenges associated with the developed methods. During the interpole states, it is difficult to extract accurate fundamental phasor data from such a short time window (theoretically 1/6 of a cycle, corresponding to 3.33 ms or 2.78 ms of data in a 50 Hz or 60 Hz system) at the

present stage of development and using the signal processing techniques available at this time. However, a number of techniques have been, and continue to be, developed to reduce the required time window for the phasor extraction process relatively recently. Paper [1] has reported on techniques which reduce the time delay for phasor extraction down to 1/3 of a cycle of the fundamental waveform. Paper [2] reports on a technique which further reduces the time required to 1/4 of a cycle (note that these techniques are in the presence of noise – it is of course possible to extract a phasor from as little as two consecutive samples if it is known that the input waveform is a perfect sinusoid). Perhaps a suitable DSP method will be developed in the future to enable the phasor extraction from even shorter time windows.

The initial investigations into the use of inter-pole states to analyse single circuit breaker operations following a fault has been extended to develop an enhanced method that analyses data from auto-reclose scheme operation. This is a prudent approach to take as permanent faults, which are of most interest from a fault location perspective, will provide more data relating to the fault due to the reclose onto the fault providing several more cycles of fault waveform data and further inter-pole status data as the circuit breaker opens for the second time during the same fault event. The basic principle is similar to the original fault location method and uses interpole states in the same fashion. Calculated data is compared with simulated data and the process proceeds iteratively as described earlier until a match is achieved within a specified tolerance error. The ranges of all possible values are reduced through the analysis of the consecutive auto-reclose scheme stages.

A 400kV, 100km transmission line model, simulated using EMTP/ATP, has been used to evaluate the performance of the based. The evaluations results verify that that the method displays high levels of immunity to the effect of R_f, n and uncertain *SCL2* over a wide range of different n (from 0-100% along the line), R_f (0-100Ω) and *SCL2* (5-30GVA). The majority of the estimated fault location errors of the proposed method are less than 0.5%.

The results of the evaluation also quantify the ability of the method to estimate values for R_f and *SCL2* in addition to the location of the faults. The results (from Table 6.7) shows that the maximum estimation error of fault resistance for low resistance fault conditions may be high (up to 20% when R_f=0.1Ω). The estimation error decreases with the value of fault resistance, the maximum estimation error of high resistance fault (R_f =100Ω) is less than 0.08%. Comparatively, *SCL2* can be accurately estimated under all conditions, the maximum error in the evaluations (from Table 6.7) is less than 1.2%. It should be noted that the primary target of the algorithm is fault location, the ability to estimate R_f and *SCL2* are merely by-products of the algorithm.

As previously stated, the performance of the method has been compared extensively with the Takagi and network impedance methods. Comparatively, the results of the Takagi method shows that R_f, n and uncertain *SCL2* have greater impact on the accuracy: the maximum estimated error can be as high as 25.2% when the fault position is close to remote end (99%) with high fault resistance (100Ω). In the same case, the maximum error of the proposed method is 0.15%. Considering the average

error across all simulated cases shows that the proposed method has an accuracy of 0.05%, while the Takagi method has an accuracy of 2.50% (Refer to Table 6.9). The network impedance method has a generally good accuracy level; the average error across all simulated cases is 0.18%. However, an extra condition associated with this method is that an accurate estimation of *SCL2* has to be known.

Investigations into the effects of inaccurate input data defining *SCL1* and measurement errors inherent in CTs and VTs have also been carried out. The estimated fault location error increases in line with increasing errors in estimations of *SCL1*. The results of evaluations illustrate that the estimated error can reach 4.75% in the case where R_f = 100Ω and there is a 10% estimation error of *SCL1*. With respect to CT and VT measurement errors, the estimated fault location error increases with measurement error, as anticipated. From the results of evaluation, the maximum error is less than 8.5% when CT and VT errors are 5% (the worst case errors evaluated, which is in line with protection class CT and VT standards [3]). However, it is believed that such errors could be reduced as the development of sensor technology continues in the future. Advanced DSP techniques, techniques for accurately estimating short circuit levels from measurement data [4-6] and advances in current and voltage measurement techniques [7-9] could all contribute to reduction, or eliminate of these errors in the future.

7.2 Future work plan

As with any research work, there is always more work that can be done. There are several possible expansions and improvements that are suggested for the methods

and concepts proposed and demonstrated in this thesis.

- Future work should focus on investigation and development of DSP techniques that are capable of extracting accurate fundamental frequency component over extremely short time windows (1/6 cycle). Recently, a number of techniques have been proposed that can reduce the time window required to extract the phasor data [10-13]. However, challenges remain with these techniques, for example high sampling frequencies are often required, and the effects of unexpected high frequency oscillations and decaying DC offset components in the signal may still impact negatively on such techniques, so more work remains to be done in this area.
- Further investigation into the effect of the circuit breakers at the line ends operating simultaneously. In the majority transmission systems, the feeders are typically supplied from both line ends (or more than two line ends in multi-terminal feeders). At the present stage, the proposed method based on circuit breaker operation is designed to operate in a two ended circuits and assumes that the local circuit breaker opens completely before the contacts of the remote end circuit breaker start to separate. However, it is noted that this situation, where one CB completely trips before another starts to operate, cannot be guaranteed. Further investigations into the effect of the timing of circuit breaker operations should be carried out.
- The evaluation of the performance of proposed fault location algorithms using recorded data from actual power systems is a natural next step for this work. In this thesis, EMTP/ATP simulated data has been used to evaluate the performance of the proposed method based on auto-reclosing operation. As the

final target of this method is implementation in practice, evaluations using actual power system data must be carried out as future work.

- Development of an executable program that implements proposed fault location method. In this thesis, a Matlab user interface program has been designed which can read EMTP/ATP generated sampled values and COMTRADE sampled value data. As the final target is the implementation of the fault locator in a practical system, an executable program should be designed.
- Integration of the fault location system with IEC 61850 measurement data should be carried out. IEC 61850 [14, 15] is a rapidly emerging suite of protocols for communication between protection, control and sensor devices and is gaining widespread acceptance by both manufacturers and utilities. Some researchers have already proposed integration of fault location functions with the IEC 60850 protocol [16-18]. An IEC 61850 compliant interface to the fault location systems proposed and developed in this thesis should be designed as an element of future work.
- Further investigation into the implementation of the method on double circuit lines should be carried out. According to the principles of the proposed method, it is believed that it is capable of application to double circuit transmission lines, as long as the mutual coupling effect of the adjacent circuit is modelled correctly.
- Further investigation into the application of the proposed algorithms in location of transient faults (e.g. by considering the effect of trapped charge in healthy phases).

7.3 References

[1] Y. Ziwen, "Fundamental Phasor Calculation With Short Delay," *Power Delivery, IEEE Transactions on*, vol. 23, pp. 1280-1287, 2008.

[2] D. Finney, *et al.*, "Ultra fast distance protection," in *Developments in Power System Protection (DPSP 2010). Managing the Change, 10th IET International Conference on*, 2010, pp. 1-5.

[3] "IEEE Standard Requirements for Instrument Transformers," *IEEE Std C57.13-2008 (Revision of IEEE Std C57.13-1993)*, pp. c1-82, 2008.

[4] M. Sumner, *et al.*, "Impedance measurement for improved power quality-Part 1: the measurement technique," *Power Delivery, IEEE Transactions on*, vol. 19, pp. 1442-1448, 2004.

[5] K. Young-Jin, *et al.*, "A fault location algorithm using estimated local source impedance," in *Power Systems Conference and Exposition, 2009. PSCE '09. IEEE/PES*, 2009, pp. 1-5.

[6] D. McIlvenna and A. Cruden, "Implementation of a fault level meter using a digital signal processing chip," in *Universities Power Engineering Conference (UPEC), 2010 45th International*, 2010, pp. 1-5.

[7] Orr P, *et al.*, "Flexible protection architectures using distributed optical sensors," presented at the Developments in Power Systems Protection, 2012, 2012.

[8] P. Orr, *et al.*, "FBG-based fibre-optic current sensors for power systems protection: Laboratory evaluation," in *Universities Power Engineering Conference (UPEC), 2009 Proceedings of the 44th International*, 2009, pp.

1-5.

[9] J. Hoark and J. Hrabliuk. *Current transformer errors and transformer inrush as measured by magnetic, optical and other unconventional CTs*.

[10] J. Buse, *et al.*, "Decaying DC offset removal operator using mathematical morphology for phasor measurement," in *Innovative Smart Grid Technologies Conference Europe (ISGT Europe), 2010 IEEE PES*, 2010, pp. 1-6.

[11] X. Chen, "Real wavelet-domain modified phasor: Principle and applications in power systems," in *Power and Energy Society General Meeting - Conversion and Delivery of Electrical Energy in the 21st Century, 2008 IEEE*, 2008, pp. 1-7.

[12] Z. Hui, *et al.*, "Fast voltage detection for a single-phase dynamic voltage restorer (DVR) using morphological low-pass filters," in *Electric Utility Deregulation and Restructuring and Power Technologies, 2008. DRPT 2008. Third International Conference on*, 2008, pp. 2042-2046.

[13] L. Yutian, *et al.*, "Real-time phasor measurement for low frequency oscillation in power system," in *Circuits and Systems, 2005. ISCAS 2005. IEEE International Symposium on*, 2005, pp. 3889-3893 Vol. 4.

[14] R. E. Mackiewicz, "Overview of IEC 61850 and Benefits," in *Transmission and Distribution Conference and Exhibition, 2005/2006 IEEE PES*, 2006, pp. 376-383.

[15] R. Kuffel, *et al.*, "Real time simulation and testing using IEC 61850," in *Modern Electric Power Systems (MEPS), 2010 Proceedings of the International Symposium*, 2010, pp. 1-8.

[16] B. Stojcevski and A. Kalam, "Fault Location in Overhead Power LinesUsing the IEC61850 International Protocol," *International Review on Modelling and Simulations*, vol. Vol. 3, N. 5, 2010.

[17] A. P. Apostolov, "Implementation of accelerated transmission line protection schemes in substations with IEC 61850," in *Transmission and Distribution Conference and Exposition, 2008. T&D. IEEE/PES*, 2008, pp. 1-6.

[18] H. K. Zadeh and M. Manjrekar, "A novel IEC 61850-based distribution line/cable protection scheme design," in *Innovative Smart Grid Technologies (ISGT), 2012 IEEE PES*, 2012, pp. 1-6.

Appendix A: Fundamental frequency phasor extraction techniques

The estimate of fault location using impedance based methods is a function of the measured voltage and current. In modern power system, the majority of computer-based protection and control functions are based on fundamental phasors of voltage and current. The extraction of these fundamental phasors is therefore required to satisfy a number of requirements, such as ability to quickly identify certain situations or phenomena, to provide immunity against frequency excursions or transients, to remain insensitive to signal pollution arising from high harmonic content, high frequency oscillations and exponential decaying DC offset components of the measured signal. There are various techniques have been developed to extract fundamental phasors, such as sinusoidal wave based methods [1-3], Fourier analysis based methods [4-8] and least squares based method [9-11]. In this section, the leading techniques, which are Discrete Fourier Transform (DFT) [8] and Modified Least Squared Method (LSM) [11] are introduced and analysed.

A.1 DFT

The DFT is basic algorithm can be directly used in modern digital protection systems [8, 12]. Such methods have the ability to extract fundamental frequency components, and other frequency components if desired, from voltage and current waveforms.

The discrete voltage/current wave can be expressed in (A.1).

$$x(k) = X_0 e^{-kT_s/\tau} + \sum_{1}^{N} X_m \cos(mw_1 kT_s - \varphi_m) \quad \text{(A.1)}$$

Where:

X_0, τ– magnitude and time constant of decaying DC component

N – number of harmonics considered;

ω – 2π/T, the radial system frequency;

ϕ_m, X_m – initial phase angle and magnitude of the m^{th} harmonic.

T_s– time

It is assumed that the transformation period is equal to the fundamental frequency period. Thus, the function of fundamental frequency phasor extraction can be represented as:

$$X(n) = \frac{2}{N} \sum_{k=0}^{N-1} x(k)\, \mathrm{e}^{-jk2\pi/\mathrm{N}} \quad \text{(A.2)}$$

An EMTP/ATP-generated fault current waveform is used to illustrate the result of

fundamental phasor extraction using DFT algorithm. Figure A.1 shows the extracted phasor magnitude versus the example input waveform. The result displays good extraction accuracy, but only from the point beyond which the waveform becomes of stable amplitude (i.e. after the DC component decays to zero). In the presence of the decaying DC offset component (which persists for a short period after fault inception and is dependent on point of wave of fault occurrence and the X/R ratio of the fault current path), the extracted magnitude is not stable. The accuracy of conventional DFT methods may therefore be compromised by the presence of decaying DC offset components.

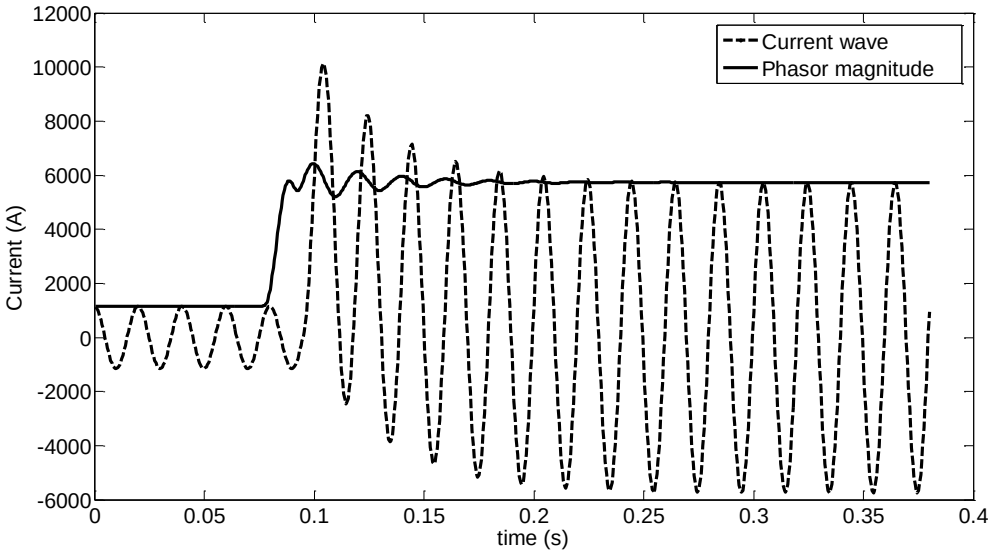

Figure A.1. Result of DFT estimation

A.2 Weighted LSM algorithm

As already stated, a fault current waveform in a transmission system typically contains a decaying DC component which has an unpredictable initial magnitude and

an uncertain time constant.

Some DSP techniques [13-20] have been designed to reduce or remove the effects of decaying DC offset and improve the accuracy of fundamental phasor extraction processes. [13] designed a digital mimic filter, which uses a pre-defined time constant, to reduce such effects. However, in this method, the effect of DC offset will not be completely eliminated in cases where the assumed time constant value deviates from the actual value. [14-17] attempt to reduce DC effects by estimating the time constant with two extra samples. And [18, 19] uses extra harmonic phasor to reduce DC effect. Reference [20] introduce a method which uses only one cycle to obtain accurate fundamental phasor without DC effect. However, potential pure DC component may influence its performance.

[11] reports the development of an algorithm, which is termed "modified Least Square Method", and this is utilised within the impedance based fault location methods reported in this thesis. This algorithm is based on a recursive full period least square filter. This estimates the fundamental phasor components with a high accuracy by rejecting the exponentially decaying DC component with additional adaptive correction for DC component. The advantage of this algorithm is that it removes the decaying DC component regardless of time constant and initial magnitude.

Assume that the signal model can be represented as shown:

$$x(t) = X_0 e^{-t/\tau} + \sum_{1}^{K} X_m \cos(mw_1 t - \varphi_m) \quad \text{(A.3)}$$

Where:

X_0, τ – magnitude and time constant of the decaying DC component

K – number of considered harmonics;

$\omega = 2\pi / T$, the radial system frequency;

ϕ_m, X_m – initial phase angle and magnitude of the m^{th} harmonic.

To estimate the fundamental phasor from M consecutive samples of the signal, a three-state LSM algorithm with the signal model matrix **H(*k*)** is composed as follows:

$$h(k-j) = [h_R(k-j), h_I(k-j), h_0(k-j)], \quad j = 0 \ldots M-1 \quad \text{(A.4)}$$

Where, $h_R(k-j) = \cos(\frac{2\pi}{N}(k-j))$,

$h_I(k-j) = -sin(\frac{2\pi}{N}(k-j))$,

$h_0(k-j) = e^{b(k-j)}, b = -\frac{T_1}{N\tau}$

The vector of estimates can be obtained using the following fundamental equation (A.5) through one full cycle window size (M=N):

$$\widehat{\mathbf{X}}(k) = \mathbf{P}(k)\mathbf{H}^{\mathbf{T}}(k)\mathbf{x}(k) \quad \text{(A.5)}$$

Where $\mathbf{P}(k) = (\mathbf{H}^{\mathbf{T}}(k)\mathbf{H}(k))^{-1}$,

$\mathbf{x}(k) = [x(k-N+1), x(k-N+2) \ldots\ldots x(k))]^T$,

$\widehat{\mathbf{X}}(k) = [X_R(k), X_I(k), X_0(k)]^T$,

Note that *T* represents the action of matrix transposition.

For this three-state LSM method, **P(*k*)** represents the full matrix, within which the off-diagonal elements are dependent on the exponential component. Consequently, the accuracy of X_R and X_I are highly dependent on the constant τ and fault inception time T_1.

A modified LSM method, which aims to convert **P(*k*)** into the form of a diagonal matrix, has been developed to reduce the effect of the constant τ and fault inception time T_1. In theory, the weighted LSM estimator h_G is the original LSM estimator multiplying the weighted factor **G**. In this method, the factor $d_c(k)$ and $d_s(k)$ have been introduced instead of the weighted factor **G**. The LSM estimator is defined as follows:

$$\mathbf{H_G}(k-j) = [h_c(k-j), h_s(k-j), h_0(k-j)], \qquad j = 0 \ldots M-1 \tag{A.6}$$

Where, $h_c(k-j) = \cos\left(\frac{2\pi}{N}(k-j)\right) - d_c(k)$,

$h_s(k-j) = -sin\left(\frac{2\pi}{N}(k-j)\right) - d_s(k)$,

$h_0(k-j) = e^{b(k-j)}, \quad b = -\frac{T_1}{N\tau}$

The requirement for $\mathbf{P_G}(k)$ is diagonal, which could be represented as:

$$\mathbf{P_G}(k) = \left[q_{i,j}\right]^T = \mathbf{H_G^T}(k)\mathbf{H}(k), \quad q_{i,j} = 0, \text{for} i \neq j \tag{A.7}$$

Based on the above condition, $d_c(k)$ and $d_s(k)$could define as:

$$d_c(k) = \frac{\sum_{j=0}^{M} \cos(\frac{2\pi}{N}(k-j))}{\exp(bk)\sum_{j=0}^{M}\exp(-bj)} \tag{A.8}$$

$$d_s(k) = \frac{-\sum_{j=0}^{M} sin(\frac{2\pi}{N}(k-j))}{\exp(bk)\sum_{j=0}^{M}\exp(-bj)} \tag{A.9}$$

Where, $b = -\frac{T_1}{N\tau}$

In the above equations, $d_c(k)$ and $d_s(k)$ could can be determined if $\exp(b)$ could can be solved. During the given transient, the time constant does not change physically. As a consequence, $\exp(b)$ can be calculated as,

$$r = \exp(b) = \frac{X_a(k)}{X_a(k-1)} \tag{A.10}$$

$$X_a(k) = \frac{2}{N}\sum_{j=0}^{N-1} x(k-j) \tag{A.11}$$

Note that $X_a(k)$ is for a sum of *N* elements of the geometric progression.

Finally, the following equation can be derived:

$$\widehat{\mathbf{X}}_\mathbf{G}(k) = \mathbf{P_G}(k)\mathbf{H_G^T}(k)\mathbf{x}(k) = [X_c(k), X_s(k), X_0(k)]^T \tag{A.12}$$

The fundamental frequency phasor is represented as shown below:

$$X(k) = X_c(k) + \mathrm{i}X_s(k) \tag{A.13}$$

An ATP generated current waveform is used to show the result of phasor estimation/extraction using this technique in Figure A.2. From the figure, it is clear that this algorithm has an excellent property of rejecting the exponentially decaying DC component.

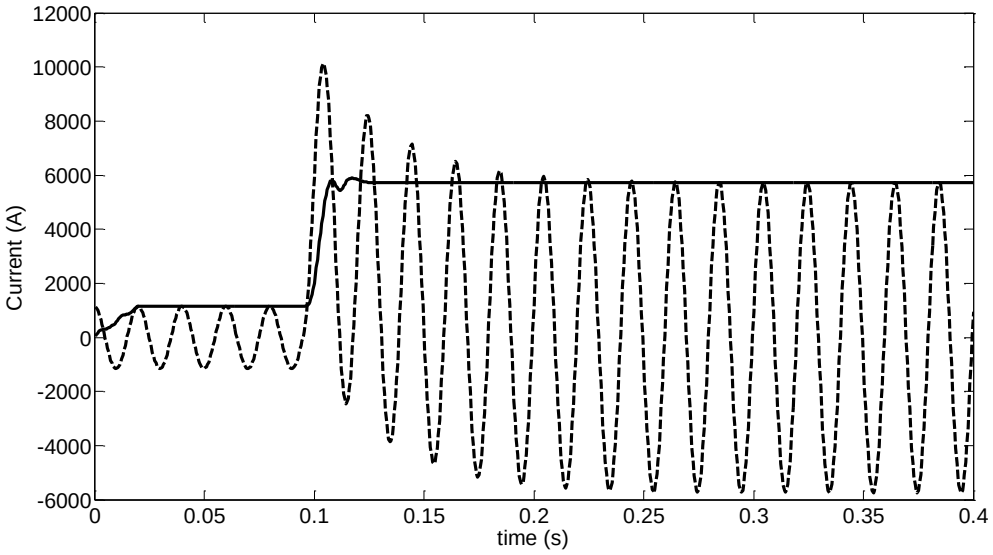

Figure A.2. Result of modified LSM estimation

A.3 References

[1] B. J. Mann and I. F. Morrison, "Digital Calculation of Impedance for Transmission Line Protection," *Power Apparatus and Systems, IEEE Transactions on,* vol. PAS-90, pp. 270-279, 1971.

[2] B. J. Mann and I. F. Morrison, "Relaying a Three Phase Transmission Line

with a Digital Computer," *Power Apparatus and Systems, IEEE Transactions on,* vol. PAS-90, pp. 742-750, 1971.

[3] J. G. Gilbert and R. J. Shovlin, "High speed transmission line fault impedance calculation using a dedicated minicomputer," *Power Apparatus and Systems, IEEE Transactions on,* vol. 94, pp. 872-883, 1975.

[4] P. G. McLaren and M. A. Redfern, "Fourier-series techniques applied to distance protection," *Electrical Engineers, Proceedings of the Institution of,* vol. 122, pp. 1301-1305, 1975.

[5] A. G. Phadke, *et al.*, "A digital computer system for EHV substations: Analysis and field tests," *Power Apparatus and Systems, IEEE Transactions on,* vol. 95, pp. 291-301, 1976.

[6] A. Wiszniewski, "How to Reduce Errors of Distance Fault Locating Algorithms," *Power Apparatus and Systems, IEEE Transactions on,* vol. PAS-100, pp. 4815-4820, 1981.

[7] A. T. Johns and M. A. Martin, "Fundamental digital approach to the distance protection of e.h.v. transmission lines," *Electrical Engineers, Proceedings of the Institution of,* vol. 125, pp. 377-384, 1978.

[8] A. T. S. S. K. Johns, *Digital protection for power systems*. London: Peter Peregrinus Ltd., 1995.

[9] A. S. AlFuhaid and M. A. El-Sayed, "A recursive least-squares digital distance relaying algorithm," *Power Delivery, IEEE Transactions on,* vol. 14, pp. 1257-1262, 1999.

[10] M. S. Sachdev and M. A. Baribeau, "A New Algorithm for Digital Impedance Relays," *Power Apparatus and Systems, IEEE Transactions on,*

vol. PAS-98, pp. 2232-2240, 1979.

[11] E. Rosołowski, *et al.*, "Adaptive measuring algorithm suppressing a decaying DC component for digital protective relays," *Electric Power Systems Research*, vol. 60, pp. 99-105, 2001.

[12] M. M. Saha and E.Rosolowski, *Fault Locaiton On Power Network*. Wrocloaw: Springer, 2011.

[13] G. Benmouyal, "Removal of DC-offset in current waveforms using digital mimic filtering," *Power Delivery, IEEE Transactions on*, vol. 10, pp. 621-630, 1995.

[14] G. Jyh-Cherng and Y. Sun-Li, "Removal of DC offset in current and voltage signals using a novel Fourier filter algorithm," *Power Delivery, IEEE Transactions on*, vol. 15, pp. 73-79, 2000.

[15] Y. Jun-Zhe and L. Chih-Wen, "A precise calculation of power system frequency and phasor," *Power Delivery, IEEE Transactions on*, vol. 15, pp. 494-499, 2000.

[16] J. F. Miñambres Argüelles, *et al.*, "A new method for decaying dc offset removal for digital protective relays," *Electric Power Systems Research*, vol. 76, pp. 194-199, 2006.

[17] Y. Chi-Shan, "A discrete Fourier transform-based adaptive mimic phasor estimator for distance relaying applications," *Power Delivery, IEEE Transactions on*, vol. 21, pp. 1836-1846, 2006.

[18] T. S. Sidhu, *et al.*, "Discrete-Fourier-transform-based technique for removal of decaying DC offset from phasor estimates," *Generation, Transmission and Distribution, IEE Proceedings-*, vol. 150, pp. 745-752, 2003.

[19] T. S. Sidhu, *et al.*, "A new half-cycle phasor estimation algorithm," *Power Delivery, IEEE Transactions on*, vol. 20, pp. 1299-1305, 2005.

[20] G. Yong, *et al.*, "Simplified algorithms for removal of the effect of exponentially decaying DC-offset on the Fourier algorithm," *Power Delivery, IEEE Transactions on*, vol. 18, pp. 711-717, 2003.

Appendix B: Interpole states modelling

Chapter 4 has introduces a novel fault location method based on the analysis of circuit breaker operation. This novel fault location method is built on the interpole states computation, which applies the superposition method. This calculation algorithm is based on a lumped R-L line model with two supplies of both ends with the assumption that remote end circuit breaker keeps closing. A single line to ground fault is involved.

The tripping sequence of three phases depends on load flow, fault inception time, fault type and fault resistance. According to phase status, there are three tripping sequences, which are F-H-H, H-F-H and H-H-F. F and H denote as faulty phase and health phase respectively. In the chapter 4, the calculation of F-H-H tripping sequence has been introduced. In Appendix A, the calculations of H-F-H and H-H-F will be presented.

B.1 H-F-H sequence computing algorithm

1) State 1

In State 1, all three poles of the circuit breaker are closed. The calculation is identical

for all scenarios of different tripping sequences, which has been introduced from (4.4) – (4.12)

$$\mathbf{V_{1L}} = \mathbf{V_L} + \mathbf{V'_{1L}} \quad \text{(B.1)}$$

$$\mathbf{I_{1L}} = \mathbf{I_L} + \mathbf{I'_{1L}} \quad \text{(B.2)}$$

Note that, $\mathbf{V_L}$ $\mathbf{I_L}$ are pre-fault voltage and current; $\mathbf{V'_{1L}}$, $\mathbf{I'_{1L}}$ are state 1 superimposed voltage and current

2) State 2

In state 2, one health phase (assume phase B) is tripped. According to superposition theory, the state 2 network is presented as the sum of state 1 network state 2 superimposed network, which is shown in Figure B.1.

In the superimposed network (Figure B.1a), the tripped pole is represented as a controlled current source I'_{2Lb}.

$$I'_{2Lb} = -I_{1Lb} \quad \text{(B.3)}$$

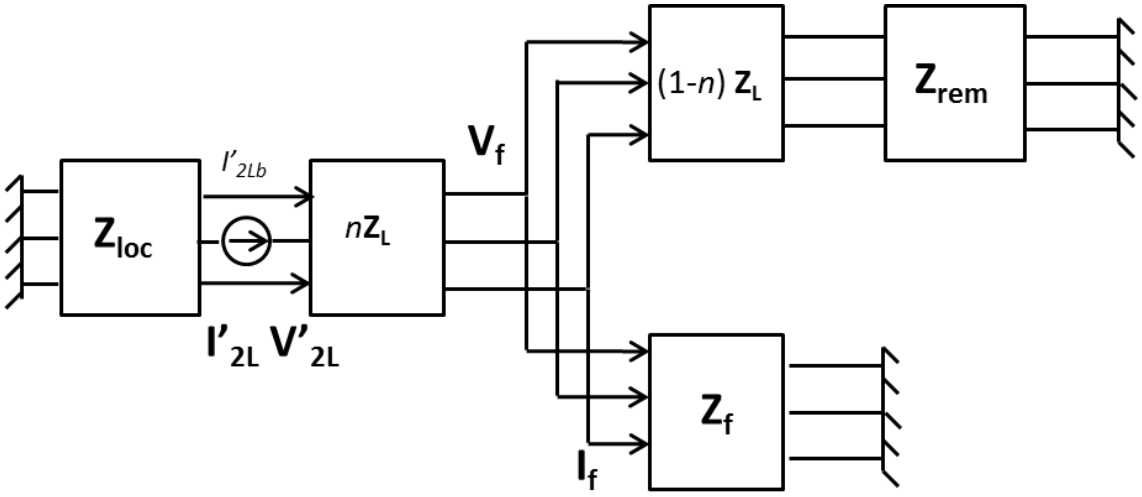

a) State 2 superimposed network

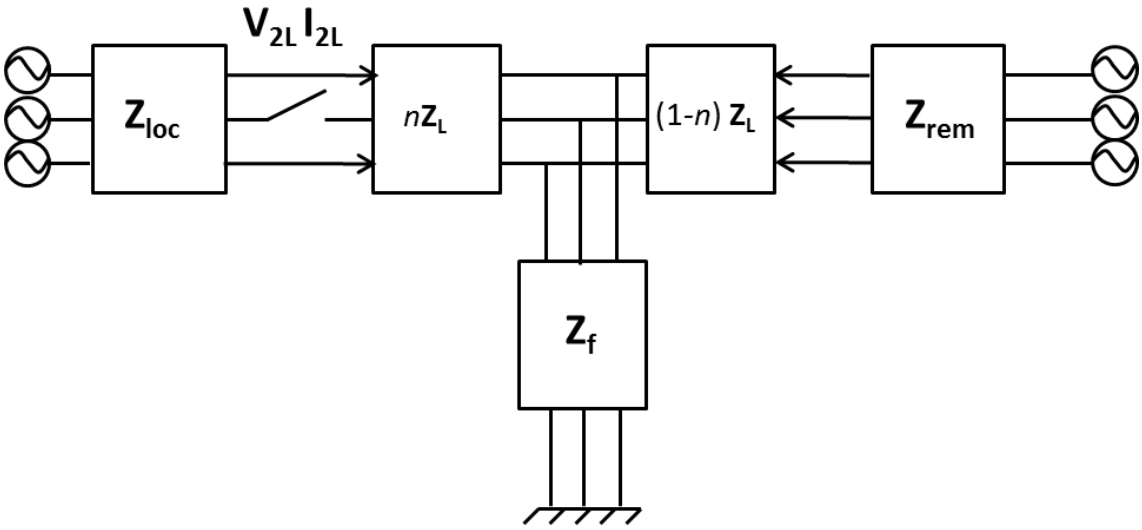

b) State 2 network

Figure B.1 State 2 network compuation

In state 2 superimposed network, the Thevenin equivalent impedance $\mathbf{Z_t}$ behind the circuit breaker is presented in (4.7). The remaining parameters in superimposed network can be calculated as:

$$\begin{bmatrix} I'_{2La} \\ I'_{2Lc} \end{bmatrix} = -I'_{2Lb} \times \begin{bmatrix} Z_{sm} + Z_{t12} \\ Z_{sm} + Z_{t23} \end{bmatrix} \times \begin{bmatrix} Z_{ss} + Z_{t11} & Z_{sm} + Z_{t13} \\ Z_{sm} + Z_{t13} & Z_{ss} + Z_{t33} \end{bmatrix} \quad \text{(B.4)}$$

$$\mathbf{I'_{2L}} = \begin{bmatrix} I'_{2La} \\ I'_{2Lb} \\ I'_{2Lc} \end{bmatrix} \quad \text{(B.5)}$$

$$\mathbf{V'_{2L}} = \mathbf{Z_f} \times \mathbf{I'_{2L}} \quad \text{(B.6)}$$

Note that Z_{ss} and Z_{sm} are self-impedance and mutual-impedance of $\mathbf{Z_{loc}}$. Z_{t11}, Z_{t12}, Z_{t13}, Z_{t23} and Z_{t33} are the elements of $\mathbf{Z_t}$. $\mathbf{Z_f}$ is the fault impedance, which is represented in (4.2).

The pre-state of state 2 is effectively state 1. Thus, $\mathbf{V_{2L}}$ and $\mathbf{I_{2L}}$ are:

$$\mathbf{V_{2L}} = \mathbf{V_{1L}} + \mathbf{V'_{2L}} \quad \text{(B.7)}$$

$$\mathbf{I_{2L}} = \mathbf{I_{1L}} + \mathbf{I'_{2L}} \quad \text{(B.8)}$$

3) State 3

The computation principle of state 3 and state 4 are the same as for state 2. In state 3, shown in Figure B.2, two poles are open. In state 3 superimposed network, one health phase (phase B) pole has already been open in state 2 and therefore is valued 0 at this stage. Pole of faulty phase (phase A) is tripped in this state, which is represented as the controlled current. So, the currents of state 3 superimposed network are

$$I'_{3La} = -I_{2La} \quad \text{(B.9)}$$

$$I'_{3Lb} = 0 \quad \text{(B.10)}$$

$$I'_{3Lac} = \frac{-I'_{3La} \times [Z_{sm} + Z_{t13}]}{Z_{ss} + Z_{t33}} \tag{B.11}$$

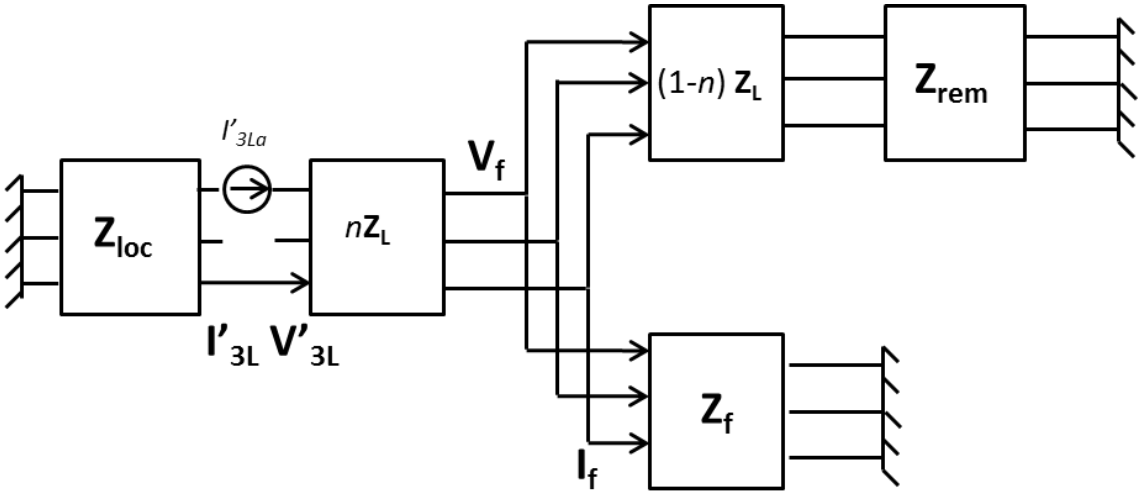

a) State 3 superimposed network

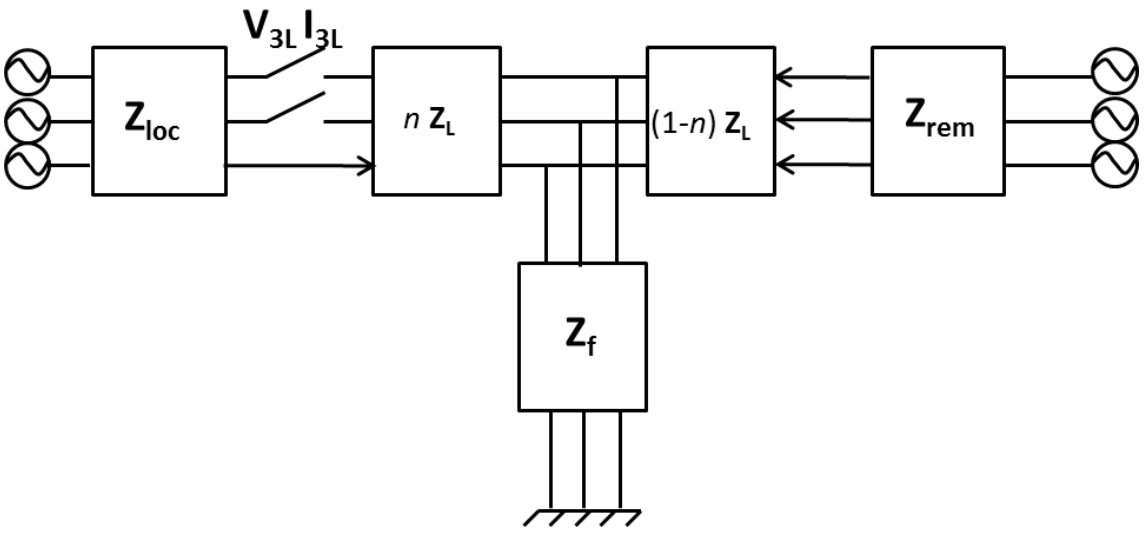

b) State 3 network

Figure B.2 State 3 network computation

Consequently, the voltages of state 3 superimposed network are

$$\mathbf{I'_{3L}} = \begin{bmatrix} I'_{3La} \\ I'_{3Lb} \\ I'_{3Lc} \end{bmatrix} \tag{B.12}$$

$$\mathbf{V'_{3L}} = \mathbf{Z_t} \times \mathbf{I'_{3L}} \tag{B.13}$$

According to superposition theory, voltage $\mathbf{V_{3L}}$ and current $\mathbf{I_{3L}}$ at state 3 are calculated as:

$$\mathbf{V_{3L}} = \mathbf{V_{2L}} + \mathbf{V'_{3L}} \tag{B.14}$$

$$\mathbf{I_{3L}} = \mathbf{I_{2L}} + \mathbf{I'_{3L}} \tag{B.15}$$

4) State 4

In state 4, all circuit breaker poles are open, shown in Figure B.3. In state 4 superimposed network, the current of health phase (phase C) is tripped and represented as controlled source. Consequently, the superimposed current and voltage are calculated as

$$I'_{4La} = 0 \tag{B.16}$$

$$I'_{4Lb} = 0 \tag{B.17}$$

$$I'_{4Lc} = -I_{3Lc} \tag{B.18}$$

$$\mathbf{I'_{4L}} = \begin{bmatrix} I'_{4La} \\ I'_{4Lb} \\ I'_{4Lc} \end{bmatrix} \tag{B.19}$$

$$\mathbf{V'_{4L}} = \mathbf{Z_t} \times \mathbf{I'_{4L}} \tag{B.20}$$

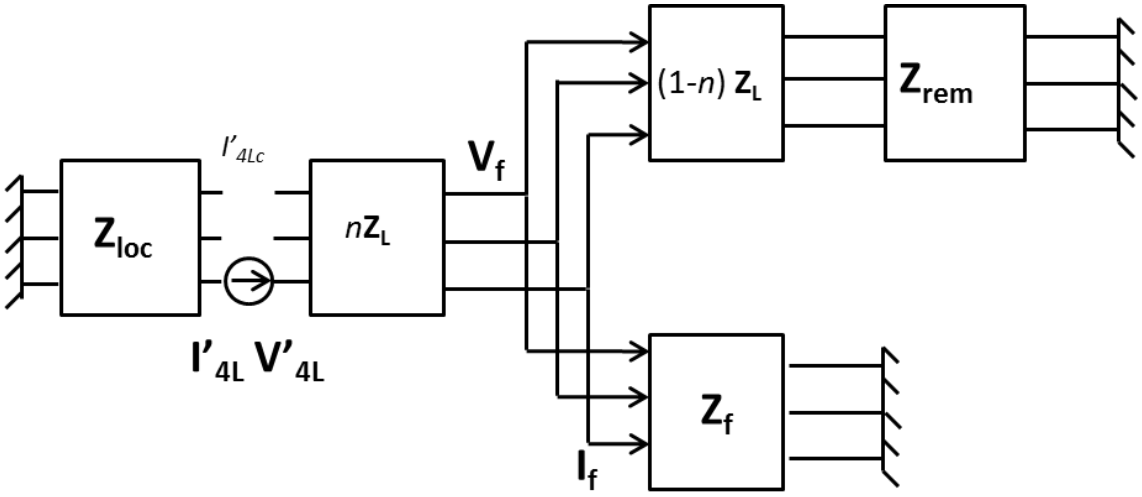

a) State 4 superimposed network

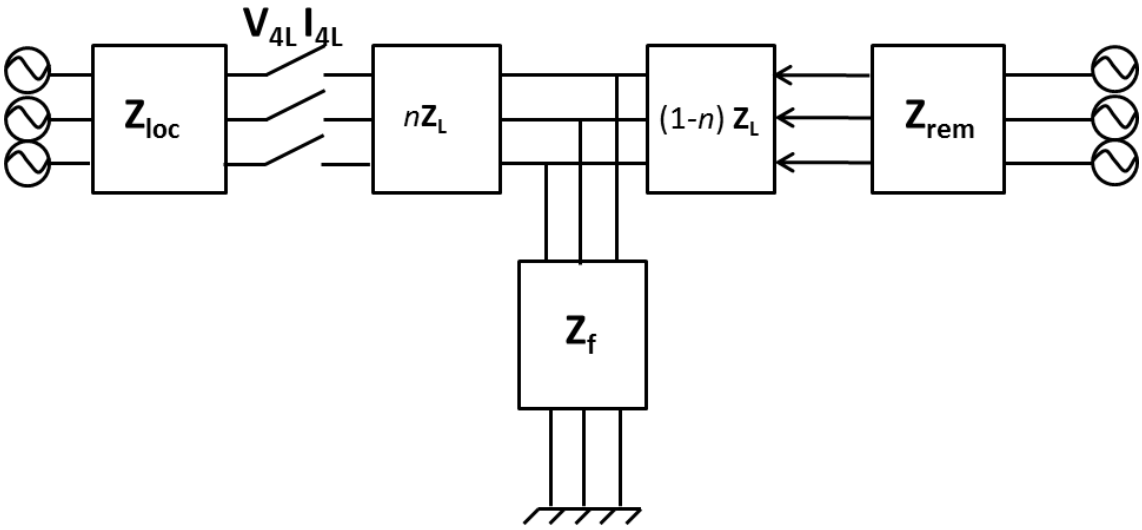

b) State 4 network

Figure B.3 State 4 network computation

Thus, the voltage $\mathbf{V_{4L}}$ and current $\mathbf{I_{4L}}$ in state 4 are as below:

$$\mathbf{V_{4L}} = \mathbf{V_{3L}} + \mathbf{V'_{4L}} \tag{B.21}$$

$$\mathbf{I_{4L}} = \mathbf{I_{3L}} + \mathbf{I'_{4L}} \tag{B.22}$$

B.2 H-H-F sequence computing algorithm

1) State 1

In State 1, all three poles of the circuit breaker are closed. The calculation is identical for all scenarios of different tripping sequences, which has been introduced from (4.4) – (4.12)

$$\mathbf{V_{1L}} = \mathbf{V_s} + \mathbf{V'_{1L}} \tag{B.23}$$

$$\mathbf{I_{1L}} = \mathbf{I_s} + \mathbf{I'_{1L}} \tag{B.24}$$

Note that, $\mathbf{V_s}$ $\mathbf{I_s}$ are pre-fault voltage and current; $\mathbf{V'_{1L}}$, $\mathbf{I'_{1L}}$ are state 1 superimposed voltage and current.

2) State 2

In state 2, one health phase (assume phase B) is tripped. According to superposition theory, the state 2 network is presented as the sum of state 1 network state 2 superimposed network, which is shown in Figure B.4

In the superimposed network (Figure B.4a), the tripped pole is represented as a controlled current source I'_{2Lb}.

$$I'_{2Lb} = -I_{1Lb} \tag{B.25}$$

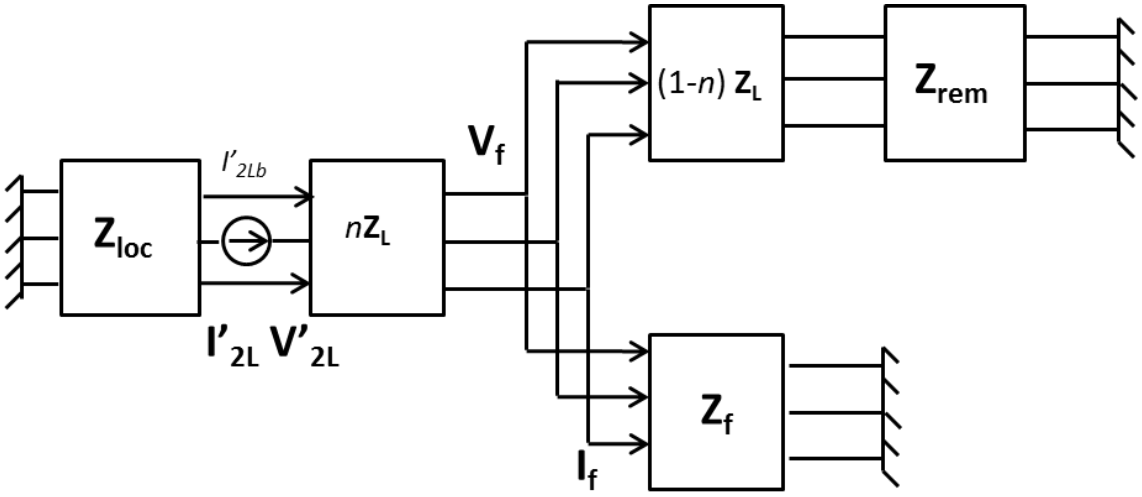

a) State 2 superimposed network

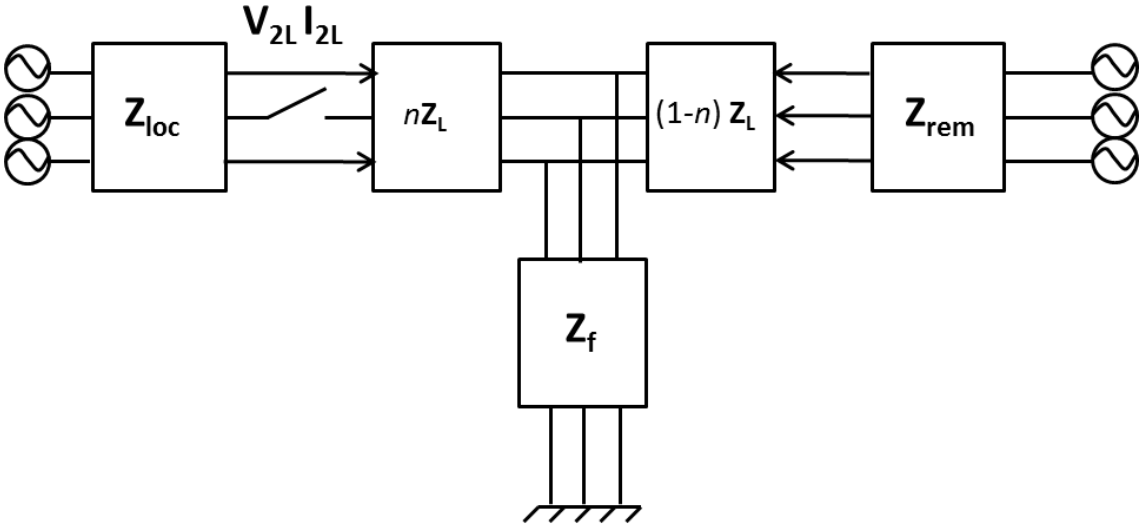

b) State 2 network

Figure B.4 State 2 network compuation

In state 2 superimposed network, the Thevenin equivalent impedance $\mathbf{Z_t}$ behind the circuit breaker is presented in (4.7). The remaining parameters in superimposed network can be calculated as:

$$\begin{bmatrix} I'_{2La} \\ I'_{2Lc} \end{bmatrix} = -I'_{2Lb} \times \begin{bmatrix} Z_{sm} + Z_{t_{12}} \\ Z_{sm} + Z_{t_{23}} \end{bmatrix} \times \begin{bmatrix} Z_{ss} + Z_{t_{11}} & Z_{sm} + Z_{t_{13}} \\ Z_{sm} + Z_{t_{13}} & Z_{ss} + Z_{t_{33}} \end{bmatrix} \tag{B.26}$$

$$\mathbf{I'_{2L}} = \begin{bmatrix} I'_{2La} \\ I'_{2Lb} \\ I'_{2Lc} \end{bmatrix} \tag{B.27}$$

$$\mathbf{V'_{2L}} = \mathbf{Z_f} \times \mathbf{I'_{2L}} \tag{B.28}$$

The pre-state of state 2 is effectively state 1. Thus, $\mathbf{V_{2L}}$ and $\mathbf{I_{2L}}$ are:

$$\mathbf{V_{2L}} = \mathbf{V_{1L}} + \mathbf{V'_{2L}} \tag{B.29}$$

$$\mathbf{I_{2L}} = \mathbf{I_{1L}} + \mathbf{I'_{2L}} \tag{B.30}$$

3) State 3

The computation principle of state 3 and state 4 are the same as for state 2. In state 3, shown in Figure B.5, two poles are tripped. In state 3 superimposed network, one health phase (phase B) pole has already been open in state 2 and therefore is valued 0 at this stage. Pole of another health phase (phase C) is tripped in this state, which is represented as the controlled current. So, the currents of state 3 superimposed network are

$$I'_{3Lb} = 0 \tag{B.31}$$

$$I'_{3Lc} = -I_{2Lc} \tag{B.32}$$

$$I'_{3La} = \frac{-I'_{3Lc} \times [Z_{sm} + Z_{t13}]}{Z_{ss} + Z_{t11}} \tag{B.33}$$

Consequently, the voltages of state 3 superimposed network are

$$\mathbf{I'_{3L}} = \begin{bmatrix} I'_{3La} \\ I'_{3Lb} \\ I'_{3Lc} \end{bmatrix} \tag{B.34}$$

$$\mathbf{V'_{3L}} = \mathbf{Z_t} \times \mathbf{I'_{3L}} \tag{B.35}$$

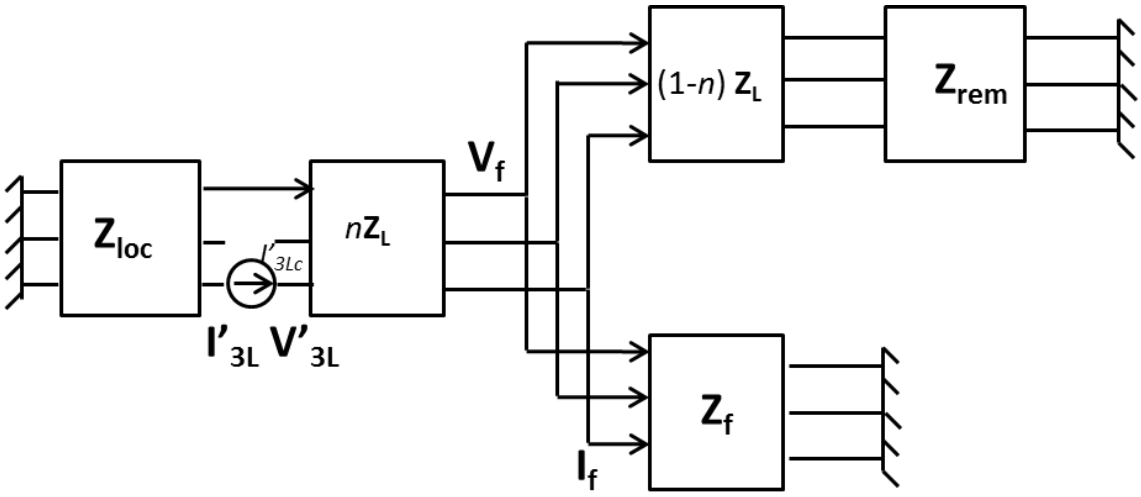

a) State 3 superimposed network

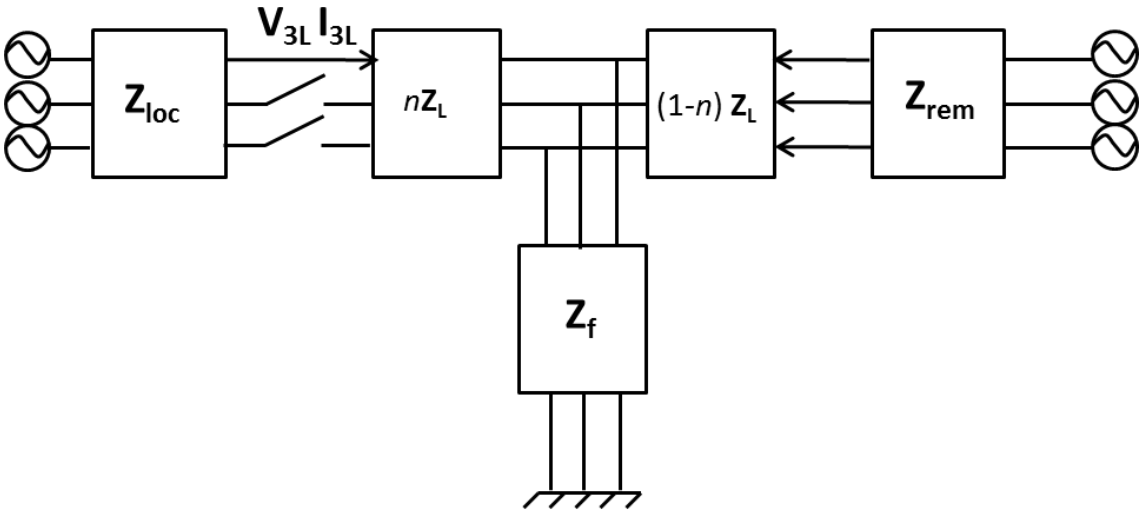

b) State 3 network

Figure B.5 State 3 network computation

According to superposition theory, voltage $\mathbf{V_{3L}}$ and current $\mathbf{I_{3L}}$ at state 3 are calculated as:

$$\mathbf{V_{3L}} = \mathbf{V_{2L}} + \mathbf{V'_{3L}} \tag{B.36}$$

$$\mathbf{I_{3L}} = \mathbf{I_{2L}} + \mathbf{I'_{3L}} \tag{B.37}$$

4) State 4

In state 4, all circuit breaker poles are open, shown in Figure B.6. In state 4 network, the current of faulty phase (phase C) is tripped. Thus, phase C represented as controlled source in state 4 superimposed network. Consequently, the superimposed current and voltage are calculated as

$$I'_{4La} = -I_{3La} \tag{B.38}$$

$$I'_{4Lb} = 0 \tag{B.39}$$

$$I'_{4Lc} = 0 \tag{B.40}$$

$$\mathbf{I'_{4L}} = \begin{bmatrix} I'_{4La} \\ I'_{4Lb} \\ I'_{4Lc} \end{bmatrix} \tag{B.41}$$

$$\mathbf{V'_{4L}} = \mathbf{Z_t} \times \mathbf{I'_{4L}} \tag{B.42}$$

Thus, the voltage $\mathbf{V_{4L}}$ and current $\mathbf{I_{4L}}$ in state 4 are as below:

$$\mathbf{V_{4L}} = \mathbf{V_{3L}} + \mathbf{V'_{4L}} \tag{B.43}$$

$$\mathbf{I_{4L}} = \mathbf{I_{3L}} + \mathbf{I'_{4L}} \tag{B.44}$$

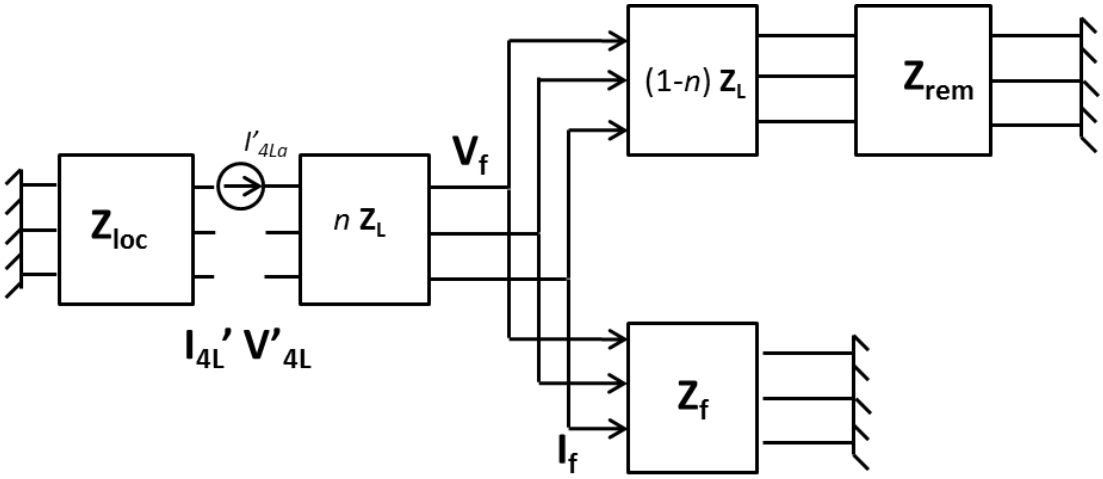

a). State 4 superimposed network

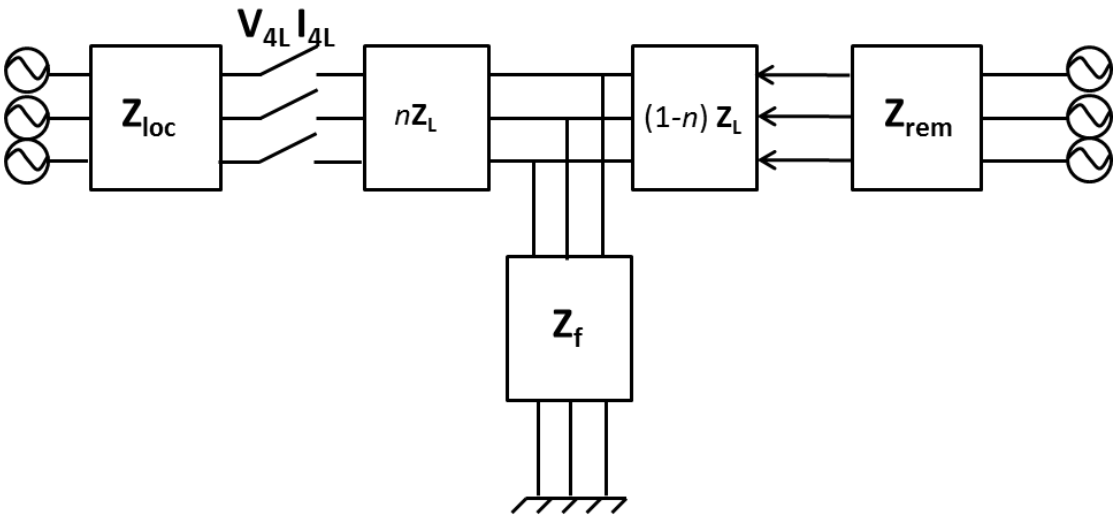

b). State 4 network

Figure B.6 State 4 network computation

Appendix C: Auto-reclose modelling

Chapter 5 has introduced a novel fault location technique which based on the auto reclose modelling. The proposed fault location algorithm is designed for a double-ended source transmission line, which is representative of the vast majority of interconnected transmission system applications. Superposition method has been applied in both state 1 and state 2 computations. In order to improve the accuracy of transmission line modelling, the distributed line model has been used instead of lumped line model in this section. Single phase to ground fault is involved at the current stage as a predominant type of fault in overhead lines. There are 4 different scenarios of auto-reclose scheme, which are

- SPAR local end reclose first;
- SPAR remote end reclose first;
- TPAR local end reclose first;
- TPAR remote end reclose first.

The modelling of scenario A is presented in chapter 5. As state 1 of all scenarios are identical, state 2 modelling of other 3 scenarios will be introduced in this section.

C.1 SPAR remote end reclose first

In this scenario state 2 superimposed network of the remote end CB recloses first. The open pole of the local circuit breaker is represented as a controlled current source, as shown in Figure C.1a, with the current equal to

$$\boldsymbol{I'_{2La} = -I_{1La}} \tag{C.1}$$

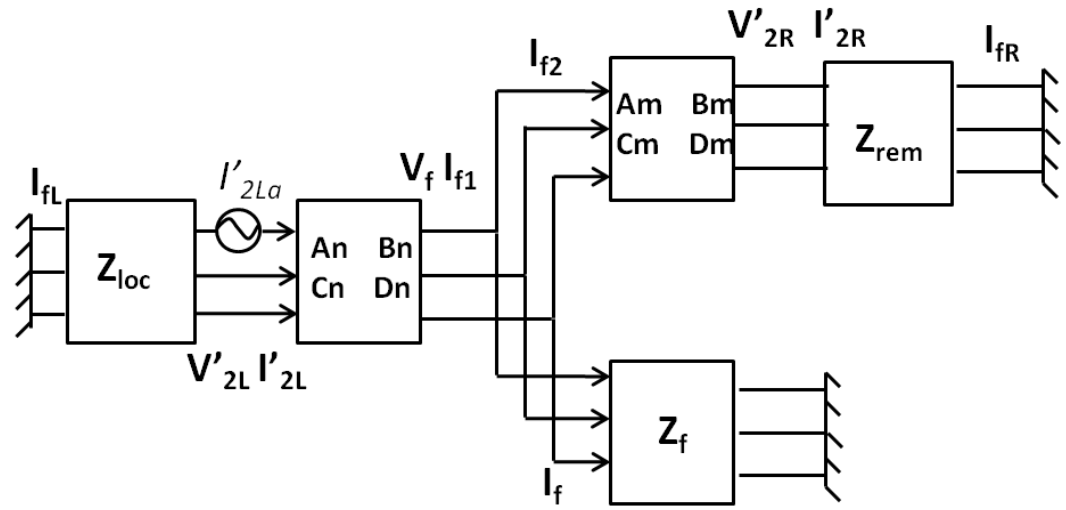

a) State 2 superimposed network

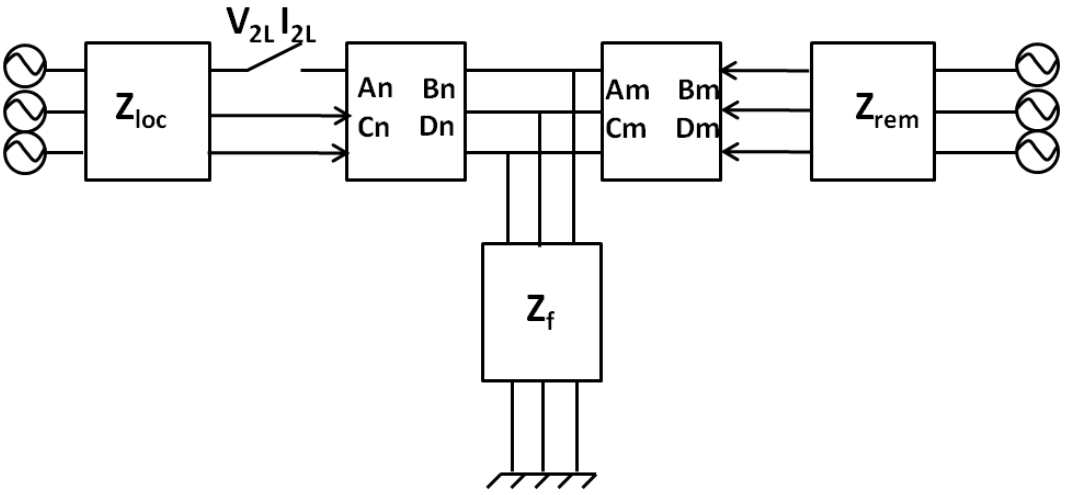

b) State 2 network during reclose

Figure C.1 Scenario of *SPAR* with remote CB reclosing first

In Figure C.1a, the distributed network section from the fault point to the remote end is represented as

$$\begin{bmatrix} \mathbf{V_f} \\ \mathbf{I_{f2}} \end{bmatrix} = \begin{bmatrix} \mathbf{A_R} & \mathbf{B_R} \\ \mathbf{C_R} & \mathbf{D_R} \end{bmatrix} \begin{bmatrix} \mathbf{0} \\ \mathbf{I_{fR}} \end{bmatrix} \tag{C.2}$$

$$\mathbf{I_{f2}} = \mathbf{D_R B_R}^{-1} \mathbf{V_f} \tag{C.3}$$

Where, $\mathbf{A_R} = \mathbf{A_m}$, $\mathbf{B_R} = \mathbf{A_m} + \mathbf{Z_{rem} B_m}$, $\mathbf{C_R} = \mathbf{C_m}$, $\mathbf{D_R} = \mathbf{C_m} + \mathbf{Z_{rem} D_m}$

The fault path from fault point to earth is represented as

$$\mathbf{I_f} = \mathbf{Z_f}^{-1} \mathbf{V_f} = {R_f}^{-1} \mathbf{K V_f} \tag{C.4}$$

From equation (C.3) and (C.4), we can obtain

$$\mathbf{I_{f1}} = \mathbf{I_f} + \mathbf{I_{f2}} = \left({R_f}^{-1} \mathbf{K} + \mathbf{D_R B_R}^{-1}\right) \mathbf{V_f} \tag{C.5}$$

The network section from the local relay point to the fault point is represented as,

$$\mathbf{V'_{2L}} = \mathbf{A_n V_f} + \mathbf{B_n I_{f1}} \tag{C.6}$$

$$\mathbf{I'_{2L}} = \mathbf{C_n V_f} + \mathbf{D_n I_{f1}} \tag{C.7}$$

Eliminating $\mathbf{V_f}$ from (C.6) and (C.7) using (C.5) gives:

$$\mathbf{V'_{2L}} = \mathbf{X}\, \mathbf{I_{f1}} \tag{C.8}$$

$$\mathbf{I'_{2L}} = \mathbf{Y}\,\mathbf{I_{f1}} \tag{C.9}$$

Where, $\mathbf{I_{f1}}$ is 3×1 matrix and **X, Y** are 3×3 matrixes, represented as

$$\mathbf{X} = [{R_f}^{-1}\mathbf{K} + \mathbf{D_R}\mathbf{B_R}^{-1}]^{-1}\mathbf{A_n} + \mathbf{B_n} \tag{C.10}$$

$$\mathbf{Y} = [{R_f}^{-1}\mathbf{K} + \mathbf{D_R}\mathbf{B_R}^{-1}]^{-1}\mathbf{C_n} + \mathbf{D_n} \tag{C.11}$$

X and **Y** depend on *n*, R_f and $\mathbf{Z_{rem}}$. Note that $\mathbf{Z_{rem}}$ is the remote end source impedance which can be calculated by *SCL2*. Assuming *n*, R_f and $\mathbf{Z_{rem}}$ are known, $\mathbf{V_f}$ can be solved using equations (C.1), (C.5), (C.8) to (C.11).

In the superimposed network, the network section from the fault point to the local end can be represented as:

$$\begin{bmatrix}\mathbf{V_f}\\ \mathbf{I_{f1}}\end{bmatrix} = \begin{bmatrix}\mathbf{A_L} & \mathbf{B_L}\\ \mathbf{C_L} & \mathbf{D_L}\end{bmatrix}\begin{bmatrix}\mathbf{0}\\ \mathbf{I'_{fL}}\end{bmatrix} \tag{C.12}$$

It is assumed that $\mathbf{I'_{2L}} = \mathbf{I_{fL}}$, Equation (C.12) can be solved for $\mathbf{I'_{2L}}$, and consequently, $\mathbf{V'_{2L}} = \mathbf{Z_{loc}}\mathbf{I'_{2L}}$. According to superposition theory, the local voltage $\mathbf{V_{2L}}$ and current $\mathbf{I_{2L}}$ in state 2 are:

$$\mathbf{V_{2L}} = \mathbf{V_{1L}} + \mathbf{V'_{2L}} \tag{C.13}$$

$$\mathbf{I_{2L}} = \mathbf{I_{1L}} + \mathbf{I'_{2L}} \tag{C.14}$$

C.2 TPAR Local end reclose first

In this scenario, all three phases of the local end circuit breaker reclose and the remote end circuit breaker remains open. Similarly to the previous cases, the superposition theory has been applied in this situation. In superimposed network (Figure C.2a), the remote opened circuit breaker is represented as a controlled current source.

$$\mathbf{I'_{2R}} = -\mathbf{I_{1R}} \tag{C.15}$$

In Figure C.2a, the distributed network section from fault point to local end is represented as:

$$\begin{bmatrix} \mathbf{V_f} \\ \mathbf{I_{f1}} \end{bmatrix} = \begin{bmatrix} \mathbf{A_L} & \mathbf{B_L} \\ \mathbf{C_L} & \mathbf{D_L} \end{bmatrix} \begin{bmatrix} \mathbf{0} \\ \mathbf{I_{fL}} \end{bmatrix} \tag{C.16}$$

Where, $\mathbf{A_L} = \mathbf{A_n}$, $\mathbf{B_L} = \mathbf{A_n} + \mathbf{Z_{loc}}\mathbf{B_n}$, $\mathbf{C_L} = \mathbf{C_n}$, $\mathbf{D_L} = \mathbf{C_n} + \mathbf{Z_{loc}}\mathbf{D_n}$, $I_{fL}=I_{2L}$

The fault path from fault point to earth and fault point to local end are represented as:

$$\mathbf{I_f} = \mathbf{Z_f}^{-1}\mathbf{V_f} = {R_f}^{-1}\mathbf{K}\mathbf{V_f} \tag{C.17}$$

$$\mathbf{I_{f1}} = \mathbf{D_L}\mathbf{B_L}^{-1}\mathbf{V_f} \tag{C.18}$$

The fault current $\mathbf{I_{f2}}$ is equal to

$$\mathbf{I_{f2}} = \mathbf{I_{f1}} + \mathbf{I_f} = \mathbf{M}\mathbf{V_f} \tag{C.19}$$

$$\mathbf{M} = R_f{}^{-1}\mathbf{K} + \mathbf{D_L}\mathbf{B_L}{}^{-1} \quad \text{(C.20)}$$

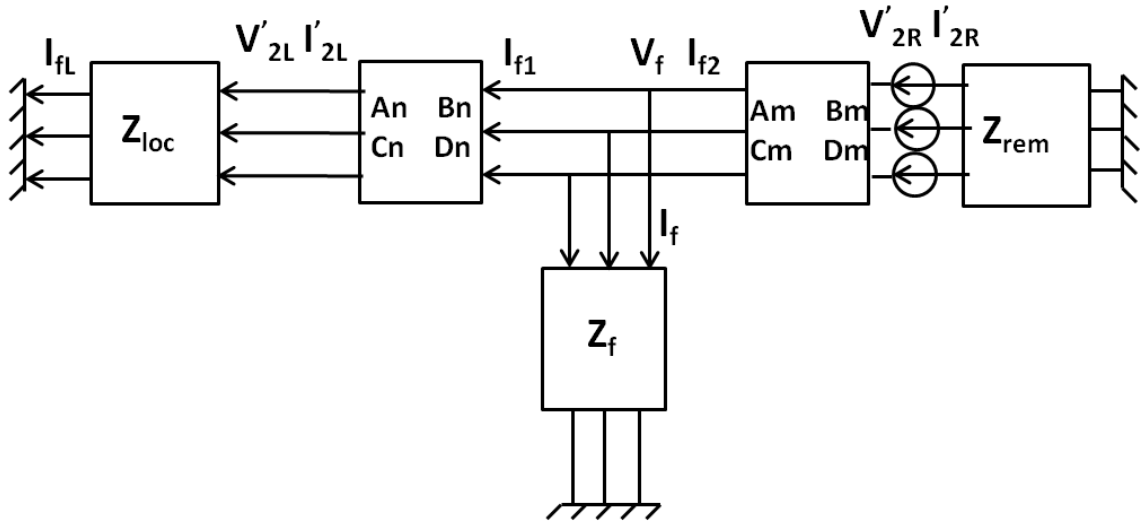

a) State 2 superimposed network

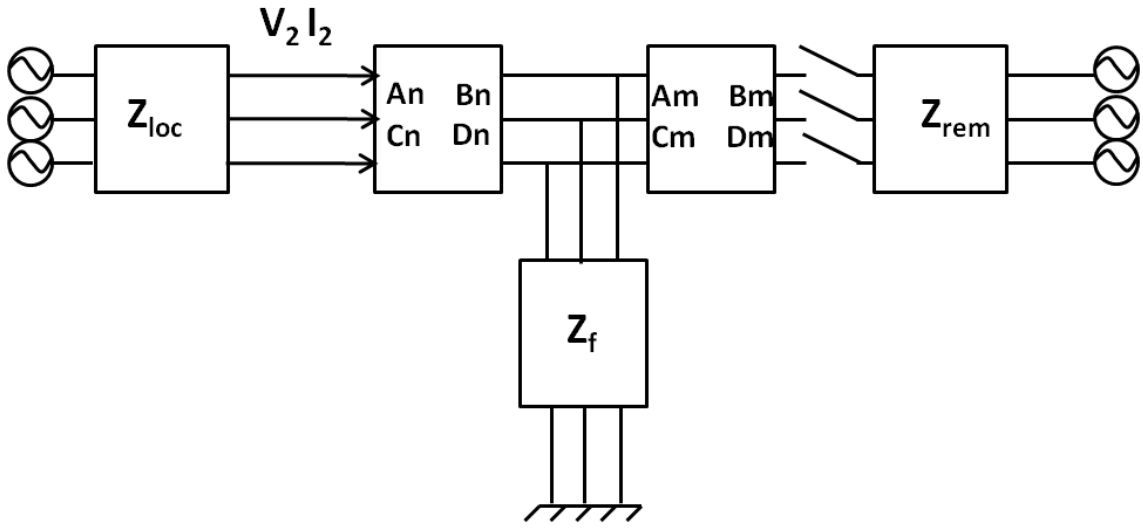

b) State 2 network during reclose

Figure C.2 Scenario of *TPAR* with local CB reclosing first

The network section from the remote relay point to the fault point is represented as:

$$\mathbf{V'_{2R}} = \mathbf{A_m V_f} + \mathbf{B_m I_{f2}} \quad \text{(C.21)}$$

$$\mathbf{I'_{2R}} = \mathbf{C_m V_f} + \mathbf{D_m I_{f2}} \quad \text{(C.22)}$$

M, $\mathbf{C_m}$ and $\mathbf{D_m}$ depend on *n*, R_f and $\mathbf{Z_{rem.}}$ Note that $\mathbf{Z_{rem}}$ is the remote end source impedance which can be calculated by *SCL2*. Assuming *n*, R_f and $\mathbf{Z_{rem}}$ are known, $\mathbf{V_f}$ can be solved using equations (C.15), (C.19), (C.20) and (C.22). Thus:

$$\mathbf{I'_{2L}} = \mathbf{B_L}^{-1}\mathbf{V_f} \quad \text{(C.23)}$$

$$\mathbf{V'_{2L}} = \mathbf{I'_{2L}} \mathbf{Z_{loc}} \quad \text{(C.24)}$$

According to superposition theory, the local end voltage and current of State 2 are:

$$\mathbf{V_{2L}} = \mathbf{V_{1L}} + \mathbf{V'_{2L}} \quad \text{(C.25)}$$

$$\mathbf{I_{2L}} = \mathbf{I_{1L}} + \mathbf{I'_{2L}} \quad \text{(C.26)}$$

C.3 TPAR Remote end reclose first

In this scenario, all three phases of the remote end circuit breaker reclose and the local end circuit breaker remains open. Similarly to the previous cases, the superposition theory has been applied in this situation. In superimposed network (Figure C.3a), the remote opened circuit breaker is represented as a controlled current source.

$$\mathbf{I'_{2L}} = -\mathbf{I_{1L}} \tag{C.27}$$

The network section from the fault point to the remote end is represented as:

$$\begin{bmatrix}\mathbf{V_f}\\ \mathbf{I_{f2}}\end{bmatrix} = \begin{bmatrix}\mathbf{A_R} & \mathbf{B_R}\\ \mathbf{C_R} & \mathbf{D_R}\end{bmatrix}\begin{bmatrix}0\\ \mathbf{I'_{2R}}\end{bmatrix} \tag{C.28}$$

$$\mathbf{I_{f2}} = \mathbf{D_R}\mathbf{B_R}^{-1}\mathbf{V_f} \tag{C.29}$$

Where, $\mathbf{A_R} = \mathbf{A_m}$, $\mathbf{B_R} = \mathbf{A_m} + \mathbf{Z_{rem}}\mathbf{B_m}$, $\mathbf{C_R} = \mathbf{C_m}$, $\mathbf{D_R} = \mathbf{C_m} + \mathbf{Z_{rem}}\mathbf{D_m}$

The fault path from fault point to earth is represented as:

$$\mathbf{I_f} = {R_f}^{-1}\mathbf{K}\mathbf{V_f} \tag{C.30}$$

In superimposed network (Figure C.3a),

$$\mathbf{I_{f1}} = \mathbf{I_f} + \mathbf{I_{f2}} = \mathbf{M}\mathbf{V_f} \tag{C.31}$$

$$\mathbf{M} = {R_f}^{-1}\mathbf{K} + \mathbf{D_R}\mathbf{B_R}^{-1} \tag{C.32}$$

The network section from the local relay point to the fault point is represented as:

$$\begin{bmatrix}\mathbf{V'_{2L}}\\ \mathbf{I'_{2L}}\end{bmatrix} = \begin{bmatrix}\mathbf{A_n} & \mathbf{B_n}\\ \mathbf{C_n} & \mathbf{D_n}\end{bmatrix}\begin{bmatrix}\mathbf{V_f}\\ \mathbf{I_{f1}}\end{bmatrix} \tag{C.33}$$

M depends on *n*, R_f and $\mathbf{Z_{rem}}$. Assuming *n*, R_f and $\mathbf{Z_{rem}}$ are known, $\mathbf{V'_{2L}}$ can be solved using equations (C.27), (C.31) to (C.33). Thus:

$$\mathbf{V'_{2L}} = (\mathbf{C_n} + \mathbf{D_n M})^{-1}(\mathbf{A_n} + \mathbf{B_n M})\mathbf{I'_{2L}} \tag{C.34}$$

According to superposition theory

$$\mathbf{V_{2L}} = \mathbf{V_{1L}} + \mathbf{V'_{2L}} \tag{C.35}$$

$$\mathbf{I_{2L}} = \mathbf{I_{1L}} + \mathbf{I'_{2L}} \tag{C.36}$$

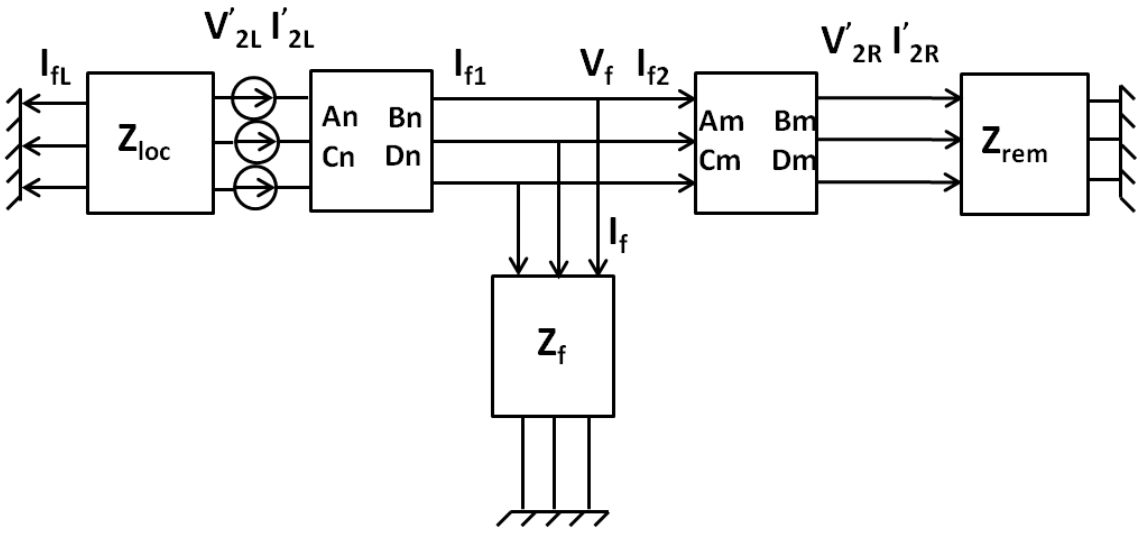

a) State 2 superimposed network

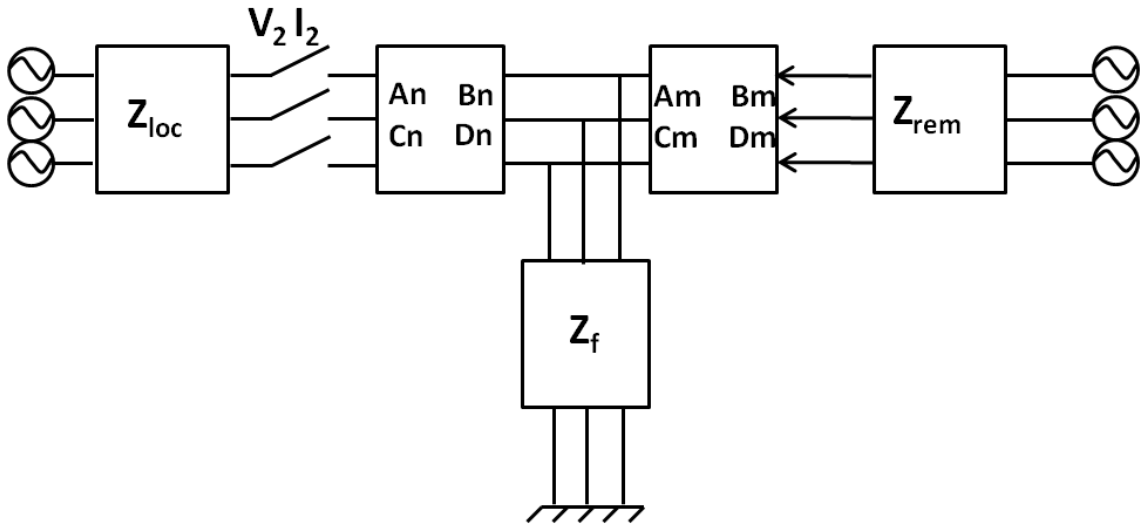

b) State 2 network during reclose

Figure C.3 Scenario of *TPAR* with local CB reclosing first

Appendix D: MATLAB user interface: design and operation

In order to facilitate convenient way of testing the proposed fault location algorithm and to enable more effective demonstration, a MATLAB graphical user interface has been designed.

Figure D.1 shows the user interface panel. Generally, there are four main elements within the user interface panel, which comprise: transmission line settings; local source settings; ATP simulated/COMTRADE data file selection; results presentation.

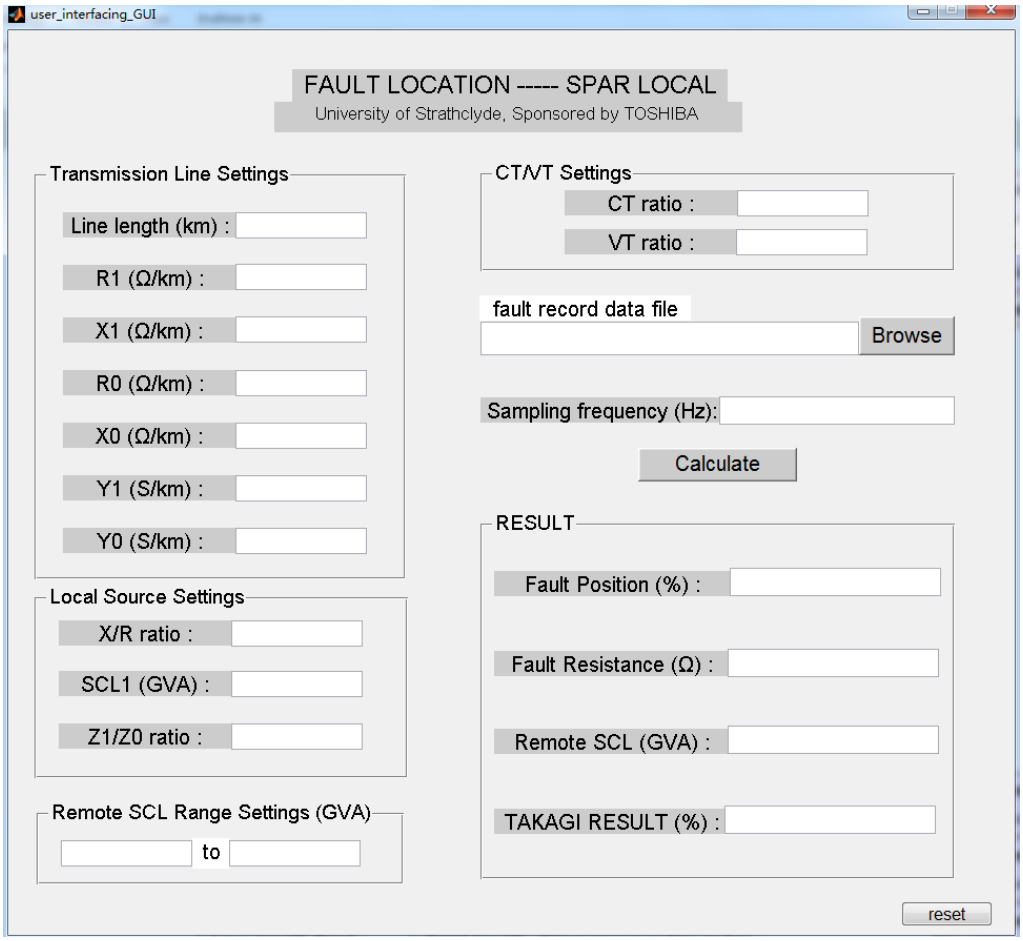

Figure D.1.User interface in MATLAB

Item	**Function**
Line length [km]	Total length of transmission line in km
R1[Ω/km]	Positive sequence resistance of transmission line
X1 [Ω/km]	Positive sequence inductance of transmission line
R0 [Ω/km]	Zero sequence resistance of transmission line
X0 [Ω/km]	Zero sequence inductance per km of transmission line
Y1 [Ω/km]	Positive sequence admittance per km of transmission line
Y0 [Ω/km]	Zero sequence admittance per km of transmission line
X/R ratio	Local source X/R ratio
SCL1	Local source short circuit level
Z1/Z0	Local source positive impedance vs zero impedance ratio
CT ratio	Current transformer ratio
VT ratio	Voltage transformer ratio
Open file	ATP simulated/COMTRADE data file selection
Sampling frequency	Sampling frequency of selected data
Locating	Debug the fault location method
Fault position	Estimated fault position by proposed fault location method
Fault resistance	Estimated fault resistance by proposed fault location method
Remote SCL	Estimated remote end short circuit level by proposed fault location method
TAKAGI RESULT	Estimated fault location using TAKAGI method
Reset	Reset fault location algorithm

Table D.1. User interface instruction

Table D.1 includes some guidance regarding the usage and the settings of the user interface. This system can estimate fault location using simulated and/or recorded fault data. The system accepts data file formats of '*.txt', '*.csv', '*.dat' and '*.xlsx'.

The operation sequence of this tool is as follows:

1. Select the fault recorder/simulation output data file using the “browse” utility

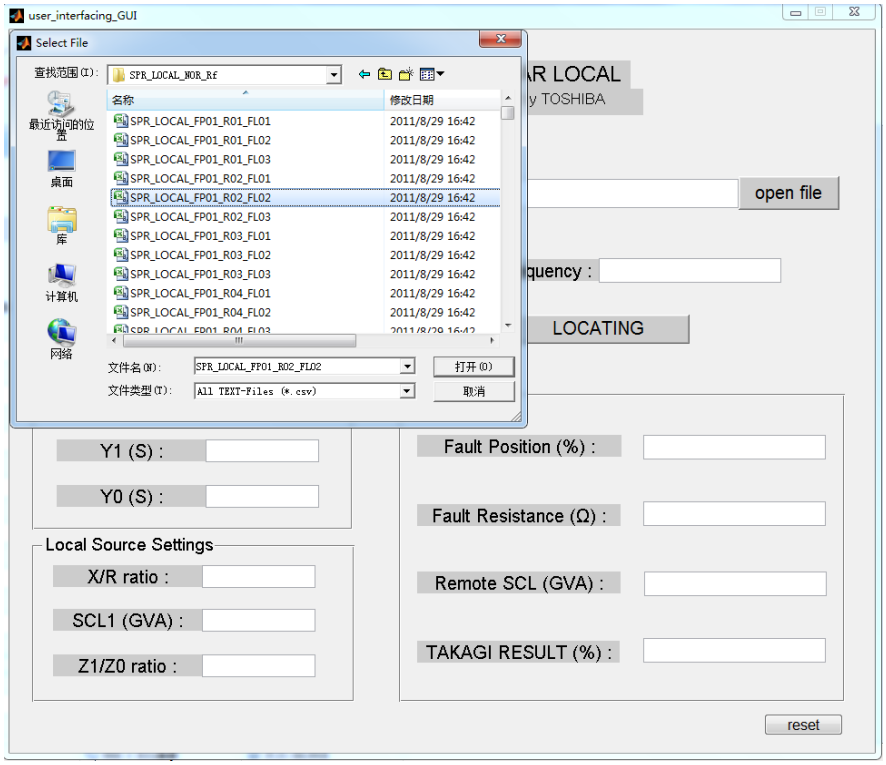

2. Input the data file sampling frequency, transmission line and local source settings

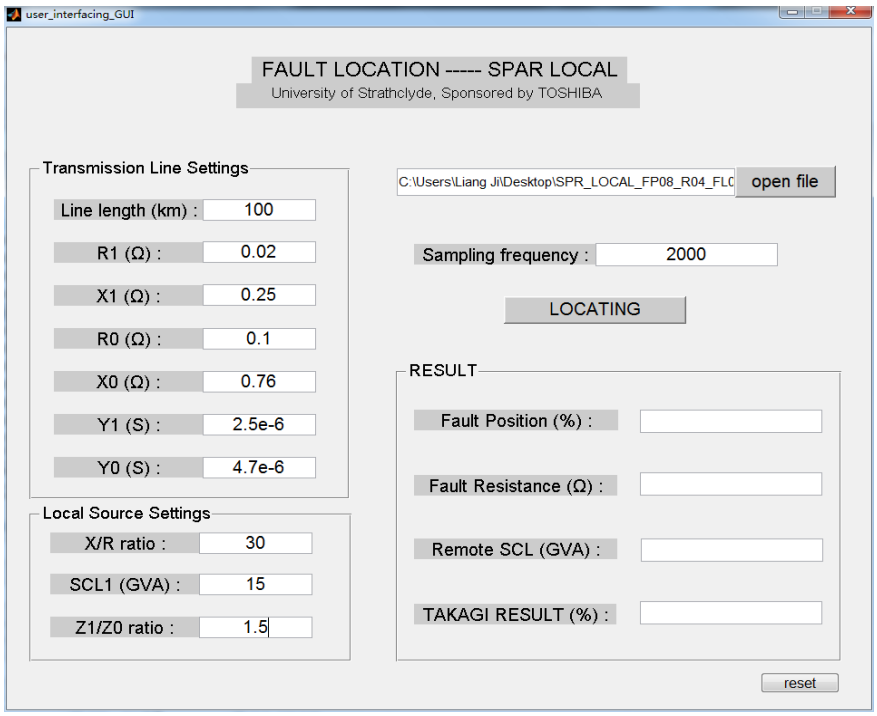

3. Press the “Calculate” button to execute the fault location algorithm

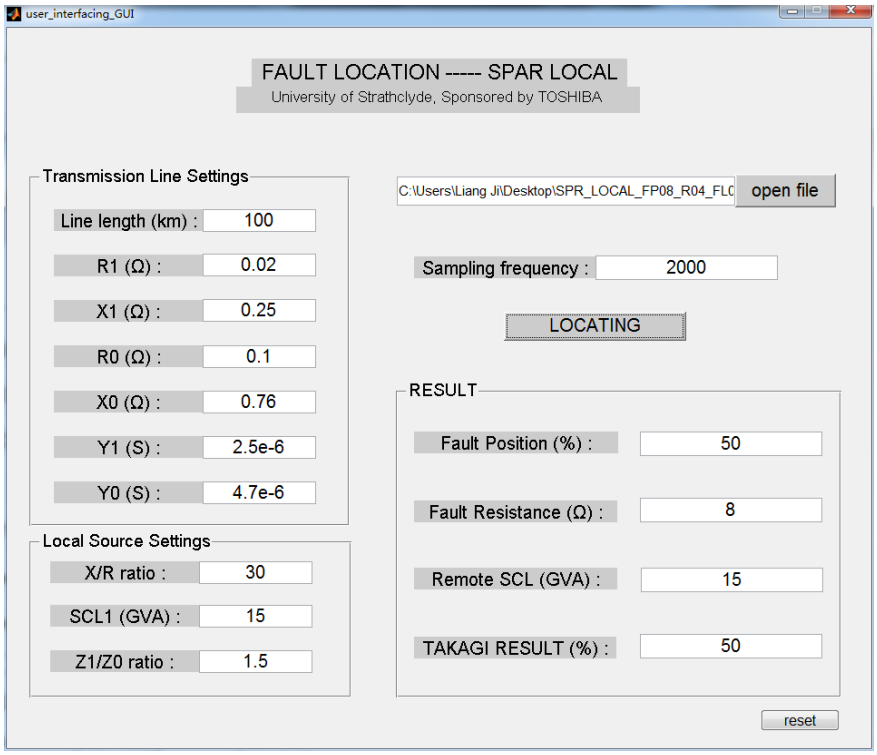

The program calculates the estimated fault position with both the proposed method and TAKAGI method.